

NASA/CR—2004-212875



Manual of Scaling Methods

David N. Anderson
Ohio Aerospace Institute, Brook Park, Ohio

March 2004

The NASA STI Program Office . . . in Profile

Since its founding, NASA has been dedicated to the advancement of aeronautics and space science. The NASA Scientific and Technical Information (STI) Program Office plays a key part in helping NASA maintain this important role.

The NASA STI Program Office is operated by Langley Research Center, the Lead Center for NASA's scientific and technical information. The NASA STI Program Office provides access to the NASA STI Database, the largest collection of aeronautical and space science STI in the world. The Program Office is also NASA's institutional mechanism for disseminating the results of its research and development activities. These results are published by NASA in the NASA STI Report Series, which includes the following report types:

- **TECHNICAL PUBLICATION.** Reports of completed research or a major significant phase of research that present the results of NASA programs and include extensive data or theoretical analysis. Includes compilations of significant scientific and technical data and information deemed to be of continuing reference value. NASA's counterpart of peer-reviewed formal professional papers but has less stringent limitations on manuscript length and extent of graphic presentations.
- **TECHNICAL MEMORANDUM.** Scientific and technical findings that are preliminary or of specialized interest, e.g., quick release reports, working papers, and bibliographies that contain minimal annotation. Does not contain extensive analysis.
- **CONTRACTOR REPORT.** Scientific and technical findings by NASA-sponsored contractors and grantees.

- **CONFERENCE PUBLICATION.** Collected papers from scientific and technical conferences, symposia, seminars, or other meetings sponsored or cosponsored by NASA.
- **SPECIAL PUBLICATION.** Scientific, technical, or historical information from NASA programs, projects, and missions, often concerned with subjects having substantial public interest.
- **TECHNICAL TRANSLATION.** English-language translations of foreign scientific and technical material pertinent to NASA's mission.

Specialized services that complement the STI Program Office's diverse offerings include creating custom thesauri, building customized databases, organizing and publishing research results . . . even providing videos.

For more information about the NASA STI Program Office, see the following:

- Access the NASA STI Program Home Page at <http://www.sti.nasa.gov>
- E-mail your question via the Internet to help@sti.nasa.gov
- Fax your question to the NASA Access Help Desk at 301-621-0134
- Telephone the NASA Access Help Desk at 301-621-0390
- Write to:
NASA Access Help Desk
NASA Center for Aerospace Information
7121 Standard Drive
Hanover, MD 21076

NASA/CR—2004-212875



Manual of Scaling Methods

David N. Anderson
Ohio Aerospace Institute, Brook Park, Ohio

Prepared under Cooperative Agreement NCC3-884

National Aeronautics and
Space Administration

Glenn Research Center

March 2004

Acknowledgments

Although this work has one author, the ideas originated with a number of people. It was jointly supported by the FAA Tech Center and the NASA Glenn Icing Branch. The author wishes to thank Jim Riley of the FAA and Tom Bond of NASA for their support, encouragement, valuable technical consultations, and direction for several years. The late Bill Olsen initiated the scaling work at NASA Glenn (then NASA Lewis), working with Gary Ruff, then of the AEDC, in complementary studies. Many of the early testing plans and approaches that led to results in this manual were based on Olsen's initial work. Jack Reinmann continued to encourage and support scaling studies after Olsen's death; Jack never grew impatient with the slow progress over time. Valuable insight into icing physics, many of the ideas for new approaches to scaling, and concepts for the tests performed through the years were the result of discussions with a number of contributors, most of whom are well known in the icing community. These include Alan Bilanin, Simon Chen, Alex Feo, Dick Kind, Mark Potapczuk, Alric Rothmayer, Gary Ruff, Paul Tsao, and Bill Wright. Finally, through a decade of testing in the NASA Glenn IRT, Dave Sheldon, Charles Andracchio, Tom Irvine, and Susan Kevdzija provided the engineering and facility support, and the IRT crew gave their ever-willing and creative technical support and patience to endure seemingly endless scaling tests on which much of the material in this manual is based. Dean Miller and Judy Van Zante gave time from their own important research to discuss, advise, and assist in testing on several occasions. My grateful appreciation is extended to all these and to numerous summer interns and high-school shadowing students who helped to run tests, digitize ice shapes, reduce data, and prepare figures for publications and presentations.

This report contains preliminary findings, subject to revision as analysis proceeds.

Available from

NASA Center for Aerospace Information
7121 Standard Drive
Hanover, MD 21076

National Technical Information Service
5285 Port Royal Road
Springfield, VA 22100

Available electronically at <http://gltrs.grc.nasa.gov>

Table of Contents

1. Nomenclature	1
2. Introduction	3
3. Similitude Analysis	4
3.1. Geometric Similarity	4
3.2. Flowfield Similarity	4
3.3. Drop Trajectory Similarity	5
3.3.1. Langmuir and Blodgett Trajectory Analysis	6
3.3.2. Simplified Trajectory Analysis	9
3.3.3. Effect of MVD on Ice Shape	10
3.4. Water Catch Similarity	10
3.5. Energy Balance Similarity	12
3.5.1. Convective Heat Transfer	13
3.5.2. Evaporation	14
3.5.3. Sublimation	15
3.5.4. Radiation	15
3.5.5. Sensible Heat of Water	15
3.5.6. Runback	15
3.5.7. Conduction	15
3.5.8. Latent Heat of Fusion	15
3.5.9. Sensible Heat of Ice	16
3.5.10. Drop Kinetic Energy	16
3.5.11. Water Inflow	16
3.5.12. Energy Balance Equation	16
3.5.13. Effect of Temperature and LWC	17
3.5.14. Validation of the Freezing Fraction Expression	21
3.6. Similarity of Surface-Water Dynamics	23
3.6.1. Forms of the Weber Number	24
3.6.2. Other Water-Film Parameters and Additional Methods to Determine Scale Velocity	27
3.7. Other Phenomena	28
3.8. Summary of Potential Scaling Parameters	28
4. Experimental Evaluation of Scaling Methods: Studies at NASA	28
4.1. NASA Glenn Icing Research Tunnel	28
4.2. Tunnel Effects	29
4.3. Tunnel Comparisons	30
4.4. Repeatability	32
4.5. IRT Scaling Models	34
4.6. IRT Scaling Test Procedures	34
5. Description and Evaluation of Scaling Methods	35
5.1. Basic Approach to Scaling Method Development	35
5.2. Methods to Scale Test Conditions	36
5.2.1. LWC	37
5.2.1.1. $LWC \times \text{Time} = \text{Constant}$	37
5.2.1.2. Olsen Method	37
5.2.2. Temperature	38
5.2.3. Drop Size	38
5.2.4. Airspeed	39

5.2.5. Pressure (Altitude)	39
5.2.6 Summary of Methods to Scale Test Parameters	40
5.3. Methods to Scale Model Size	40
5.3.1. Ingelman-Sundberg	40
5.3.2. ONERA	41
5.3.3. Ruff (AEDC)	42
5.3.4. Methods to Choose Scale Velocity	43
5.3.5. Size Scaling for Intercycle Ice Studies	47
5.3.6. Acceptable Parameter Variations	48
5.3.7. Recommended Method to Scale Size	48
5.3.8. Practical Limitations to Size Scaling	50
6. Recommended Future Studies in Scaling	51
Appendix A: Resources for Scaling Calculations	53
A.1. Properties of Air, Water and Ice and General Relationships	53
A.2. Similarity Parameters and Other Terms	56
Appendix B: Sample Scaling Calculations	59
B.1. Sample Calculations for Size Scaling (Ruff Method with Constant WeL)	59
B.2. Sample Calculations for LWC Scaling (Olsen Method)	61
B.3. Procedures for Scaling Drop Size and Temperature	65
Appendix C: References	71

Manual of Scaling Methods

David N. Anderson
Ohio Aerospace Institute
Brook Park, Ohio 44142

Abstract

This manual reviews the derivation of the similitude relationships believed to be important to ice accretion and examines ice-accretion data to evaluate their importance. Both size scaling and test-condition scaling methods employing the resulting similarity parameters are described, and experimental icing tests performed to evaluate scaling methods are reviewed with results. The material included applies primarily to unprotected, unswept geometries, but some discussion of how to approach other situations is included as well. The studies given here and scaling methods considered are applicable only to Appendix-C icing conditions. Nearly all of the experimental results presented have been obtained in sea-level tunnels. Recommendations are given regarding which scaling methods to use for both size scaling and test-condition scaling, and icing test results are described to support those recommendations. Facility limitations and size-scaling restrictions are discussed. Finally, appendices summarize the air, water and ice properties used in NASA scaling studies, give expressions for each of the similarity parameters used and provide sample calculations for the size-scaling and test-condition scaling methods advocated.

1. Nomenclature

a_i constants in curve fit for water vapor pressure over ice, where i ranges from 0 to 6
 A empirical constant in expression for Nu , dimensionless
 A_c accumulation parameter, dimensionless
 AOA angle of attack, °
 b relative heat factor, dimensionless
 b_i constants in curve fit for water vapor pressure over water, where i ranges from 0 to 6
 B empirical power dependency of Nu on Re , dimensionless
 c airfoil chord, in
 $c_{p,a}$ constant-pressure specific heat of air, Btu/lbm R
 $c_{p,ws}$ specific heat of water on model surface, Btu/lbm R
 $c_{p,is}$ specific heat of ice on model surface, Btu/lbm R
 $c_{v,a}$ constant-volume specific heat of air, Btu/lbm R
 Ca capillary number, dimensionless
 C_D drag coefficient of drop, dimensionless
 C_f skin-friction coefficient, dimensionless

d cylinder diameter or twice the airfoil leading-edge radius, in
 D_v diffusivity of water vapor in air, ft²/s
 $e1, e2, e3$ powers in supplemental similarity parameter, P , equation (3.65), dimensionless
 E exponent in latent heat of evaporation expression, dimensionless
 h_c convective heat transfer coefficient, Btu/hr ft² R
 h_{film} water-film thickness, in
 h_G gas-phase mass transfer coefficient, lbm/hr ft²
 k thermal conductivity, Btu/hr ft R
 k_l constant in equation (3.15) – (3.17)
 K inertia parameter (eq. (3.5)), dimensionless
 \bar{K} Bragg's trajectory scaling parameter, dimensionless
 K_0 modified inertia parameter, dimensionless
 ℓ span-wise length of control volume, in
 L undefined length proportional to model diameter or chord, in
 LWC liquid water content of cloud, lbm/ft³
 m mass flux of water per unit time, lbm/ft² s
 m_e mass flux of water evaporated, lbm/ft² s
 m_s mass flux of ice sublimated, lbm/ft² s
 M Mach number, dimensionless
 n freezing fraction, dimensionless
 n_0 freezing fraction at stagnation, dimensionless
 n_a analytical value of freezing fraction, dimensionless
 n_e freezing fraction found from leading-edge thickness of experimental ice shapes, dimensionless
 Nu Nusselt number based on cylinder diameter or twice the airfoil leading-edge radius, dimensionless
 Nu_c Nusselt number based on airfoil chord, dimensionless
 p pressure, psi
 p_{wi} vapor pressure of water over ice, psia
 p_{ww} vapor pressure of water over liquid water, psia
 p_w vapor pressure of water in the atmosphere, psia
 P supplemental similarity parameter, equation (3.65), dimensionless
 Pr Prandtl number of air, dimensionless
 q_c surface heat loss due to convection, Btu/hr ft²
 q_{cond} surface heat loss due to conduction, Btu/hr ft²
 q_e surface heat loss from evaporation, Btu/hr ft²
 q_f surface heat gain from release of latent heat of fusion, Btu/hr ft²

q_i	surface heat gain from ice cooling to surface temperature, Btu/hr ft ²	x	horizontal coordinate, in
q_k	surface heat gain from kinetic energy of water drops, Btu/hr ft ²	X	drop position vector, dimensionless
q_r	surface heat loss from radiation, Btu/hr ft ²	y	vertical coordinate, in
q_{rb}	surface heat loss due to water run-back, Btu/hr ft ²	β	catch efficiency, dimensionless
q_s	surface heat loss from sublimation, Btu/hr ft ²	β_0	catch efficiency at stagnation, dimensionless
q_w	surface heat loss to raise temperature of impinging water to freezing, Btu/hr ft ²	γ	ratio of specific heats for air, 1.4
r	recovery factor, dimensionless	δ	drop median volume diameter (MVD), μm
r_{le}	leading-edge radius, in	Δ	ice thickness, in
r_A	evaporative-to-convective heat transfer term, dimensionless	ΔC_p	change in pressure coefficient on airfoil, dimensionless
R_a	gas constant for air, lbf ft/lbm R	ε	emissivity of surface, dimensionless
Re	Reynolds number based on cylinder diameter or twice the airfoil leading-edge radius, dimensionless	θ	air energy transfer parameter, R
Re_c	Reynolds number based on airfoil chord and free-stream temperature, dimensionless	Θ	dimensionless time
Re_{film}	Reynolds number based on airfoil chord and film temperature, dimensionless	κ	exponent on Reynolds number for ($C_D Re/24$) dependency (eq. 3.15), dimensionless
Re_{rel}	Reynolds number of drop relative to airstream, dimensionless	λ	drop range in absence of gravity, ft
Re_δ	Reynolds number of drop, dimensionless	λ/λ_{Stokes}	drop range parameter, dimensionless
s	surface distance from stagnation, in	λ_{Stokes}	drop range in absence of gravity if Stokes' law applies, ft
Sc	Schmidt number of air, dimensionless	A_f	latent heat of freezing, Btu/lbm
t	temperature, °F	A_s	latent heat of sublimation, Btu/lbm
t_{bl}	temperature of air in boundary layer, °F	A_v	latent heat of vaporization, Btu/lbm
t_{film}	film temperature, °F	μ	viscosity, lbm/ft s
T	absolute temperature, R	ρ	density, lbm/ft ³
u	air velocity vector, dimensionless	σ	Stefan-Boltzmann constant, $.1714 \times 10^{-8}$ Btu/hr ft ² R ⁴
U_a	local air velocity, mph	σ_{wa}	Surface tension of water against air, lbf/ft
U_δ	local drop velocity, mph	τ	icing time, min
U_w	water-film velocity, mph	ϕ	drop energy transfer parameter, R
V	free-stream velocity (air speed), mph	ξ	chord-wise dimension of control volume, in
We_c	Weber number based on model length dimension, dimensionless	General Subscripts:	
We_δ	Weber number based on water drop diameter, dimensionless	0	stagnation value
We_h	Weber number based on water-film thickness, dimensionless	a	air
We_k	Weber number based on water-film thickness and water-film edge velocity, using Feo correlations, dimensionless	c	based on airfoil chord
We_L	Weber number based on length L , dimensionless	f	at the freezing point of water
We_t	Weber number based on water-film thickness, using Kind analysis, dimensionless	i	ice
We_w	Weber number based on water-film thickness and water-film edge velocity, using Feo analysis, dimensionless	R	reference conditions
We_{wK}	Weber number based on water-film thickness, using alternate Kind analysis, dimensionless	s	at the surface
		S	scale conditions
		st	static
		tot	total
		w	water

2. Introduction

Icing poses a hazard both to aircraft on the ground preparing for flight and after take off. Ice can accumulate on upper surfaces of aircraft on the ground due to the freezing of precipitation. The ice layer is sometimes invisible but always introduces additional risks at take-off, because it typically increases drag and decreases lift. This type of icing is protected against by spraying de-icing fluids, which depress the freezing temperature, on the upper surfaces of wings and tail planes prior to take off. The scaling discussed in this manual applies only to in-flight icing encounters, and ground icing will not be discussed further.

In-flight icing results when aircraft fly through supercooled clouds. Supercooling is the state in which water exists as a liquid at a temperature less than 32°F. Suspended water drops in clouds are frequently supercooled when ambient temperatures are below freezing. Supercooled water freezes when it impacts surfaces, and the resulting ice accretions can have a dangerous effect on aircraft. Aircraft flying through supercooled clouds are susceptible to ice formations on the leading edges of engine inlets, tail planes, wings or rotors and instrumentation probes. Engine inlet icing can distort the airflow, and when shed ice is ingested compressor blades can be damaged and combustors may experience flame-out. On aerodynamic surfaces icing generally decreases lift and increases drag. Iced probes produce false instrument readings leading to possible pilot confusion and sometimes fatal mistakes. Large transport aircraft are protected against ice by bleeding hot air from the engine compressor to maintain critical surfaces warm enough to vaporize water. Some surfaces may not need to be protected, and smaller aircraft often use intermittent impulse methods to remove small amounts of ice repeatedly.

Aircraft and component manufacturers must thoroughly test new products to determine the effect of icing on their performance. This testing is performed both during the design process and for certification purposes. Flight-testing is necessary but is expensive and can only be done when atmospheric icing conditions exist. Furthermore, it can be very time consuming to find in nature the extremes in the cloud drop size and liquid-water content envelope required for certification testing. Icing wind tunnels can simulate natural icing with water-spray and refrigeration systems and provide control of cloud conditions, temperature and airspeed to permit safe, convenient and relatively inexpensive testing. Some measurement of lift and drag changes can be made in the icing tunnel, and ice shapes are usually recorded. Knowing the ice shape which results from testing at given simulated flight and cloud conditions, researchers can obtain

more precise aerodynamic-penalty information either in flight or in an aerodynamic wind tunnel. This can be done by attaching a reproduction of the ice shape fabricated from suitable materials (e.g., wood, plastic) to the leading edge of the airfoil.

A scaling method is a procedure to determine the scaled test conditions to produce the same result as exposing the reference model to the desired cloud conditions. Because of test-section blockage limitations, many components cannot be tested full size in an icing wind tunnel. Furthermore, facilities that simulate natural icing can provide only limited ranges of air speed, cloud drop size, and liquid-water content. When the reference (full-size) model is too large for a given facility, model-size scaling is applied, and when the desired test conditions are outside the facility operating capability, test-condition scaling is required.

The objectives of such scaling are usually to insure that the amount of ice relative to the model size, the shape of the ice accreted, dimensionless ice accretion limits, and the aerodynamic penalties due to the ice are the same as would have been obtained with the desired, or reference, model size or test conditions. It has always been assumed that for adequate scaling, characteristic features, such as glaze horns, need to be simulated in size, location, angle and shape, but how closely these characteristics need to match between scale and reference accretions has never been shown. For testing of ice-protection systems, the main objectives may be to match scale and reference non-dimensional impingement limits or water loading. In any case, it is important to establish reliable methods to scale model size or test conditions. In this manual, the emphasis will be on ice-accretion scaling rather than scaling for ice-protection systems.

Accurate scaling requires that similitude of geometry, flowfield, drop trajectory, drop catch and heat transfer are satisfied. The similitude analyses result in equations that can be solved for the scale icing conditions that will simulate the reference icing encounter. However, these relationships may sometimes lead to conflicting values for one or more of the test conditions; thus, the similitude equations cannot always be rigorously applied, and simplifications are usually necessary to permit their use in practical scaling situations. To address this problem a number of scaling methods have been derived from the basic set of similitude equations with different simplifications and assumptions. These methods provide guidance for the researcher in establishing proper scaling conditions.

For the testing of airfoils, when the desired model size cannot be accommodated in a test facility, an alternative approach to attempting to apply simplifications to the

similitude equations is to use a hybrid scaling method^{1,2,3}. In this approach, a full-size leading-edge portion of a wing section is attached to a flapped section of reduced size. The flap is adjusted such that the flowfield around the leading-edge region of the scale model is the same as that of the full-size airfoil. In reference 1, this flowfield match was accomplished by trial and error. References 2 and 3 presented a method in which the design of the test article behind the full-size leading edge was determined using computer flowfield analysis tools. In the hybrid method, scale test temperature, airspeed, liquid-water content, median volume drop diameter and icing time are the desired full-size values. However, multiple models need to be fabricated for different flow conditions and angles of attack. The hybrid method will not be addressed in this manual.

Efforts to establish icing scaling methods in which either the entire model is scaled in size or test conditions are scaled began in the 1950's and continue to the present. In general, to test scaling methods, an ice shape is recorded for a reference condition that represents the full-size or desired test, the scaling equations are applied to find the appropriate scaled conditions from the reference values, and the scaled ice shape is recorded. The two ice shapes are then compared. If size has been scaled, the comparison can be facilitated if the ice-shape coordinates are normalized with respect to some characteristic dimension of the model; for example, the chord of an airfoil. Whether the two shapes agree is frequently dependent on subjective judgment, and the quality of agreement when the match isn't perfect has always been difficult to define.

In this manual, the similitude relationships are reviewed, a number of scaling methods are described and compared, and experimental icing tests performed to evaluate scaling methods are reviewed with results. The primary emphasis in the studies discussed has been on insuring that scale and reference ice accretions have the same non-dimensional quantity and shape. The analyses and test results reported are for unprotected, unswept geometries, but some discussion of a preliminary study of inter-cycle-ice scaling is included as well. The icing conditions for which the tests and analyses of this manual were made fall entirely within the FAA Part 25 Appendix-C envelope,⁴ which includes drop sizes from 15 to 50 μm median volume diameter (MVD). Supercooled large drop conditions (SLD), for which drop sizes are larger than 50 μm MVD will not be discussed because studies of the physics required to understand phenomena related to SLD icing are just beginning. For some SLD situations (low airspeed and drop sizes not far above the Appendix-C envelope) the scaling methods described will be adequate. In general, however, the scaling described

here should be considered valid only for Appendix-C conditions. Although some of the scaling methods discussed deal with altitude scaling, nearly all of the experimental results presented have been obtained in sea-level tunnels. Recommendations are given regarding which scaling methods might be most effective for both size scaling and test-condition scaling. Restrictions on scale size ratio are discussed with respect to practical considerations, including facility limitations. Finally, recommendations for additional study are outlined.

3. Similitude Analysis

To achieve similarity in ice accretion, it is necessary for the scale test to simulate the geometry, the flowfield, the drop trajectories, the total water catch, the heat transfer and, probably, the surface phenomena of the desired icing encounter. The similitude analyses performed for scaling studies through the 1970's was made with the objective of deriving a series of closed-form equations that could be solved for the scale test conditions. Fewer simplifications need to be made if equations can be programmed for computer solution, and most of the results to be given here used the latter approach.

3.1. Geometric Similarity

The alternative to the hybrid scaling mentioned in the Introduction is to make the reference and scaled models geometrically similar over the entire model. In this manual, the discussion will assume geometric scaling. As ice grows on the model, the shape must continue to be similar for flowfield similarity to be maintained. This basic requisite will be assumed satisfied in subsequent derivations from other similitude requirements.

3.2. Flowfield Similarity

Similarity of the flowfield would suggest that the Reynolds and Mach numbers for the scaled test need to be matched to their respective full-size, or reference, values. The usual definitions for these parameters will be used:

$$Re_a = \frac{V d \rho_a}{\mu_a} \quad (3.1)$$

$$M_a = \frac{V}{\sqrt{\gamma R_a T_{st}}} \quad (3.2)$$

In equation (3.1) the length scale d represents either the diameter if the model is a cylinder or twice the leading-edge radius if the model is an airfoil. For many analyses, the chord of the airfoil has been chosen as the characteristic length; however, the main ice accretion occurs in the region near the leading edge. Therefore, in studying scaling similarity it seems reasonable to define similarity

parameters in terms of a length scale representative of the leading-edge region. The convention of using d to represent either cylinder diameter or twice the airfoil leading-edge radius will be used in the definition of all similarity parameters in this manual.

Icing occurs in the atmosphere only within the limited range of absolute temperature, T , of 420 to 492°R (233 to 273 K). Thus, because γ and R_a are constant properties of air, equating the Mach number for the scaled and reference cases requires that the velocities for the two cases be very nearly the same. However, to match the Reynolds numbers when the scale model is, for example, half the reference size, it is necessary for the scale velocity to be approximately double the reference. Clearly, then, Mach and Reynolds numbers cannot be simultaneously matched when the scale model is other than full size.

Most scaling analyses avoid this dilemma simply by disregarding both of these parameters. The rationale for this approach is that, for most icing conditions, the Mach number is relatively low and compressibility effects can be neglected. The Reynolds number has been ignored by arguing that ice accretions occur mostly at the leading edge of surfaces where the boundary layer is initially thin, and viscous effects are small. Farther downstream, as ice accretes it often causes the boundary layer to transition to turbulent flow, whose characteristics are nearly independent of Reynolds number. However, when the effects of surface-water phenomena are considered (see section 3.6), the Reynolds number may need to be included in the analysis.

In addition to Mach and Reynolds number considerations, simulation of the flowfield requires that the velocity, pressure and temperature distributions over the scale model must simulate those of the reference case. However, scaling methods proposed to date do not explicitly attempt to satisfy these requirements. In spite of this, some success with scaling methods has been achieved, probably because significant ice accretions are limited to the leading-edge region.

3.3. Drop Trajectory Similarity

The mass of water reaching each part of the surface of each model must be similar. The drop trajectory determines if an individual drop will impinge on the surface of the model and, if so, where on the body. Thus, similarity of drop trajectory between scale and reference cases must be satisfied. An analysis of the drop trajectories will be made in this section, and expressions will be derived which relate the scaled and reference values of some of the operating and test parameters of importance. The quantity of water reaching the surface will be discussed in section 3.4.

Several simplifications are required to derive workable equations. It is assumed that the trajectories in both the scaled and the reference clouds can be adequately represented by that of one typical drop diameter for each. Bragg, et al⁵ showed that for the typical distributions of drop size and relative velocity of Appendix-C icing experiments, the drop motion in the flowfield and eventual impingement on a surface can be accurately represented by using the drop MVD. Note that this simplification may not be valid for SLD drop sizes, for which the drop distribution may have an effect on the accreted ice shape. The small size of cloud water drops involved in Appendix-C icing minimizes the effect of gravity relative to other forces; therefore, gravity will be neglected. The non-dimensional drop momentum equation describing the motion of a single drop relative to the airstream is then given by (see, for example, Bragg⁶ and Ruff⁷)

$$\frac{d^2 X}{d\Theta^2} = \frac{C_D Re_{rel}}{24K} \left(u - \frac{dX}{d\Theta} \right) \quad (3.3)$$

where the relative drop Reynolds number, Re_{rel} , is based on the local relative velocity between the air and drop:

$$Re_{rel} = \frac{\delta \rho_a \left| u - \frac{dX}{d\Theta} \right|}{\mu_a} \quad (3.4)$$

In equation (3.3), K is the non-dimensional inertia parameter defined by Langmuir and Blodgett⁸ as

$$K = \frac{\rho_w \delta^2 V}{18 d \mu_a} \quad (3.5)$$

In Langmuir and Blodgett's paper the cylinder radius was used in place of the dimension d . Thus, for cylinders, the radius should be used in equation (3.5). Bragg⁶ and Ruff⁷ used a length c which they defined as a characteristic dimension. Airfoil chord is commonly used in evaluating the inertia parameter for aircraft icing applications. For scaling, however, the use of chord means that for a general trajectory analysis the same inertia parameter could result for airfoils of the same chord but different forms, whether thick or thin. By setting d to twice the leading-edge radius, this problem is avoided. Maximum airfoil thickness might also be considered for the characteristic length, but the use of twice the leading-edge radius leads to collection efficiencies consistent with those from the LEWICE ice-accretion code,⁹ as will be shown below.

Because equation (3.3) is non-dimensional, if the reference and scale flows approaching the models are similar, the trajectories are the same for both reference and scaled cases if

$$\left. \frac{C_D Re_{rel}}{24} \right)_S = \left. \frac{C_D Re_{rel}}{24} \right)_R \quad (3.6)$$

and

$$K_S = K_R \quad (3.7)$$

$C_D Re_{rel}/24$ is the ratio of the actual drag on a sphere, C_D , to the Stokes-law drag, $24/Re_{rel}$. It is a function only of Reynolds number. Thus, if the Reynolds number and inertia parameter, K , for the scaled case were matched to the values for the reference case, drop trajectory similarity would be satisfied. Unfortunately, in practical situations it is not always possible to satisfy both parameters simultaneously. The modified inertia parameter, K_0 , introduced by Langmuir and Blodgett⁸, offers a solution to this problem. It combines the effects of the inertia parameter and the Reynolds Number and thereby provides a single similarity parameter to satisfy. The Langmuir and Blodgett analysis will be presented next, then in section 3.3.2 a simplified form will be given.

3.3.1. Langmuir and Blodgett Trajectory Analysis

Langmuir and Blodgett's expression for modified inertia parameter is

$$K_0 = \frac{1}{8} + \frac{\lambda}{\lambda_{Stokes}} \left(K - \frac{1}{8} \right), \text{ for } K > \frac{1}{8} \quad (3.8)$$

In equation (3.8) λ_{Stokes} is the range of the drop if it were released in still air at an initial velocity of V with the drag given by Stokes' law, and λ is its range with the actual drag. The dimensionless range parameter, λ/λ_{Stokes} was defined by Langmuir and Blodgett as the average drag ratio over the Reynolds number range, 0 to Re_δ , experienced during the drop trajectory

$$\frac{\lambda}{\lambda_{Stokes}} = \frac{1}{Re_\delta} \int_0^{Re_\delta} \frac{d Re_{rel}}{C_D Re_{rel} / 24} \quad (3.9)$$

The drop Reynolds number, Re_δ , is given by:

$$Re_\delta = \frac{V \delta \rho_a}{\mu_a} \quad (3.10)$$

It can be seen that the range parameter is a function only of drop Reynolds number.

By using the parameter K_0 , equations (3.6) and (3.7) can be combined and replaced by equation (3.11):

$$K_{0,S} = K_{0,R} \quad (3.11)$$

Langmuir and Blodgett noted that for $K \leq 1/8$ drop impingement would not occur. This fact is reflected in

equation (3.8), which is only valid if K is greater than $1/8$. Figure 3.3.1 shows plots of inertia parameter as a function of V/d for drops of 4 – 10 μm . The $K = 1/8$ limit is noted on the figure. Several runs of the LEWICE ice-accretion code⁹ were made with drops of 4, 5, 6 and 7 μm . Although the code's drop trajectory routine has not been validated for drops smaller than 10 μm , its results were reasonably consistent with the Langmuir and Blodgett impingement lower bound. At a V/d of 7.7 (m/s)/cm LEWICE predicts no accretion for 5- μm drops, accretion only at the leading edge ($\beta_0 = 1.4\%$) for 6- μm drops, and accretion with a leading-edge collection efficiency of 2.7% for 7- μm drops. The Langmuir and Blodgett limit would suggest no accretion would occur below a drop size of 7 μm . At a V/d of 19.3 (m/s)/cm LEWICE predicts no accretion for 4- μm drops, but accretion with a leading-edge collection efficiency of 2.7% for 5- μm drops. The Langmuir and Blodgett limit also indicates no accretion with a 4- μm drop, but that accretion should occur with a 5- μm drop.

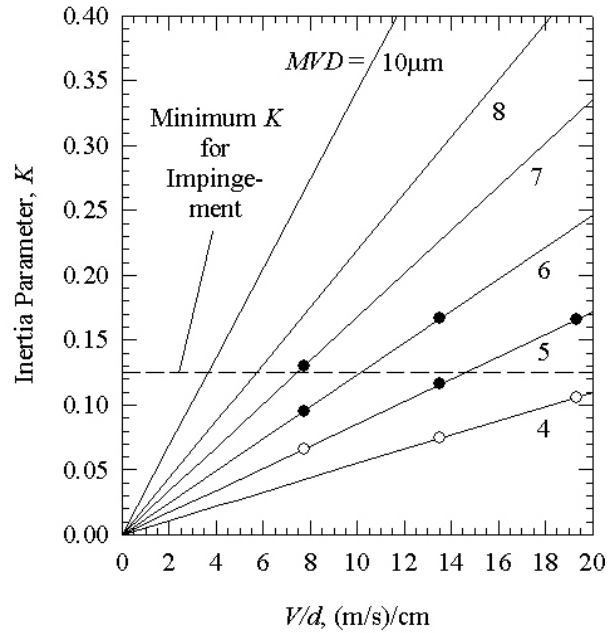


Figure 3.3.1.—Drop Impingement for Small Values of Inertia Parameter. For $K \leq 1/8$ drops will not impinge on the model. Solid symbols are the result of LEWICE 2.0⁹ calculations showing some impingement. Open symbols are the result of LEWICE 2.0 calculations for which no impingement occurred. All LEWICE calculations were for a 1.83-m chord NACA 0012 airfoil ($d = 5.78$ cm).

The range parameter, λ/λ_{Stokes} , in equation (3.8) was tabulated by Langmuir and Blodgett as a function of the drop Reynolds number, Re_δ . A fit to the Langmuir and Blodgett tabulation is

$$\frac{\lambda}{\lambda_{Stokes}} = \left(\frac{0.8388 + 0.001483Re_\delta}{+0.1847\sqrt{Re_\delta}} \right)^{-1} \quad (3.12)$$

Equation (3.12) gives range parameters within $\pm 0.2\%$ of Langmuir and Blodgett's values for $14 \leq Re_\delta \leq 600$. The error increases to 0.4% for a Re_δ of 800. For a static temperature of 0°F , Re_δ for icing encounters range from 18 to 760, for airspeeds from 100 to 400 mph, drop median-volume diameters from 10 to $50 \mu\text{m}$ and air pressures of 6.8 to 14.7 psia (corresponding to altitudes from 20,000 ft to sea level, respectively).

The local catch efficiency, or collection efficiency, of the model is defined by considering the projection of a stream tube from the undisturbed flow upstream of the model onto the model surface at the location of interest. The stream tube contains water drops with the distribution of sizes and the liquid water content of interest. The fraction of the original water content that actually impacts the model is the local catch efficiency. The smaller drops in the distribution will tend to follow the air streamlines around the model, while the larger drops will turn less easily, and are more likely to strike the surface. The catch efficiency, β , varies over the model surface with a value β_0 at the stagnation line. Langmuir and Blodgett⁸ published tables of the stagnation-point catch efficiency as a function of the inertia parameters, K and K_0 for cylinders. They showed that fairly accurate values of β_0 could be calculated from equation (3.13) if the inertia parameter, K , is less than or equal to 7.5:

$$\beta_0 = \frac{1.40 \left(K_0 - \frac{1}{8} \right)^{.84}}{1 + 1.40 \left(K_0 - \frac{1}{8} \right)^{.84}} \quad (3.13)$$

where K_0 is the modified inertia parameter from equation (3.8). A sample set of conditions which would produce a value of $K = 7.5$ at 0°C is $d = 1.0$ in (2.5 cm), $V = 330$ mph (147.5 m/s) and $\delta = 20 \mu\text{m}$. For an NACA 0012 airfoil, $d = 1$ in corresponds with a chord of 31.6 in (80.3 cm). Larger model sizes, lower velocities or smaller drops would result in smaller values of K . We will see in the next paragraph, however, that equation (3.13) gives values of β_0 that are consistent with LEWICE calculations over a wide range of conditions.

Figure 3.3.2 compares the collection efficiency calculated from equation (3.13) with values found from the LEWICE ice accretion code. The LEWICE code deter-

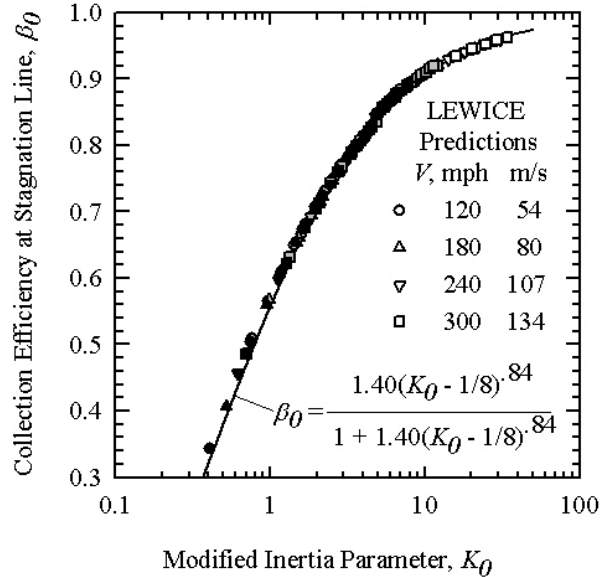


Figure 3.3.2.—Stagnation Collection Efficiency for NACA 0012 Airfoils at 0° Angle of Attack. Static Temperature, 10°F ; Static Pressure, 14 psia; Airspeed, 120 to 300 mph; Water Drop Median Volume Diameter, 10 to $50 \mu\text{m}$; Liquid-Water Content, 1 g/m^3 . Open Symbols, 7-in Chord; Shaded Symbols, 21-in Chord; Solid Symbols, 31.5-in Chord. Data Represented by Symbols are from LEWICE⁹ Predictions.

mines the local catch efficiency by integrating the equations of motion of the drops assuming they are rigid spheres acted upon by drag and gravity forces. This process gives the trajectories, thus determining the drop impingement locations on the model surface. By comparing the release locations of several adjacent drops in the undisturbed flow upstream with the trajectory intersections on the model surface, the local collection efficiency can be determined. The code was run with NACA 0012 models with chords of 7.0 – 31.5 in (17.8 – 80.0 cm), velocities from 120 – 300 mph (53.6 – 134.1 m/s) and mono-dispersed drop sizes of 10 – $50 \mu\text{m}$. Figure 3.3.2 shows that equation (3.13) gives leading-edge collection efficiencies that closely match those found by the more detailed procedure of the LEWICE code. The equation (3.13) value for β_0 ranged from 4.7% lower than the LEWICE value at $K_0 = 0.4$ to 0.23% higher at $K_0 = 34$. The conditions considered in figure 3.3.2 provide a range of inertia parameter, K , of 0.72 to 202, suggesting that Langmuir and Blodgett's upper limit of $K = 7.5$ for equation (3.13) is very conservative.

Figure 3.3.3 compares LEWICE determinations of leading-edge collection efficiency at angles of attack of 0 and 10° with those from equation (3.13). For the NACA 0012 airfoil used for these computations β_0 varies little from 0 to 10° AOA. If the scale model is mounted at the

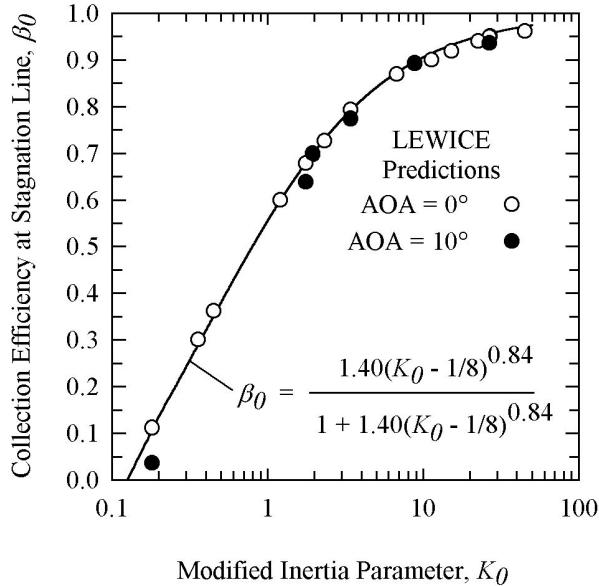


Figure 3.3.3.—LEWICE⁹ Predictions of Effect of Angle of Attack on Collection Efficiency for NACA 0012 Airfoils of Various Chord. Static Temperature, -30 to 25°F ; Static Pressure, 14 psia; Airspeed, 100 and 400 mph; Water Drop Median Volume Diameter, 10 to $100\ \mu\text{m}$; Liquid-Water Content, $1\ \text{g}/\text{m}^3$. Open Symbols, AOA, 0° ; Solid Symbols, AOA, 10° .

identical AOA as the reference, matching of K_{θ} will still produce the correct drop trajectories for the scale test although there may be a small error in β_{θ} if equation (3.13) is used.

Langmuir and Blodgett also gave a β_{θ} expression for cylinders for $K > 7.5$. However, because equation (3.13) has been validated in figure 3.3.2, there is no reason to use any other expression for wing icing situations.

Equation (3.13) shows that to match β_{θ} between scale and reference values, it is only necessary to match K_{θ} . Because K_{θ} is easy to calculate, it has been universally adopted in scaling methods as the similarity parameter to use to insure similarity of drop trajectories.

The initial capture efficiency is assumed to be that at the stagnation line of a clean surface. It can be argued for scaling, however, that aft of the stagnation line, because scale and reference models are geometrically similar, the collection efficiencies must vary in the same way for both models. This agreement of scale and reference collection efficiencies is shown in figure 3.3.4, which gives LEWICE predictions for two NACA 0012 airfoils of different sizes. The conditions for the smaller model were scaled from those of the larger such that the stagnation K_{θ} (and therefore β_{θ}) for the two matched. The two curves are indistinguishable over the range for which

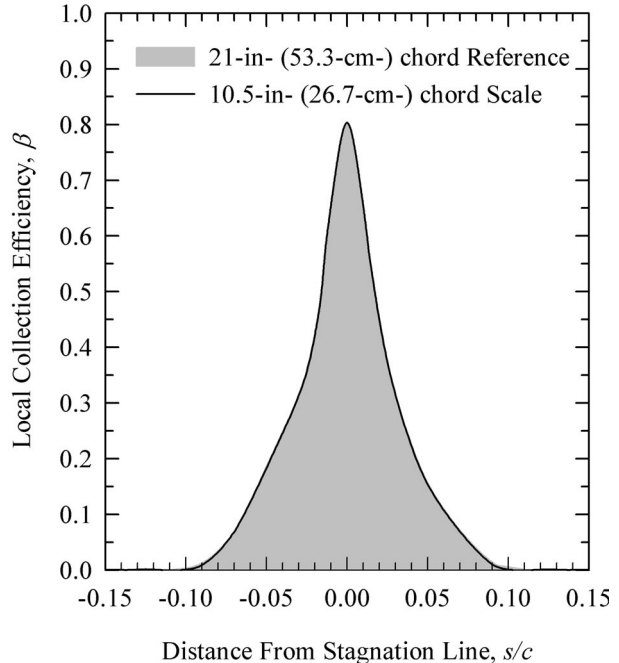


Figure 3.3.4.—LEWICE-Predicted Reference and Scale Collection Efficiencies. NACA 0012 Airfoils at 0° AOA. Reference Conditions: c_R , 21 in (53.3 cm); V_R , 150.0 mph (67 m/s); δ_R , $30.0\ \mu\text{m}$. Scale Conditions: c_S , 10.5 in (26.7 cm); V_S , 262.5 mph (117 m/s); δ_S , $15.6\ \mu\text{m}$.

accretion occurs. Therefore, to help identify the curve for the reference case the area under that plot has been shaded. Other reference conditions and their resultant scale conditions have also been tested with LEWICE. The scale and reference beta curves matched consistently. Consequently, it is only necessary to match the stagnation K_{θ} to properly scale drop trajectories over the entire clean airfoil. It is assumed that as ice accretes, because the geometry changes in the same way for both models, the time-varying collection efficiency will continue to match everywhere.

Derivation of the equations for trajectory similitude assumed that a single drop diameter, the median volume diameter, adequately represents the cloud and its trajectory. At any instant during icing, the size of a drop impacting a particular location on the model surface cannot be predicted. Thus, in glaze ice conditions in particular, features of the ice shape tend to be subject to a certain randomness, with the history of drop impact at each surface location having some small effect on the final accretion there. The resulting surface variations mean that icing encounters repeated with the same model and identical test conditions cannot be expected to produce identical ice shapes.

Noticeable macroscopic-scale differences in ice shapes produced with repeated test conditions are usually minor,

however. Although Olsen and Walker¹⁰ reported a strong effect of intermediate ice shape on final shape, others have not observed as much influence. Anderson and Shin¹¹ found that 10-min glaze ice shapes were not affected by initial 1/2-min ice accretions at different test conditions. In these tests, the final conditions determined the shape. Hansman and Turnock¹² found that ice shapes were independent of the initial surface material. Apparently, for glaze ice, initial roughness features, whether inherent in the uniced surface or produced by a short-time ice accretion, are masked by subsequent ice deposits and eventually have little or no noticeable effect on the final shape. This is fortunate, since there is no easy way to include the random effect of drop size in the scaling equations. The cloud drop distribution and individual drop impingement have been found to be adequately represented by the median volume diameter, MVD. Furthermore, characterization of the initial uniced surface is not necessary when dealing with substantial ice accretions.

3.3.2. Simplified Trajectory Analysis

For making quick calculations or estimates, a closed-form expression for scale drop size can be developed by applying two simplifications to Langmuir and Blodgett's analysis. The first is to define the modified inertia parameter as:

$$K_0 = K \frac{\lambda}{\lambda_{Stokes}} \quad (3.14)$$

The second simplification is to develop an approximate expression for $C_D Re_{rel}/24$ that can be easily integrated. Figure 3.3.5 is a plot of $C_D Re_{rel}/24$ as a function of Re_{rel} . Although in general the data cannot be fit by a simple power law, over limited ranges of relative Reynolds number the relationship

$$\frac{C_D Re_{rel}}{24} = k_1 Re_{rel}^\kappa \quad (3.15)$$

can be used to represent the data. k_1 and κ are constants. Figure 3.3.5 shows that the $\kappa = 0.38$ power approximately describes the $C_D Re_{rel}/24$ -vs- Re_{rel} data over the range of relative Reynolds number from 5 to 100, and $\kappa = 0.45$ is satisfactory for the range $10 < Re_{rel} < 300$. When equation (3.15) is substituted into the expression for the range parameter, equation (3.9), and the integration performed, the range parameter becomes:

$$\frac{\lambda}{\lambda_{Stokes}} = \frac{1}{k_1 (1-\kappa)} Re_\delta^{-\kappa} \quad (3.16)$$

When the definition of Re_δ from equation (3.10) is included in equation (3.16) and equations (3.5) and (3.16)

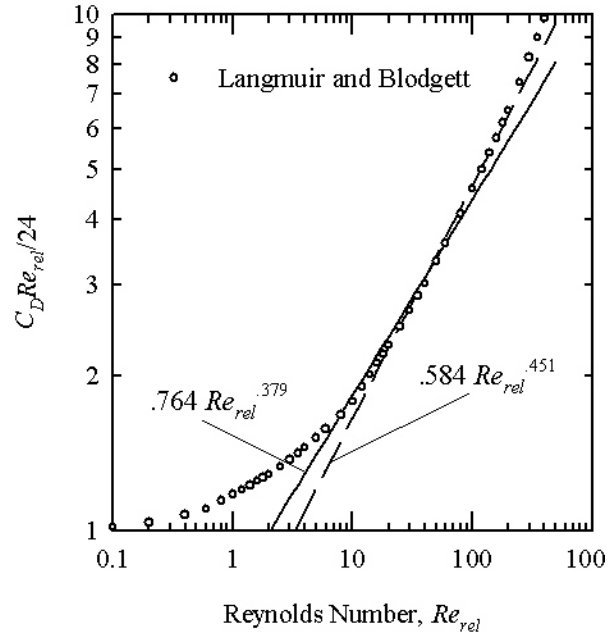


Figure 3.3.5.—Ratio of Actual Drag, C_D , to Stokes-Law Drag, $24/Re_{rel}$. Drag values from Langmuir and Blodgett.⁸

are substituted into (3.14), the modified inertia parameter in terms of the test conditions and physical properties is obtained:

$$K_0 = \left[\frac{\rho_w R_a^\kappa}{18k_1 (1-\kappa) \mu_a^{1-\kappa}} \right] \frac{\delta^{2-\kappa} V^{1-\kappa} T^\kappa}{d p^\kappa} \quad (3.17)$$

The density of water (ρ_w) and the viscosity of air vary little over the relatively narrow temperature range (-40°F to 32°F) at which icing occurs. Thus, these parameters have been included in the brackets along with the constants in equation (3.17). When the scale and reference values of K_0 are equated, the term in brackets cancels, and an expression is obtained which approximately satisfies drop trajectory similarity and from which the scale drop size can easily be determined:

$$\frac{\delta_S}{\delta_R} = \left(\frac{d_S}{d_R} \right)^{\frac{1}{2-\kappa}} \left(\frac{p_S}{p_R} \right)^{\frac{\kappa}{2-\kappa}} \left(\frac{V_S}{V_R} \right)^{\frac{\kappa-1}{2-\kappa}} \left(\frac{T_S}{T_R} \right)^{-\frac{\kappa}{2-\kappa}} \quad (3.18)$$

This expression has been widely used with different values for κ . Olsen¹³ at NASA used $\kappa = 0.38$, Charpin and coworkers^{14,15} at ONERA and Sibley and Smith¹⁶ at Lockheed used $\kappa = 0.39$ and Dodson at Boeing¹⁷ used $\kappa = 0.45$. Equation (3.18) can be used to obtain the scale drop size that gives an approximate match to scale and reference K_0 . Alternately, equation (3.11) can be solved using equations (3.8), (3.5) and (3.12). Depending on the software used, this latter approach may require an

iterative solution for which equation (3.18) can be used to provide an initial guess of scale drop size.

As a practical matter, for typical sizes and conditions for wing icing, K_0 found from equation (3.14) will differ from that using equation (3.8) by less than 5%. The scale δ 's found from equation (3.18) are almost always within 1 μm of those using equations (3.11) and the analysis of section 3.3.1.

Bragg⁶ presented some alternative approaches. The first was to replace the simplification of equation (3.15) with an integratable expression that represents the drag curve over the entire Re_{rel} range. The result was a closed-form expression for K_0 :

$$K_0 = 18K \left[Re_\delta^{-2/3} - \sqrt{6} Re_\delta^{-1} \arctan \left(\frac{Re_\delta^{1/3}}{\sqrt{6}} \right) \right] \quad (3.19)$$

Although equation (3.19) may represent greater accuracy over a wider range of Re_δ , than the method that led to equation (3.18), finding scale drop MVD by matching the scale and reference K_0 from equation (3.19) is not as convenient as using equation (3.18), and we have already seen that equation (3.18) produces results with acceptable accuracy.

Bragg also proposed an alternative scaling parameter to K_0 . It was derived by applying the drag approximation of equation (3.15) directly to the drop trajectory equation (3.3) instead of using it in the averaging process that defined the range parameter, equation (3.9). Bragg defined his trajectory scaling parameter as

$$\bar{K} = \frac{K}{Re_\delta^\kappa} \quad (3.20)$$

Because Re_{rel} (equation (3.4)) and Re_δ (equation (3.10)) differ only by the dimensionless relative velocity between the air and drop, equation (3.3) was now rewritten with the single similarity parameter of equation (3.20). Thus, to satisfy drop trajectory similarity it is only necessary to match scale and reference values of \bar{K} . Matching scale and reference values of \bar{K} from equation (3.20) also results in equation (3.18); thus, \bar{K} differs from the approximate K_0 of equation (3.17) by only a constant. Bragg also found that a value of κ of 0.35 best represented icing conditions, consistent with most of the studies cited following equation (3.18).

3.3.3. Effect of MVD on Ice Shape

It is necessary to establish the importance of each similarity parameter and test parameter. In this section we will review the effect of drop size on ice shape. In 1998 Chen¹⁸ performed icing tests to compare shapes produced with drop MVD's of 20, 36 and 55 μm . The tests

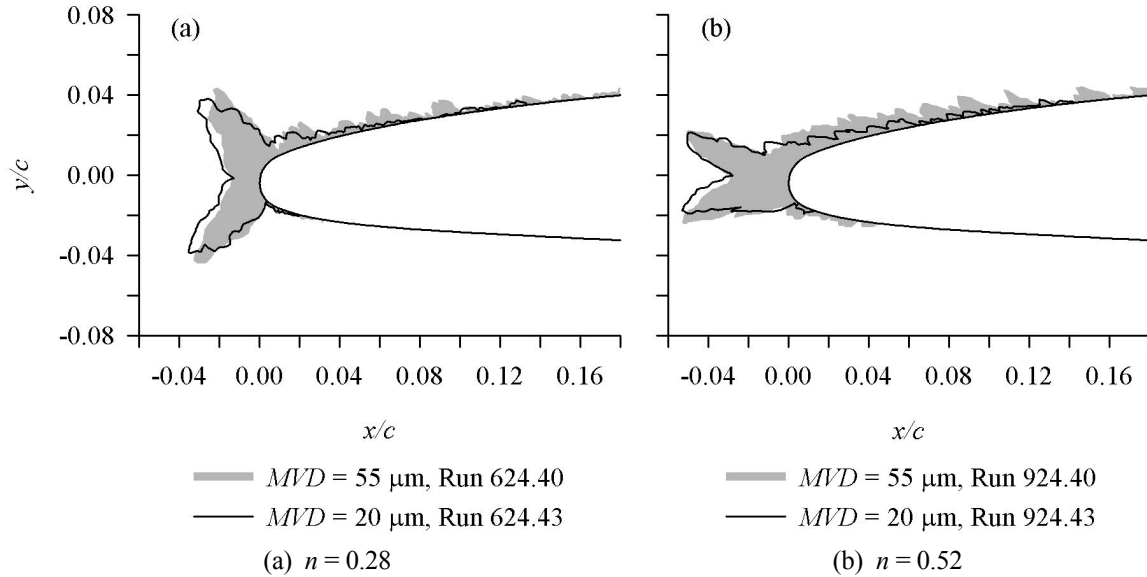
were made in the IRT using a 61-cm-chord GLC 305 airfoil model with constant t_{st} , V , and accretion time. LWC was adjusted to maintain constant n_0 of 0.3 and 0.5. With fixed velocity and model size β_0 varied with MVD. The quantity of ice collected is determined by the product $\beta_0 A_c$, and this value was maintained within about 10%. Results for drop sizes of 55 and 20 μm are given in figure 3.3.6. Although β_0 changed from about 92 to 74% for this change in δ , the reduction in drop size and collection efficiency appeared to have no effect on the main ice shape. Undoubtedly, the impingement limit would have changed with drop size (that is, with β_0), but this characteristic was not measured.

Additional ice-shape comparisons from tests using NACA 0012 airfoils at 4°AOA were reported in Anderson¹⁹ and are shown in figure 3.3.7. The ice shapes were recorded in the NASA Glenn Icing Research Tunnel in 1997 tests by Harold E. Addy and 1998 tests by Colin S. Bidwell and Judith K. Van Zante. The digitized data are available from a 2-CD set accompanying Wright.²⁰ As with the GLC 305 ice shapes of figure 3.3.6, the shapes compared in figure 3.3.7 reveal no significant effect of drop MVD on the main ice shape.

The implications of these results for scaling are significant. Within the Appendix-C envelope, the main ice shape appears to be virtually independent of drop size, and, thus, K_0 . Therefore, if calculated conditions for a scale model test involve drop sizes outside the available range for a particular test facility a different δ can be substituted providing the key parameters $\beta_0 A_c$ and n_0 are maintained at the reference values. The accumulation parameter, A_c , and freezing fraction, n , will be introduced and discussed in the next section. When scaled tests need to provide information about impingement limits, however, the scale K_0 must match the reference. If necessary, impingement limits can be found from tests with scale velocity and model size chosen such that K_0 matches the reference. The test conditions for impingement-limit tests would likely be different from those required to satisfy proper scaling for the main ice shape.

3.4. Water Catch Similarity

The quantity of ice accreted at a specified location on the model depends on (1) the amount of water in the cloud, (2) the portion of that water that reaches the given surface location (dependent on the drop trajectories as discussed in the previous section) and (3) the fraction of water having reached the surface that freezes in that location. The concept of the freezing fraction, n , is due to Messinger.²¹ For some conditions it is possible that there is no local freezing of water; in that case, $n = 0$. On the other hand, if all the water that reaches the surface of the model freezes on impact, $n = 1$. The freezing fraction is



Run	c , in	t_{st} , °F	V , mph	δ , μm	LWC , g/m ³	τ , min	β_0 , %	A_c	$\beta_0 A_c$	n_0	b	ϕ , °F	θ , °F	Re_a , 10 ⁴	We_δ , 10 ³	We_c , 10 ³	We_L , 10 ⁶
(a) 624.40	24	14	200	55	1.16	6.1	91.6	2.53	2.32	0.28	0.84	16.1	20.3	10.9	6.76	2.49	2.02
624.43	24	14	198	20	1.31	6.1	73.9	2.83	2.09	0.30	0.76	15.9	20.2	10.8	2.44	2.44	1.98
(b) 924.40	24	2	200	55	1.16	6.1	91.7	2.53	2.32	0.51	0.84	28.6	36.8	11.4	6.77	2.56	2.02
924.43	24	2	200	20	1.30	6.1	74.0	2.83	2.09	0.54	0.76	28.5	36.7	11.4	2.46	2.54	2.00

Figure 3.3.6.—Effect of Drop MVD on Ice Shape. GLC 305 Airfoil at 0°AOA. Ice-Shape Data from Tests by Chen¹⁸.

another similarity parameter and will be discussed further in the following section. The rate of growth of ice with time when $n = 1$ is given by

$$\frac{d\Delta}{d\tau} = \frac{\dot{m}}{\rho_i} \quad (3.21)$$

In equation (3.21) \dot{m} is the total mass of water striking a unit area of surface per unit time:

$$\dot{m} = LWC V \beta \quad (3.22)$$

Here LWC is the liquid-water content of the cloud and β is the local catch efficiency. Although β can be expected to vary with time as the ice shape changes, assuming both β and ρ_i are constant as ice is accreted, equation (3.21) can be integrated over the accretion time to give the ice thickness, Δ :

$$\Delta = \frac{LWC V \beta \tau}{\rho_i} \quad (3.23)$$

One goal of properly scaling the ice accretion is that the local thickness of ice normalized by the characteristic model dimension will be the same for the scaled and reference cases; thus,

$$\left. \frac{\Delta}{d} \right)_S = \left. \frac{\Delta}{d} \right)_R \quad (3.24)$$

Then,

$$\left. \frac{LWC V \beta \tau}{\rho_i d} \right)_S = \left. \frac{LWC V \beta \tau}{\rho_i d} \right)_R \quad (3.25)$$

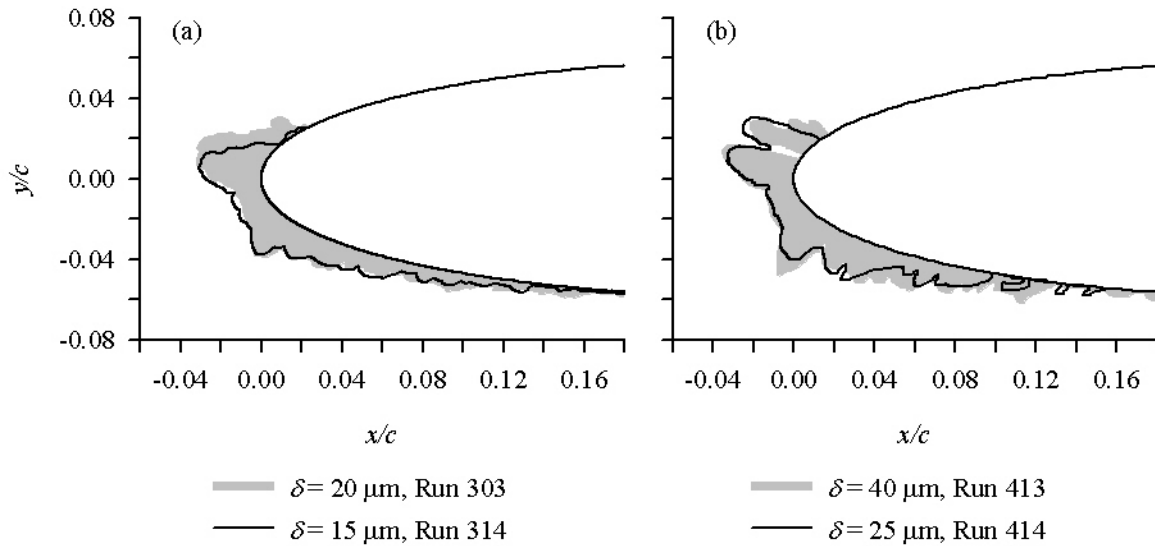
The accumulation parameter, A_c , is defined as

$$A_c = \frac{LWC V \tau}{\rho_i d} \quad (3.26)$$

From the previous section we know that to insure trajectory similarity it's necessary to match scale and reference values of Langmuir and Blodgett's modified inertia parameter, K_0 . And from equation (3.13) if the K_0 match, so do the β_0 . Figure 3.3.4 indicated that if β_0 is matched, so too are all local catch efficiencies. Therefore, equation (3.25) is the same as requiring that equation (3.11) be satisfied along with

$$A_{c,S} = A_{c,R} \quad (3.27)$$

to insure properly scaled ice thickness everywhere on the model when $n = 1$ everywhere. If it is not possible to find scaled conditions that permit a match of K_0 (and therefore β_0), it is recommended that the product of $\beta_0 A_c$ be matched. Thus,



(a) April 1997 Tests by Addy.

(b) January 1998 Tests by Bidwell and Van Zante.

Run	c , in	t_{st} , °F	V , mph	δ , μm	LWC_s , g/m ³	τ , min	β_0 , %	A_c	n_0	b	ϕ , °F	θ , °F	Re_a , 10 ⁴	We_δ , 10 ³	We_c , 10 ³	We_L , 10 ⁶
(a) 303	21	13	230	20	0.55	7.0	75	1.54	0.50	0.36	16.7	19.5	13.0	3.25	3.40	2.74
314	21	13	230	15	0.60	6.4	66	1.53	0.52	0.34	16.7	19.5	13.0	2.44	3.40	2.74
(b) 413	21	12	230	40	0.50	7.7	88	1.54	0.51	0.38	17.7	20.9	13.0	6.50	3.40	2.74
414	21	13	230	25	0.55	7.0	80	1.54	0.48	0.38	16.7	19.5	13.0	4.06	3.40	2.74

Figure 3.3.7.—Effect of Drop MVD on Ice Shape. NACA 0012 Airfoil at 4°AOA. Ice-Shape Data from Tests by Addy, April 1997 and Bidwell and Van Zante, January 1998, reported in data CD's accompanying Wright.²⁰

$$\beta_{0,S} A_{c,S} = \beta_{0,R} A_{c,R} \quad (3.28)$$

should be applied in this case. The use of equation (3.28) is not as desirable in general as satisfying equations (3.11) and (3.27) separately, and should only be used when no other alternatives are available. Only when the two collection efficiencies, $\beta_{0,S}$ and $\beta_{0,R}$, are within 10%, can equation (3.28) be expected to give acceptable agreement of the quantities of the scale and reference ice accretions.

For glaze ice, the freezing fraction is less than unity and varies with position on the model. The local accumulation depends not only on what impinges but is the result of a mass balance that includes evaporation and surface water flowing into and away from the location of interest. Thus, for glaze it is not simple to quantify the incoming liquid water except at the stagnation line, where there is no incoming surface water flow. The general non-dimensional ice thickness at the stagnation line depends on three things: the potential ice accumulation, A_c , the collection efficiency, β_0 , and the fraction of water reaching the surface that freezes there, n_0 . Thus,

$$\frac{A_0}{d} = n_0 A_c \beta_0 \quad (3.29)$$

The freezing fraction, n_0 , represents the heat balance at the ice surface; as such it is an additional similarity parameter that needs to be matched between reference and scale situations. It will be discussed in the next section. With both n_0 and β_0 matched, when the scale non-dimensional ice thickness at stagnation is equated with the reference, equation (3.27) again results. With the additional assumption that ρ_i is the same for scaled and reference cases, equations (3.26) and (3.27) can be rearranged to solve for the ratio of scale-to-reference accretion time:

$$\frac{\tau_S}{\tau_R} = \left(\frac{d_S}{d_R} \right) \left(\frac{V_S}{V_R} \right) \left(\frac{LWC_S}{LWC_R} \right) \quad (3.30)$$

For airfoils, of course, the ratio (c_S/c_R) can be used here in place of (d_S/d_R) because these ratios have the same value.

3.5. Energy Balance Similarity

If all the water impinging on a surface were to freeze on impact, equations (3.11) (or (3.18)) and (3.30) would be sufficient to satisfy scaling. This situation applies to rime ice formation. However, the fraction of water that freezes, n , is not always unity, and energy-balance similarity must be satisfied for glaze ice accretions.

The rate at which water freezes on a surface depends on the local heat balance. Tribus, et al²² studied heat transfer for a heated cylinder in icing conditions. Their analysis is useful for thermal deicing or anti-icing systems. Messinger²¹ later performed the classical energy-balance analysis for freezing at an unheated surface. Messinger's work was further developed by Ruff.⁷ The similitude relations to be presented here are for an unheated surface and are based primarily on the Messinger and Ruff analyses. The energy terms for this case, expressed per unit area, are listed here. The analyses will be done at the stagnation line.

(1) Heat lost from the surface by convection through the boundary layer:

$$q_c = h_c(t_s - t_{bl})$$

(2) Heat lost from the surface due to evaporation of water:

$$q_e = \dot{m}_e A_v$$

(3) Heat lost from the surface due to sublimation of ice:

$$q_s = \dot{m}_s A_s$$

(4) Heat lost from the surface due to radiation:

$$q_r = \sigma \epsilon (T_s^4 - T_{st}^4)$$

(5) Heat lost from the surface to raise the temperature of the impinging liquid to the freezing point:

$$q_w = \dot{m} c_{p,ws} (t_f - t_{st})$$

(6) Heat lost from the surface by water flowing out of the control volume to a neighboring location:

$$q_{rb} = [(1-n)\dot{m} - \dot{m}_e] c_{p,ws} (t_s - t_f)$$

(7) Heat lost from the surface due to conduction through the ice into the model:

$$q_{cond} = k_i \frac{\Delta}{\xi \ell} \left(t_s - t_{st} - r \frac{V^2}{2c_{p,a}} \right)$$

(8) Heat gained by the surface due to release of latent heat of fusion from the freezing water:

$$q_f = \dot{m} n A_f$$

(9) Heat gained by the surface due to release of sensible heat from the ice as it cools from the freezing temperature to the surface temperature:

$$q_i = \dot{m} n c_{p,is} (t_f - t_s)$$

(10) Heat gained by the surface from the kinetic energy of the water drops striking the surface:

$$q_k = \dot{m} (V^2 / 2)$$

(11) Heat gained by the surface by water flowing into the control volume from a neighboring location.

These terms will be discussed individually in greater detail in the following subsections.

3.5.1. Convective Heat Transfer

In term (1) the film coefficient, h_c , varies with position on the model. For scaling, this term in the heat balance will be evaluated only at the stagnation line. It is assumed that if scale and reference conditions are matched there, they will also match everywhere. In addition, the heat balance on the clean airfoil (before ice begins to accrete) is used; if the clean heat balance matches for two models and similarity is maintained in all the physical phenomena that affect the shape of the accreting ice, the heat balance, although changing with time, will be the same for the two models as ice develops.

Experimental convective heat transfer data is typically correlated in the form²³

$$Nu_a = A Re_a^B \quad (3.31)$$

where A and B are constants,

$$Nu_a = \frac{h_c d}{k_a} \quad (3.32)$$

and Re_a is the form defined in equation (3.1). Kreith²⁴ gives the following relationship for Nu_a for the stagnation line of a cylinder:

$$Nu_a = 1.14 Pr_a^{0.4} Re_a^{0.5} \quad (3.33)$$

where

$$Pr_a = \frac{c_{p,a} \mu_a}{k_a} \quad (3.34)$$

and Re_a was given by equation (3.1). The air properties for Nu_a , Pr_a , and Re_a in equation (3.33) are evaluated at the film temperature, which is taken as the average of the free-stream and surface temperatures,

$$t_{film} = \frac{1}{2} (t_s + t_{st}) \quad (3.35)$$

For glaze ice the surface temperature is 0°C, and over a free-stream temperature range of -40 to 0°C, the range of interest to icing, the Pr_a evaluated at film temperatures varies only from 0.708 to 0.705; thus, $1.14 Pr_a^{0.4}$ has a nearly constant value of 0.992. Then

$$Nu_a = 0.992 Re_a^{0.5} \quad (3.36)$$

Equation (3.33) was used to find the convective heat transfer coefficient by Ruff⁷ for both cylinders and airfoils. Heat transfer measurements were made along the surface of airfoils by Gelder and Lewis²⁵ and Poinatte²⁶ and around a cylinder by Van Fossen, et. al.²⁷ At the stagnation line of a clean, smooth NACA 0012 airfoil at 0° AOA in the NASA Glenn Icing Research Tunnel (IRT), Poinatte found

$$Nu_{a,c} = 6.818Re_{a,c}^{0.472} \quad (3.37)$$

where $Nu_{a,c}$ and $Re_{a,c}$ are based on airfoil chord rather than twice the leading-edge radius:

$$Nu_{a,c} = \frac{h_c c}{k_a} \quad (3.38)$$

and

$$Re_{a,c} = \frac{V c \rho_a}{\mu_a} \quad (3.39)$$

For consistency with the above expressions for Nu_a based on twice the nose radius, equation (3.37) can be converted using (for an NACA 0012) $d = 0.0316c$. Then $Nu_{a,c} = Nu_a/0.0316$ and $Re_{a,c} = Re_a/0.0316$, and equation (3.37) is equivalent to

$$Nu_a = 1.100Re_a^{0.472} \quad (3.40)$$

Poinatte's IRT data at 4° AOA correlated with

$$Nu_a = 0.903Re_a^{0.498} \quad (3.41)$$

The coefficients in Poinatte's study had an uncertainty of about ±5%.

Poinatte also conducted flight tests for which the turbulence level can be expected to be less than that in the IRT. At the leading edge of a clean, smooth NACA 0012 airfoil, the Nusselt number was

$$Nu_a = 2.618Re_a^{0.388} \quad (3.42)$$

Using a turbulence level of 0.5%, the approximate level in the NASA Glenn IRT, and for a smooth cylinder with no ice accretion, Van Fossen, et al reported

$$Nu_a = 1.244Re_a^{0.477} \quad (3.43)$$

Thus, the Poinatte 0012 IRT data correlations gave coefficients and exponents within 10% of those quoted by Kreith for a cylinder. Van Fossen's clean, smooth cylinder tests for IRT turbulence levels produced a coefficient about 25% higher than Kreith's and an exponent on Re_a within 5%. For scale testing in an icing tunnel with tur-

bulence levels similar to those of the IRT, it is recommended that Kreith's expression for Nu_a be used because it is consistent with these recent experimental data for both cylinder and airfoil models.

Charpin and coworkers^{14,15} used a Nusselt number of the form

$$Nu_a = ARe_a^{0.8} \quad (3.44)$$

Exponents on Re_a near 0.8 were obtained by both Poinatte and Van Fossen, et al only in regions where separation would probably have occurred or for very high turbulence levels. For example, for an NACA 0012 with roughened surface in the IRT Poinatte reported an exponent of 0.809 at a location well aft of the leading edge. And Van Fossen, et al found that for a cylinder with simulated smooth 15-min horn-glaze ice and with 0.5% turbulence an exponent of 0.798 occurred just aft of the horns. For the same test, near the leading edge the Nu_a dependency was $Re_a^{0.62}$. With roughness added to the ice, the exponent at the measuring station nearest the leading edge was 0.68. However, scaling calculations are based on parameters evaluated for a clean airfoil at the leading edge, so these exponents are not relevant in justifying equation (3.44).

The effect of using $Nu_a = Re_a^{0.8}$ on the value of the freezing fraction will be discussed in section 3.5.14.

The boundary-layer temperature, $t_{bl} = t_{st} + rV^2/2c_{p,a}$, where r is the recovery factor. The recovery factor has a theoretical value of 0.85 for laminar airflow and 0.87 - 0.88 for turbulent airflow over a flat plate at temperatures of interest to icing.²⁸ Experimental measurements for a flat plate give values of 0.88 - 0.90 for both flow regimes.²⁸ For a cylinder in crossflow at subsonic speeds, the recovery factor based on free-stream conditions decreases from 1 at the stagnation point to about 0.6 at 80° (ref. 28). Messinger²¹ used $r = 0.875$ as an average value to cover most situations. For the purposes of this manual, the analysis will be limited to the stagnation line, where $r = 1$, and, therefore, the convection term becomes $h_c(t_s - t_{st} - V^2/2c_{p,a})$.

3.5.2. Evaporation

The mass of water which evaporates, \dot{m}_e , in term (2) is

$$\dot{m}_e = h_G \frac{(p_{ww} - p_w)}{p_{st}} \quad (3.45)$$

Here the driving force for evaporation is the difference between the partial pressure of vapor at the surface, p_{ww} , and that in the atmosphere, p_w . The vapor pressure over water at the surface is assumed the saturation pressure at the surface temperature.

A compressible form of equation (3.45) was developed by Ruff. It is

$$m_e = h_G \left(\frac{\frac{p_{ww} - p_{tot} p_w}{T_{st} T_{tot} p_{st}}}{\frac{1}{0.622} \frac{p_{tot} - p_{ww}}{T_{tot}} - \frac{p_w}{T_{st}}} \right) \quad (3.46)$$

A curve fit for the saturation pressure of vapor over water was given by Pruppacher and Klett²⁹ for the range of -50°C to 50°C and can be found in Appendix A of this manual.

The gas-phase convective mass transfer coefficient, h_G , is analogous to the convective heat-transfer coefficient. The theoretical relationship between h_G and h_c can be expressed in terms of the Schmidt and Prandtl numbers as (see, for example, ref. 24):

$$h_G = \frac{h_c}{c_{p,a}} \left(\frac{Pr_a}{Sc_a} \right)^{0.67} \quad (3.47)$$

In equation (3.47) the Prandtl and Schmidt numbers, Pr_a and Sc_a , are those for air, with properties evaluated at the film temperature, t_{film} , from equation (3.35). The Prandtl number was given by equation (3.34) and the Schmidt number is

$$Sc_a = \frac{\mu_a}{\rho_a D_v} \quad (3.48)$$

An expression to calculate the diffusivity of water vapor in air was given by Pruppacher and Klett and is presented in Appendix A.

Measurements of h_G do not agree precisely with the values from equation (3.47), but that equation is useful for making estimates. At 0°C equation (3.47) gives $h_G/h_c = 4.81$ lbm R/Btu. Messinger used an experimental value of 2.90 lbm R/Btu for this ratio. Results shown in this manual were based on the value from equation (3.47).

3.5.3. Sublimation

Similar to the mass of ice that evaporates in term (2), the mass of ice which sublimates to vapor, \dot{m}_s , in heat-balance term (3) can be written

$$\dot{m}_s = h_G \frac{(p_{wi} - p_w)}{p_{st}} \quad (3.49)$$

where h_G is the convective mass transfer coefficient, equation (3.47). The driving force for sublimation is the difference between the partial pressure of vapor at the surface and that in the atmosphere. At the surface, the partial pressure of vapor is the saturation pressure of water vapor over ice. Pruppacher and Klett provide a

useful curve fit for the saturation pressure of vapor over ice (see Appendix A). However, sublimation of ice is small compared with evaporation of liquid. Therefore, this term will not be included in the energy balance equation.

3.5.4. Radiation

When hot-air or electrothermal anti- or deicing systems are not used, the surface temperature and ambient temperature are not sufficiently different for term (4) to be important. Therefore, for this analysis, radiation will be neglected.

3.5.5. Sensible Heat of Water

In term (5) the impinging mass of water is found from equation (3.22) for a general location. Because other terms of the energy balance have been formulated for the stagnation line the following form will be used

$$\dot{m} = LWC V \beta_0 \quad (3.50)$$

The impinging water is assumed to be at the ambient static temperature; therefore, the temperature has to be increased from the static temperature to the freezing temperature before freezing can occur.

3.5.6. Runback

Term (6) evaluates the heat carried away from the control volume by water run-back. For rime ice $n = 1$, and the term has a value of 0. On the other hand, for glaze ice $t_s = t_f$, and the term again disappears. Thus, this term can be ignored except for the case of thermal ice protection for which $t_s \neq t_f$. Scaling for thermal ice protection will not be considered in this manual.

3.5.7. Conduction

Ruff⁷ included an expression for conduction into the model surface. Conduction effects can be neglected for icing times greater than a few seconds because the ice quickly produces an insulating layer over the model surface. Even for short times, however, conduction similitude can be satisfied implicitly by requiring that the scale and reference models be identical in material and structure. Therefore, term (7) will be omitted.

3.5.8. Latent Heat of Fusion

The mass flux entering the control volume at stagnation is given by equation (3.50). The portion of this incoming mass that freezes is found by multiplying by the stagnation freezing fraction, n_0 . Then term (8) becomes

$$q_f = LWC V \beta_0 n_0 A_f \quad (3.51)$$

3.5.9. Sensible Heat of Ice

Term (9) is valid only for rime ice. For glaze, the surface temperature, t_s , is equal to the freezing temperature, t_f ; therefore, this term disappears.

3.5.10. Drop Kinetic Energy

Term (10) needs no further explanation.

3.5.11. Water Inflow

The contribution due to term (11) cannot be assessed easily except at stagnation. There, water enters the control volume only through impingement, and this term can be ignored in the heat balance.

3.5.12. Energy Balance Equation

When the surface temperature reaches steady state, the net heat transfer is zero. Thus, the energy-balance equation at an unheated stagnation surface for glaze ice, neglecting terms (2), (4), (6), (7), (9) and (11) is

$$q_c + q_e + q_w = q_f + q_k \quad (3.52)$$

or

$$h_c \left(t_s - t_{st} - \frac{V^2}{2c_{p,a}} \right) + h_G \left(\frac{\frac{p_{ww} - p_{tot} p_w}{T_{st} T_{tot} p_{st}}}{\frac{1}{0.622} \frac{p_{tot} - p_{ww}}{T_{tot} T_{st}}} \right) A_v \quad (3.53)$$

$$+ \dot{m} c_{p,ws} (t_f - t_{st}) = \dot{m} n_0 A_f + \dot{m} \frac{V^2}{2}$$

This equation includes compressibility effects for the evaporation term. The incompressible form of the energy equation is

$$h_c \left(t_s - t_{st} - \frac{V^2}{2c_{p,a}} \right) + h_G \left(\frac{p_{ww} - p_w}{p_{st}} \right) A_v \quad (3.54)$$

$$+ \dot{m} c_{p,ws} (t_f - t_{st}) = \dot{m} n_0 A_f + \dot{m} \frac{V^2}{2}$$

Several similarity parameters can be incorporated to simplify the expression of equation (3.53). Tribus²² introduced the dimensionless parameter b , known as the relative heat factor:

$$b = \frac{\dot{m} c_{p,ws}}{h_c} = \frac{LWC V \beta_0 c_{p,ws}}{h_c} \quad (3.55)$$

It relates the total heat capacity of the impinging water to the ability of the surface to convect heat. The convective heat transfer coefficient, h_c can be found from equations (3.32) and (3.33).

Two other parameters often used for convenience are ϕ and θ which have dimensions of temperature and relate to the drop energy transfer and air energy transfer, respectively:

$$\phi = t_f - t_{st} - \frac{V^2}{2c_{p,ws}} \quad (3.56)$$

and

$$\theta = \left(t_s - t_{st} - \frac{V^2}{2c_{p,a}} \right) + \frac{h_G}{h_c} \left(\frac{\frac{p_{ww} - p_{tot} p_w}{T_{st} T_{tot} p_{st}}}{\frac{1}{0.622} \frac{p_{tot} - p_{ww}}{T_{tot} T_{st}}} \right) A_v \quad (3.57)$$

Equation (3.57) includes compressibility effects. It was used by Ruff and will be used in this manual. The incompressible form, based on equation (3.45) has also been widely used. It is

$$\theta = \left(t_s - t_{st} - \frac{V^2}{2c_{p,a}} \right) + \frac{h_G}{h_c} \left(\frac{p_{ww} - p_w}{p_{st}} \right) A_v \quad (3.58)$$

If equation (3.47) is substituted into equation (3.58) along with Messinger's experimental value of 0.693 gK/joule for $(1/c_{p,a})(Pr/Sc)^{0.667}$ the form of θ used by Olsen and by Charpin and coworkers results. For aircraft icing conditions, compressibility is rarely an issue. Therefore, it is not surprising that the values of θ from equations (3.57) and (3.58) are nearly the same.

The energy balance, equation (3.53), can be rewritten in terms of the parameters b , ϕ and θ . Then, the energy balance for glaze ice becomes

$$n_0 = \left(\frac{c_{p,ws}}{A_f} \right) \left(\phi + \frac{\theta}{b} \right) \quad (3.59)$$

This formulation of the freezing fraction includes simplifications and evaluations that apply strictly to the stagnation line. It is often the practice in scaling publications to omit the subscript θ from n , but for this manual, the subscript will be retained to emphasize that the analysis is for the stagnation line. By using n_0 as the heat-balance parameter to match for scale studies, the implicit assumption is that if $n_{0,S} = n_{0,R}$ then n will also match everywhere. Furthermore, equation (3.59) applies to a clean airfoil. As ice accretes, the stagnation freezing fraction can be expected to change because the geometry is continually changing. Thus, for scaling it is necessary to assume additionally that n_0 varies with time in such a way that if $n_{0,S} = n_{0,R}$ at the initiation of spray, freezing fractions will continue to match during the course of ice accretion. This is not an unreasonable assumption be-

cause the goal of scaling is to maintain similar ice shapes for scale and reference.

It was shown earlier that if the stagnation collection efficiency, β_0 , matched for scale and reference, LEWICE predicted collection efficiencies that matched everywhere on the airfoil. Similarly, Oleskiw, Kind and McCullough³⁰ presented LEWICE predictions showing that when the stagnation n_0 matched, reference and scale local freezing fractions also matched from the stagnation line back to about $s/c = \pm 0.02$. This is the region of greatest interest to icing because most of the main ice shape is accreted in this range. However, it's important to keep in mind that LEWICE predictions of freezing fraction have not been validated experimentally the way collection efficiencies have, and therefore there is less confidence in the LEWICE values of n .

Experimental evidence to validate the formulation of the expression for stagnation freezing fraction will be presented below in section 3.5.2.

For rime ice, because water freezes on impact, the energy balance does not affect the ice shape. Consequently, no energy balance needs to be considered when scaling rime. However, for glaze ice, the energy balance similarity is typically satisfied by matching scale and reference values of one or more of the parameters n_0 , ϕ , θ and b . If any three of these are satisfied, it can be seen from equation (3.59) that the fourth is, as well.

Kind^{31,32} used an additional parameter that related the evaporative and convective heat transfer rates. He matched scale and reference values of a convective-to-latent heat ratio that will be called r_A :

$$r_A = \frac{\left(1 + \frac{q_e}{q_c}\right) h_c (t_s - t_{st})}{LWC V A_f} \quad (3.60)$$

Typically, $q_e \ll q_c$. Then, substituting the definition of b from equation (3.55), equation (3.60) becomes

$$r_A \approx \left(\frac{\beta_0 c_{p,ws}}{A_f}\right) \left(\frac{t_s - t_{st}}{b}\right) \approx \text{constant} \left(\frac{t_s - t_{st}}{b}\right) \quad (3.61)$$

3.5.13. Effect of Temperature and LWC

Studies with both cylinders and NACA 0012 airfoils^{33,34} have shown how ice shapes change with temperature and LWC . Some of the 0012 results will be given here. The effect of incremental changes in temperature on ice shape is shown in figure 3.5.1. The tests were performed in the NASA Glenn IRT using 21-in- (53.3-cm-) chord NACA 0012 airfoil models. In each portion of the figure, two

ice shapes are compared for which the temperature was different with all other test conditions held constant. For all tests K_0 was the same to give a fixed value of β_0 of 0.85, A_c was 1.88 and b was 0.58. As temperature decreased, the parameters n_0 , ϕ and θ increased.

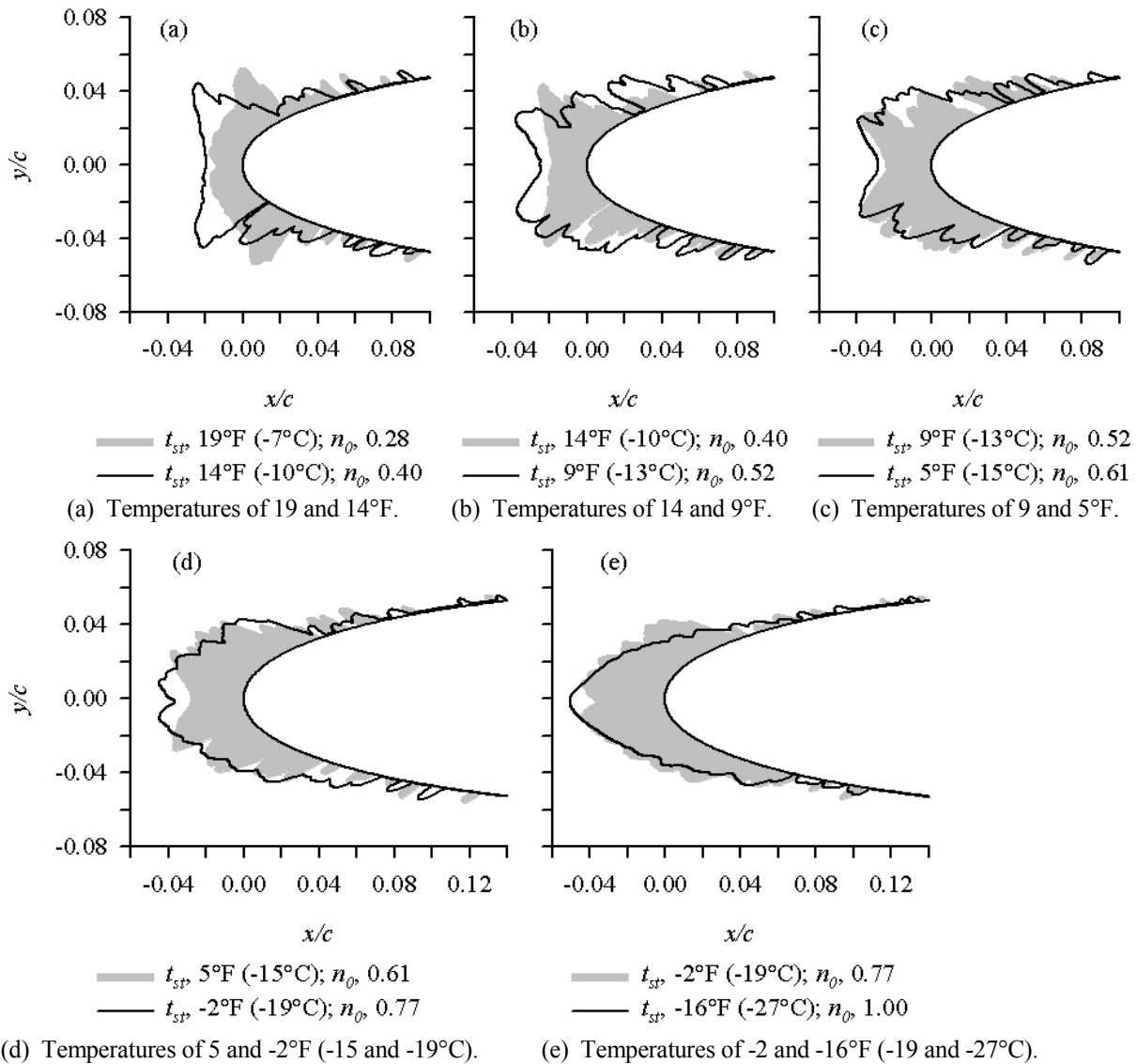
The ice shape for the warmer temperature of each pair is shown shaded while the colder of the two is represented with a solid line. With each incremental decrease in temperature (and consequent increase in n_0) the horns moved forward and the leading-edge ice thickness increased (consistent with equation (3.29)). The total quantity of ice produced appeared to be the same for each pair of profiles. The same trends were observed with a 36-in-chord GLC 305 model when temperature decreased from 14 to 1°F. Again, the horns moved forward and the leading-edge thickness increased when the temperature decreased.¹⁸

With constant test conditions c , V , δ , LWC , and τ and constant similarity parameters K_0 (β_0), A_c and b for the range of temperatures tested in figure 3.5.1, it must be reasoned that only the varying parameters n_0 , ϕ or θ can be responsible for the changes observed in ice shape. Further evidence will be shown next to isolate which of these three has the greatest impact on shape.

Figure 3.5.2 presents results of another series of tests; this time, the test conditions c , t_{st} , V , and δ were maintained constant while LWC varied. The icing time was adjusted to keep A_c the same from test to test. For these experiments, the similarity parameters K_0 (β_0), A_c , ϕ and θ were unchanged as LWC was decreased. n_0 increased with decreasing LWC , and b also decreased. Again, the model was a 21-in- (53.3-cm-) chord NACA 0012 tested in the NASA Glenn IRT. The shaded ice shape in each portion of the figure was recorded for the higher LWC . As the LWC was decreased from 1.4 to 1.0 g/m³ (fig. 3.5.2 (a)) the horns on the main ice shape moved forward and the leading-edge thickness tended to increase, similar to the effect of decreasing the static temperature shown in figure 3.5.1. A further reduction in LWC from 1.0 to 0.8 g/m³ (fig. 3.5.2 (b)) produced a small additional narrowing of the horn angle.

Finally, figure 3.5.3 gives results of tests in which both temperature and LWC were varied in such a way that the freezing fraction was maintained constant. The LWC was again reduced from 1.4 to 1.0 g/m³ (fig. 3.5.3 (a)) and from 1.0 to 0.8 g/m³ (fig. 3.5.3 (b)). The fixed similarity parameters were K_0 (β_0), A_c and n_0 , while b , ϕ and θ varied from test to test. Ice shapes now were unchanged as LWC varied.

For the range of temperature and LWC tested, these results led to the conclusion that neither temperature nor

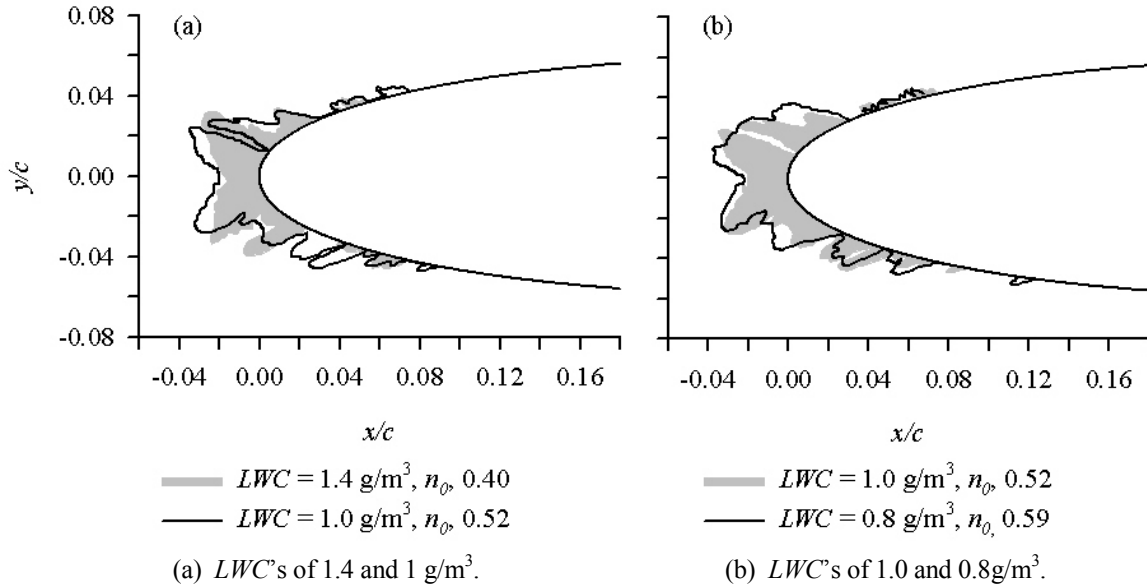


(d) Temperatures of 5 and -2°F (-15 and -19°C).

(e) Temperatures of -2 and -16°F (-19 and -27°C).

Date/Run	c , in	t_{st} , °F	V , mph	δ , μm	LWC , g/m^3	τ , min	β_0 , %	A_c	n_0	b	ϕ , °F	θ , °F	Re_{δ} , 10^4	We_{δ} , 10^3	We_{σ} , 10^3	We_L , 10^6
(a) 11-13-00/1	21	19	149	38	1.00	7.3	84.9	1.88	0.28	0.58	11.8	16.2	8.56	2.61	1.47	1.15
11-13-00/3	21	14	149	38	1.00	7.3	84.9	1.88	0.40	0.58	16.7	23.2	8.72	2.61	1.48	1.15
(b) 11-13-00/3	21	14	149	38	1.00	7.3	84.9	1.88	0.40	0.58	16.7	23.2	8.72	2.61	1.48	1.16
11-13-00/5	21	9	150	38	0.99	7.3	84.9	1.88	0.52	0.58	21.6	29.9	8.91	2.62	1.51	1.16
(c) 11-13-00/5	21	9	150	38	0.99	7.3	84.9	1.88	0.52	0.58	21.6	29.9	8.91	2.62	1.51	1.16
11-13-00/6	21	5	150	38	0.99	7.3	84.9	1.88	0.61	0.58	25.8	35.3	9.03	2.61	1.52	1.16
(d) 11-13-00/6	21	5	150	38	0.99	7.3	84.9	1.88	0.61	0.58	25.8	35.3	9.03	2.61	1.52	1.16
11-13-00/7	21	-2	150	38	0.99	7.3	84.9	1.88	0.77	0.58	32.9	44.1	9.29	2.62	1.55	1.16
(e) 11-13-00/7	21	-2	150	38	0.99	7.3	84.9	1.88	0.77	0.58	32.9	44.1	9.29	2.62	1.55	1.16
11-13-00/8	21	-16	150	38	0.99	7.3	84.9	1.88	1.00	0.58	47.2	60.6	9.80	2.62	1.59	1.16

Figure 3.5.1.—Effect of Static Temperature on Ice Shape. NACA 0012 Airfoil at 0°AOA.



Run	c , in	t_{st} , °F	V , mph	δ , μm	LWC , g/m ³	τ , min	β_0 , %	A_c	n_0	b	ϕ , °F	θ , °F	Re_{δ} , 10 ⁴	We_{δ} , 10 ³	We_{ϕ} , 10 ³	We_L , 10 ⁶
(a) 10-25-95/11	21	11	150	30	1.40	5.2	80.3	1.90	0.40	0.77	20.4	28.2	8.90	2.08	1.52	1.17
10-25-95/9	21	10	150	30	1.00	7.3	80.4	1.90	0.52	0.55	21.2	29.4	8.91	2.08	1.51	1.17
(b) 10-25-95/9	21	10	150	30	1.00	7.3	80.4	1.90	0.52	0.55	21.2	29.4	8.91	2.08	1.51	1.17
10-25-95/10	21	11	150	30	0.80	9.1	80.3	1.90	0.59	0.44	20.4	28.2	8.87	2.08	1.51	1.16

Figure 3.5.2.—Effect of Liquid-Water Content on Ice Shape. Constant Static Temperature. NACA 0012 Airfoil at 0° AOA.

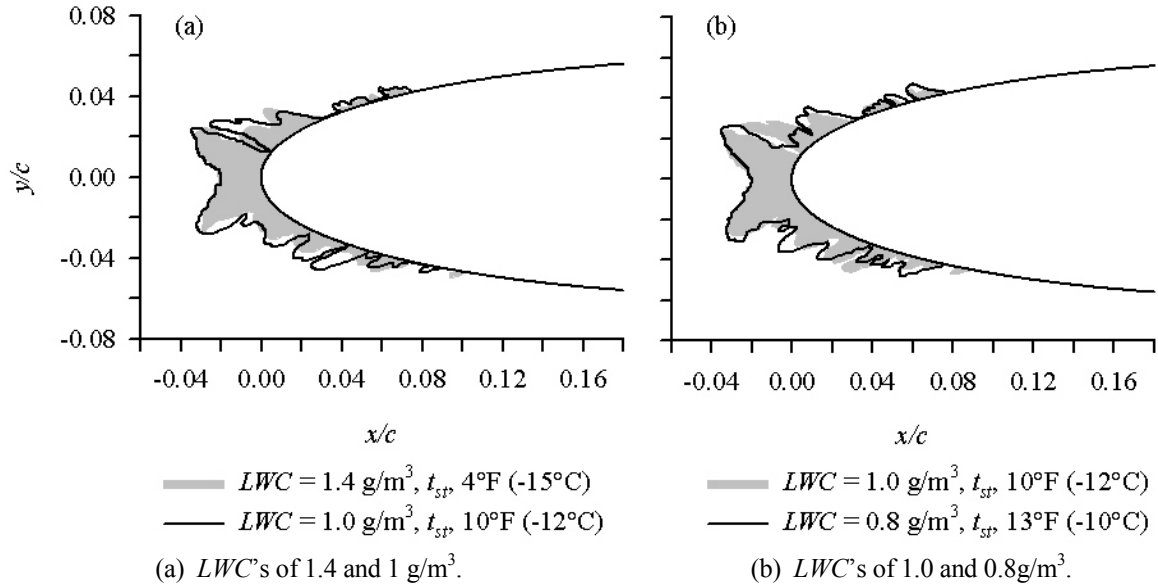
LWC has an effect on ice shape independent of the freezing fraction. The results of the three test series shown in figures 3.5.1, 3.5.2 and 3.5.3 demonstrate not only the very strong effect of freezing fraction on ice shape, but also the apparent unimportance of the other energy parameters by themselves. b , ϕ and θ are related to n_0 through equation (3.59) but appear to have little or no independent effect on ice shape. These results also show that when tests must be performed to simulate an LWC that cannot be obtained in a test facility, it is only necessary to adjust temperature in such a way that freezing fraction matches the desired value. This approach to scaling test conditions is known as the Olsen method.¹³ The Olsen method will be discussed in section 5.2.1.2.

This ability to match shape by matching c , V , δ and n_0 fails if the scale total temperature is too high. Obviously, ice will not accrete if the scale total and static temperatures are above freezing. If the static temperature is below freezing while the total is above, ice will accrete over some part of the model, but the quantity of ice at the leading edge will be less than would result at the same freezing fraction but with a total temperature below freezing. An example³⁵ with a static temperature of 20°F and a total temperature of 32°F is shown in figure 3.5.4. Here, instead of well-defined horns, ridges of ice formed

adjacent to the stagnation region while there was little accumulation at the leading edge. Inspection showed this accretion to be wet. Other investigators^{36,37} have reported that slushy ice forms when total temperatures are near freezing.

The temperatures reported in figure 3.5.4 were averaged over the run time. For this test, the variation in temperature over time was approximately $\pm 0.5^\circ\text{F}$. Therefore, at times, the stagnation temperature would have been below freezing, and at others, above. Away from the stagnation line, the recovery temperature would have been somewhat below the stagnation (total) value. Consequently, more freezing was possible aft of stagnation, accounting for the ice ridges adjacent to the leading-edge region. Another case, for a total temperature of 33°F, was also reported in reference 35. The ice shape was very similar in appearance to that in figure 3.5.4.

Unpublished ice shapes recorded by the author in the IRT showed that even for temperatures as much as 4 – 5°F below freezing accretions look different from those formed at lower temperatures at the same n_0 . Figure 3.5.5 gives an example. Here shapes obtained at different total temperatures but with constant n_0 are compared. In figure 3.5.5 (a) ice shapes are shown for total



Run	c , in	t_{st} , °F	V , mph	δ , μm	LWC , g/m ³	τ , min	β_0 , %	A_c	n_0	b	ϕ , °F	θ , °F	Re_a , 10 ⁴	We_δ , 10 ³	We_σ , 10 ³	We_L , 10 ⁶
(a) 10-2595/13	21	4	150	30	1.40	5.2	80.3	1.90	0.52	0.77	26.6	36.4	9.09	2.07	1.53	1.17
10-25-95/9	21	10	150	30	1.00	7.3	80.4	1.90	0.52	0.55	21.6	29.4	8.91	2.08	1.51	1.17
(b) 10-25-95/9	21	10	150	30	1.00	7.3	80.4	1.90	0.52	0.55	21.6	29.4	8.91	2.08	1.51	1.17
10-25-95/7	21	13	150	30	0.80	9.1	80.4	1.90	0.52	0.44	17.8	24.7	8.80	2.09	1.50	1.17

Figure 3.5.3.—Effect of Liquid-Water Content. Temperature Adjusted for Constant n_0 . NACA 0012 Airfoil at 0°AOA.

temperatures of 24.9 and 27.6°F. The same model was used for both tests and the velocity and drop MVD were unchanged. To maintain the freezing fraction at 0.30, the LWC was decreased from 1.22 to 0.80 g/m³ when the

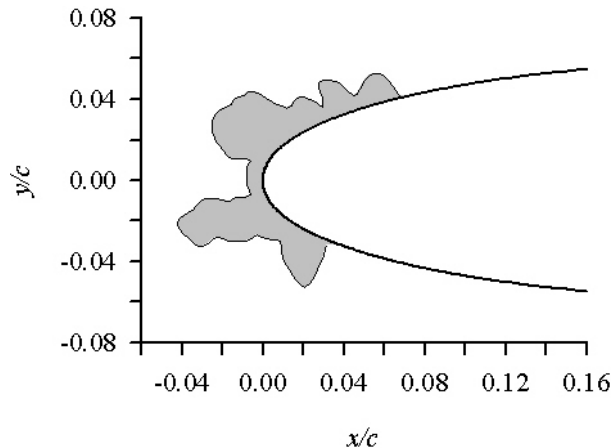
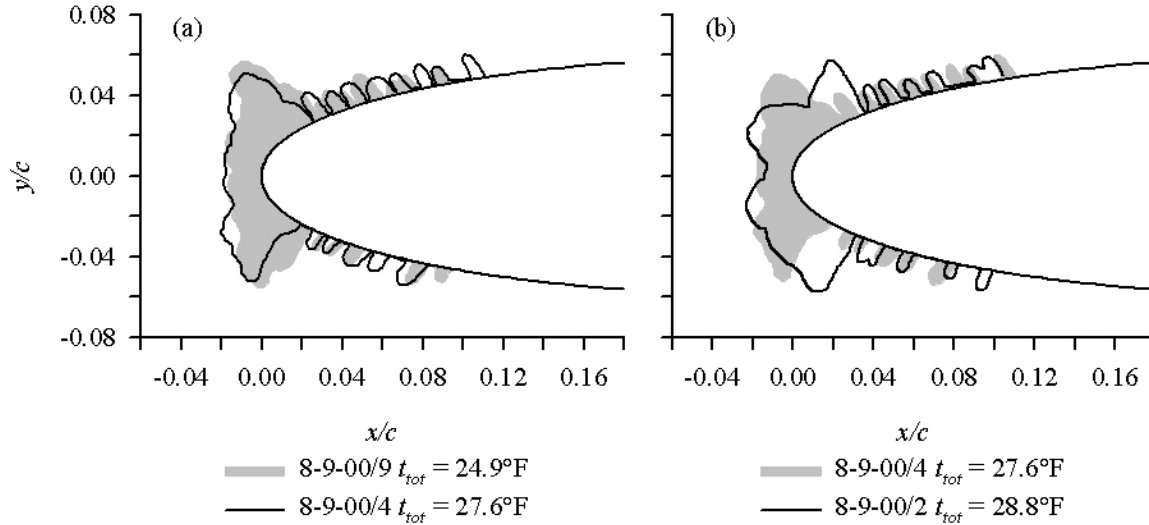


Figure 3.5.4.—Ice Shape for Total Temperature of 32°F.³⁵ NACA 0012 at 0° AOA Tested in the IRT, 3-23-98 Run 2; c , 10.5 in; t_{st} , 20°F; V , 264 mph; δ , 21 μm; LWC , 0.49 g/m³; τ , 4.3 min; β_0 , 85.8; A_c , 1.96; n_0 , 0.22; b , 0.29; ϕ , 9.1°F; θ , 6.5°F; Re , 7.11×10^4 ; We , 4.44×10^3 ; We_L , 1.80×10^6 .

temperature was increased. The two ice-shapes agreed within the typical repeatability of shapes for low freezing fractions such as this. There were no major differences in the horn size, horn location or leading-edge thickness between the two.

In figure 3.5.5 (b) the 27.6°F test shown in 3.5.5 (a) is compared with one at 28.8°F. Again, the freezing fraction was maintained the same for the two tests by lowering the LWC when the temperature was raised. All other test conditions were the same. In contrast to the minimal effects of a 2.7°F total temperature change in 3.5.5 (a), the increase in total temperature of just over 1°F in 3.5.5 (b) produced a dramatic change in the shape. For the 28.8°F shape the leading-edge thickness has decreased and ice ridges have appeared adjacent to the stagnation region. Horn-like structures were located significantly farther aft than those seen at temperatures from 24.9 to 27.6°F.

These observations suggest that, with constant model size, velocity and drop size, matched freezing fractions will insure matched ice shapes only for total temperatures below 27°F in the IRT. Test results to define this temperature limit have not been published for models other than the NACA 0012, but there is no reason to sup-



(a) Total Temperatures of 24.9 and 27.6°F

(b) Total Temperatures of 27.6 and 28.8°F

Date/Run	<i>c</i> , in	<i>t_{st}</i> , °F	<i>t_{tot}</i> , °F	<i>V</i> , mph	δ , μm	<i>LWC</i> , g/m ³	τ , min	β_0 , %	<i>A_c</i>	<i>n₀</i>	<i>b</i>	ϕ , °F	θ , °F	<i>Re_a</i> , 10 ⁴	<i>We_s</i> , 10 ³	<i>We_c</i> , 10 ³	<i>We_L</i> , 10 ⁶
(a) 8-9-00/9	10.5	12.6	24.9	262	21	1.22	1.7	85.7	1.89	0.29	0.696	16.5	17.4	7.12	4.38	2.12	1.78
8-9-00/4	10.5	15.3	27.6	262	20	0.80	2.6	85.4	1.89	0.30	0.455	13.8	13.5	7.06	4.31	2.11	1.78
(b) 8-9-00/4	10.5	15.3	27.6	262	20	0.80	2.6	85.4	1.89	0.30	0.455	13.8	13.5	7.06	4.31	2.11	1.78
8-9-00/2	10.5	16.6	28.8	262	20	0.68	3.1	85.5	1.91	0.30	0.39	12.5	11.7	7.01	4.31	2.10	1.77

Figure 3.5.5—Effect of Total Temperature near Freezing on Ice Shape. NACA 0012 Airfoils at 0° AOA.

pose the effects shown in figures 3.5.4 and 3.5.5 would be different for other airfoil profiles. The results shown are for 10.5-in-chord models, and it is not known how the temperature limit might vary with model size. Other facilities would be expected to show similar practical limitations, as well, although the value of the upper temperature limit may be different from that in the IRT.

3.5.14. Validation of the Freezing Fraction Expression

When experimental ice shapes are available, there are two ways to determine the stagnation freezing fraction, n_0 . First, an experimental stagnation freezing fraction, n_e , can be found using measurements from the ice shapes. From equation (3.29),

$$n_e = \frac{\Delta_0}{d} \frac{1}{A_c \beta_0} \quad (3.62)$$

where Δ_0 is the leading-edge thickness of the ice, and β_0 and A_c are calculated from equations (3.13) and (3.26), respectively, using the conditions at which the ice was accreted. Second, an analytical stagnation value can be determined from equation (3.59), also using the conditions of the test,

$$n_a = \left(\frac{c_{p,ws}}{A_f} \right) \left(\phi + \frac{\theta}{b} \right) \quad (3.63)$$

No experimental results are needed to calculate n_a . The freezing fractions found from equations (3.62) and (3.63) should agree.

Anderson and Tsao³⁸ compared values of n_e and n_a for a number of experimental ice shapes obtained in the IRT using NACA 0012 models with chords of 10.5 – 31.5 in (26.7 – 80 cm), velocities of 106 – 257 mph (48 – 115 m/s) and drop MVD's of 21.5 – 46 μm . The experimentally-derived freezing fractions are plotted against the analytical values in figure 3.5.6. Open symbols were measured from ice tracings taken at mid-span (CL) and the solid from the tracings 1 in (2.5 cm) above mid-span (CL+2.5 cm). The solid line represents perfect agreement of the two freezing fractions and the shaded band indicates the limits for $\pm 10\%$ agreement. A linear fit to the data is shown as a dashed line.

There was significant uncertainty in the ice thickness values found from tracings at low freezing fractions. The data scatter in figure 3.5.6 at the lowest freezing fraction tested was a consequence of this uncertainty. The linear fit to the data fell within the $\pm 10\%$ agreement band, although on average n_e values tended to be about 5% lower than the n_a . The value of n_e found from equation (3.62) is inversely proportional to the value of LWC through the accumulation parameter (eq. (3.26)). Because the uncer-

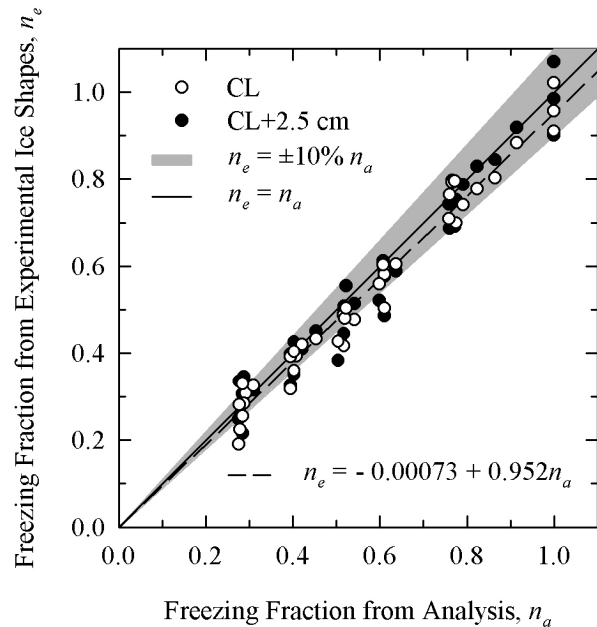


Figure 3.5.6.—Experimental (eq. (3.62)) and Analytical (eq. (3.63)) Stagnation Freezing Fractions of Anderson and Tsao.³⁸

tainties for the LWC and A_c were both estimated to be about $\pm 10\%$, this agreement is quite good.

While $n_a = 1$ suggests fully rime ice, n_e is susceptible to the uncertainties in both the LWC calibration and the tracing technique and can therefore be greater or less than unity. n_e values for experimental rime shapes in this study were within $\pm 10\%$ of 1.

Bilanin³⁹ performed a similar study using a limited set of ice-shape data from Ruff. Bilanin found agreement of n_e and n_a at rime, but the two deviated significantly for the lowest freezing fractions. He concluded that the Messinger analysis for freezing fraction had serious deficiencies, probably because surface-water effects, particularly splashing, were not included in the heat balance. However, Bilanin did not consider the possibility that his results might be explained by experimental complications, such as possible problems with the facility LWC calibration and the uncertainty in the leading-edge thickness for low freezing fractions.

Unlike Bilanin's results, the experimentally-determined freezing fractions for the Anderson and Tsao study in figure 3.5.6 showed no systematic deviation from the analytical values at low freezing fractions. This consistently good agreement between n_e and n_a over a range of conditions including both fully rime and fairly warm glaze argued against the contention that the Messinger freezing fraction formulation neglects any important effects, such as surface-water phenomena. On the contrary, for Appendix C icing conditions, the experimental

results appeared to validate the Messinger freezing fraction formulation expressed in equation (3.59) (or eq. (3.63)).

Besides the consistency between n_e and n_a over the range of freezing fractions evaluated, Anderson and Tsao showed that when conditions were such that equation (3.63) gave $n_a = 1$, fully rime ice resulted, as evidenced both by the shapes and the white appearance. The maximum temperature for the given model size, velocity, drop size, and LWC at which rime should occur was determined using equation (3.63). Figure 3.5.7 compares ice shapes obtained at this temperature, which should have produced fully rime, with ones at slightly higher temperatures. Ice shapes at these higher temperatures would be expected to deviate from fully rime appearance if the formulation for n_a is correct.

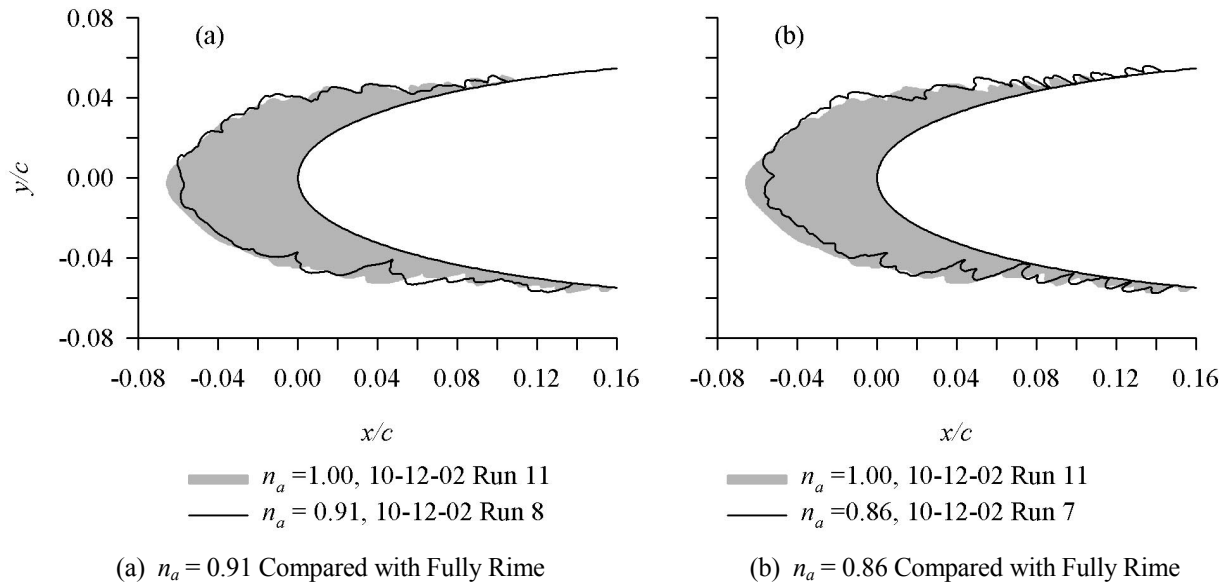
The rime shape (10-12-02 run 11) used for comparison in both portions of the figure is shown with a shaded cross section. It was accreted at a static temperature of -13°F . Figure 3.5.7 (a) compares this shape with one produced at -7°F , giving an analytical stagnation freezing fraction of 0.91. The outline of this shape is plotted with a solid line and no shading. The shape at the lower freezing fraction differed from the rime in that a narrow strip of ice at the leading edge changed from the characteristic white appearance of rime to a slightly transparent form. At the same time, the smooth, convex shape of rime was replaced with a slight valley right at the leading edge. The remainder of the ice aft of this narrow strip maintained the rime appearance. A further increase in temperature to -5°F reduced the analytical stagnation freezing fraction to 0.86 (fig. 3.5.7 (b)). This change in n_0 caused the leading-edge depression to deepen slightly without changing the appearance aft of the leading edge.

These results show that the use of the Messinger analysis leads to a consistency between the analytical freezing fraction and experimental ice shapes for rime and nearly-rime ice.

Anderson and Tsao also looked at the effects of calculating the analytical freezing fraction with 2 minor modifications. The first was to use the model chord instead of twice the leading-edge radius, and the second substituted the average Nu_a around a cylinder²⁴

$$Nu_a = 0.0239 Re_a^{0.805} \quad (3.64)$$

for the stagnation value of equation (3.33). Each of these changes led to somewhat poorer agreement between n_e and n_a , but more significantly gave analytical freezing fractions of 0.82 to 0.89 for the conditions yielding ice with the appearance of fully rime ice.



Run	c , in	t_{st} , °F	V , mph	δ , μm	LWC , g/m ³	τ , min	β_0 , %	A_c	n_a	b	ϕ , °F	θ , °F	Re_a , 10 ⁴	We_δ , 10 ³	We_σ , 10 ³	We_L , 10 ⁶
(a) 10-12-02/11	21	-13	114	40	1.14	10.8	84.0	2.43	1.00	0.57	44.5	58.9	7.37	1.59	0.91	0.67
10-12-02/8	21	-7	115	40	1.13	10.8	84.1	2.44	0.91	0.57	38.5	52.0	7.29	1.62	0.92	0.68
(b) 10-12-02/11	21	-13	114	40	1.14	10.8	84.0	2.43	1.00	0.57	44.5	58.9	7.37	1.59	0.91	0.67
10-12-02/7	21	-5	115	40	1.13	10.8	84.0	2.44	0.86	0.57	36.1	49.3	7.23	1.62	0.92	0.68

Figure 3.5.7.—Sensitivity of Ice Shape to Freezing Fraction at and near $n_a = 1$. NACA 0012 Airfoil at 0°AOA.

These comparisons illustrate how it is possible to apply simple checks of experimental consistency to expose problems with particular analytical methods for calculating freezing fraction. At the same time, because fully rime is easy to recognize, equation (3.62) provides a simple way to validate facility LWC calibrations. Conditions to give $n_a = 1$ can be calculated using equation (3.63), then validated by the appearance of the ice actually produced. With β_0 determined from equation (3.13) and the stagnation ice thickness measured from the experimental accretion, when equation (3.26) is substituted for A_c , equation (3.62) can be rearranged to solve for the actual LWC .

3.6. Similarity of Surface-Water Dynamics

Scaling methods developed from the 1950's through the 1970's relied on matching scale and reference values of some or all of the parameters K_0 , A_c , and n_0 . Given a set of reference conditions and choosing scale model size, ONERA and Ruff (see section 5.3) used these parameters plus ϕ and θ from equations (3.56) and (3.57) to provide five equations to solve for scale temperature, pressure, drop MVD, cloud LWC and spray duration. Some of these earlier methods permitted the user the arbitrary choice of scale velocity. In this section, it will be shown

that velocity has an effect on ice shape independent of its effect on the similarity parameters identified so far. This effect of velocity appears to be associated with surface-water phenomena, as will be seen.

In 1988 Bilanin³⁹ presented a Buckingham- π analysis in which he concluded that surface-water phenomena had to be included in icing scaling methods. Olsen and Walker¹⁰ and Hansman, et al^{12,40,41} studied surface effects and surface water during ice accretion, presenting additional evidence that these were important phenomena to consider in ice accretion. From the close-up photographs of these research studies, it was observed that for glaze ice accretion unfrozen water on the ice surface tended to coalesce to form beads. These beads sometimes were swept downstream and sometimes froze in place. Bilanin^{39,42} also argued that drop splashing on impact might affect the shape of the ice accreted.

Hansman and Turnock¹² found that when a surfactant was added to the icing spray water, the ice shape appearance and shape changed significantly, with the glaze horns moving toward the leading edge. Clearly, then, surface tension, and by implication, surface phenomena, have a significant role in the physics of ice accretion.

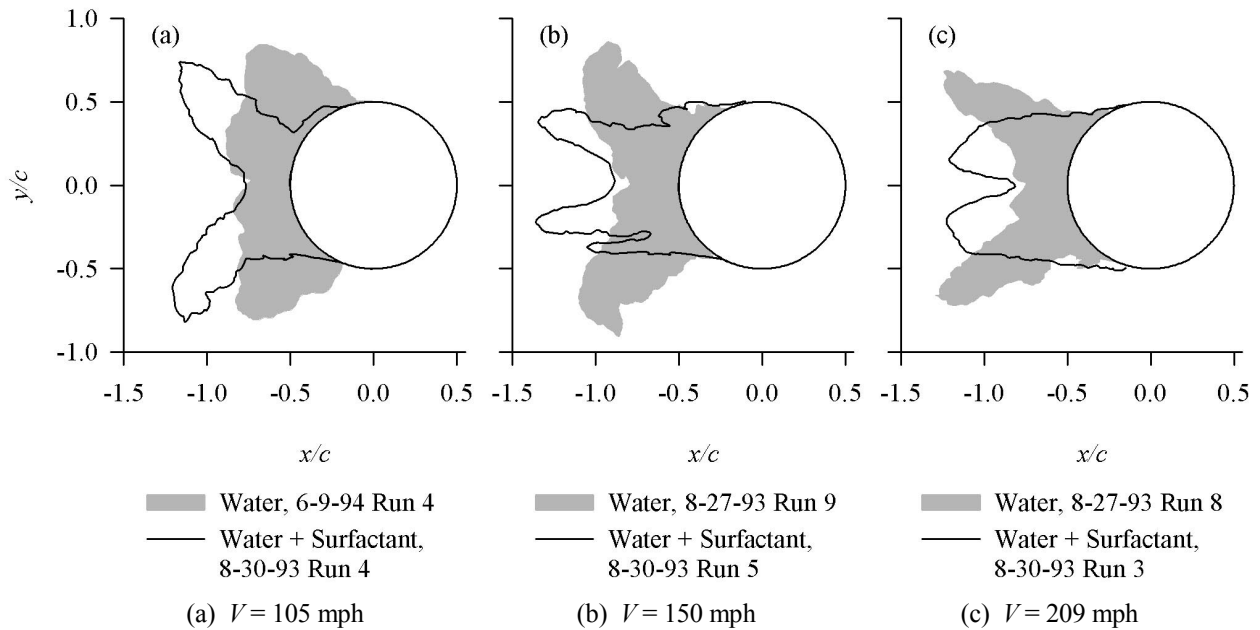
3.6.1. Forms of the Weber Number

Similar observations were made by Bilanin and Anderson.⁴² Figure 3.6.1 includes published and unpublished data from their studies and compares ice shapes with and without surfactant addition to the spray for velocities of 105, 150 and 209 mph. The shaded ice shapes were obtained with the NASA Glenn Icing Research Tunnel (IRT) spray bar system de-mineralized water supply with no surfactant added, and the shape represented by the solid line resulted from surfactant addition to the water. Other than the addition of surfactant the same test conditions were used for each pair of tests, as shown in the accompanying table. Surfactant addition reduced the surface tension to roughly half that of water. Because n_0 , β_0 and A_c were the same for each pair of tests, the leading-edge ice thickness was also nearly the same. However, the included angle between the horns decreased dramatically when surfactant was added. Horn angle also decreased when velocity increased as can be seen by comparing figure 3.6.1(a) with (b) and (c). All the re-

sults shown for different velocities were from tests made at approximately the same freezing fraction. Thus, both surface tension and velocity have an effect on ice shape independent of freezing fraction. Clearly, then, scale velocity cannot be chosen arbitrarily, and a similarity parameter dependent on the ratio $V^{e1}/\sigma_{w/a}^{e2}$ must be included in scaling methodology, where the powers $e1$ and $e2$ need to be determined.

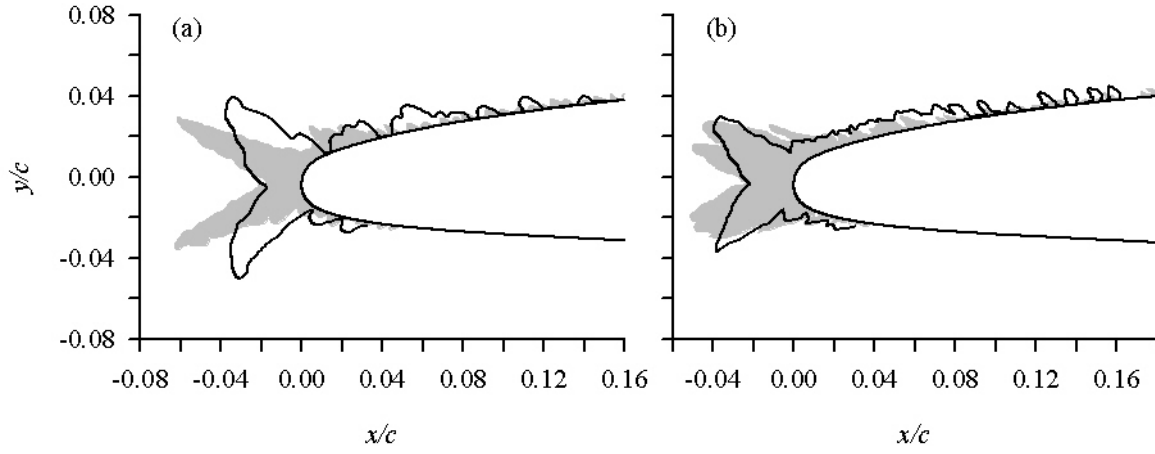
Chen's¹⁸ results for GLC 305 airfoils, shown in figure 3.3.6, as well as NACA 0012 results, shown in figure 3.3.7, show that drop size and collection efficiency appear to have little effect on the main ice shape for at least much of the range of Appendix-C conditions. Therefore, the parameter being sought cannot be dependent on δ .

The effect of model size was also evaluated by Chen. Figure 3.6.2 illustrates that with β_0 , A_c , n_0 , b , ϕ and θ constant a reduction in chord from 91 to 30 cm moved the glaze horns rearward. This is the same effect shown in figure 3.6.1 for decreasing velocity.



Date/Run	d , in	t_{sb} , °F	V , mph	δ , μm	LWC , g/m ³	τ , min	$\sigma_{w/a}$, dyne/ cm	β_0 , %	A_c	n_0	b	ϕ , °F	θ , °F	Re_{as} , 10 ⁴	We_{δ} , 10 ³	We_c , 10 ³	We_L , 10 ⁶
(a) 6-9-94/4	2	18	105	40	1.16	16.0	65	77.7	1.12	0.25	0.89	13.5	20.1	18.5	1.36	2.29	1.72
8-30-93/4	2	18	105	40	1.17	16.0	30	77.7	1.13	0.25	0.90	13.5	20.1	18.5	2.94	4.83	3.72
(b) 8-27-93/9	2	11	150	34	1.39	10.2	65	77.2	1.22	0.29	1.28	20.0	27.8	26.7	2.35	4.54	3.51
8-30-93/5	2	11	150	34	1.39	10.2	30	77.2	1.22	0.29	1.28	20.0	27.8	26.7	5.11	9.85	7.61
(c) 8-27-93/8	2	10	209	30	1.10	9.0	65	77.2	1.19	0.29	1.21	20.1	25.3	36.3	4.03	8.60	6.82
8-30-93/3	2	10	209	30	1.10	9.2	30	77.2	1.22	0.29	1.21	20.1	25.3	36.3	8.73	18.6	14.8

Figure 3.6.1.—Effect of Surfactant and Velocity on Ice Shape. Vertical Cylinders Tested in the NASA Glenn IRT. Published and Unpublished Ice-Shape Data from Tests by Bilanin and Anderson.



— $c = 36\text{-in}$, Run 2-8-36
 — $c = 12\text{-in}$, Run 2-8-12

— $c = 36\text{-in}$, Run 0-14-8-3
 — $c = 12\text{-in}$, Run 0-14-8-0

(a) $n = 0.4$

(b) $n = 0.5$

Run	c , in	t_{st} , °F	V , mph	δ , μm	LWC , g/m ³	τ , min	β_0 , %	A_c	n_0	b	ϕ , °F	θ , °F	Re_{ap} , 10 ⁴	We_δ , 10 ³	We_c , 10 ³	We_L , 10 ⁶
(a) 2-8-36	36	10	265	44	0.58	14.6	87.2	2.67	0.40	0.57	19.5	21.2	21.4	9.54	6.41	5.28
2-8-12	12	8	280	26	0.91	3.0	90.0	2.68	0.41	0.55	20.2	21.2	7.5	6.29	2.36	1.96
(b) 0-14-8-3	36	5	271	38	0.55	13.5	84.9	2.40	0.52	0.54	24.0	26.7	22.2	8.59	6.76	5.54
0-14-8-0	12	5	270	20	0.96	2.6	85.9	2.42	0.50	0.54	23.5	26.1	7.4	4.54	2.23	1.83

Figure 3.6.2.—Effect of Model Size on Ice Shape. GLC 305 Airfoil at 0° AOA. Ice-Shape Data from September 1998 IRT Tests by Chen.¹⁸

The previous section showed that the temperature and LWC do not have effects on the ice shape independent of the freezing fraction. Thus, the effect of these test conditions are adequately accounted for by n_0 , and the supplementary parameter does not need to include them. and Its general form must then be

$$P = \text{constant} \frac{V^{el} c^{e3}}{\sigma_{w/a}^{e2}} \quad (3.65)$$

This form suggests a Weber number based on chord:

$$We_c = \frac{V^2 c \rho_a}{\sigma_{w/a}} \quad (3.66)$$

Studies by Bartlett^{43, 44} and Oleskiw, et al⁴⁵ found no measurable effect of pressure on ice shape. These observations rule out the dependence on air density in equation (3.66), making water density a better choice. Furthermore, the length may not be chord itself but rather some physical characteristic related to the accreting ice that is proportional to chord; for example, the water-film thickness. Because this length is not yet identified, L will be used to represent it, with the understanding that

$$L \propto c \quad (3.67)$$

or, since the leading-edge radius is proportional to chord,

$$L \propto d \quad (3.68)$$

and the likely form of the Weber number is then

$$We_L = \frac{V^2 L \rho_w}{\sigma_{w/a}} \quad (3.69)$$

The trends apparent in figures 3.6.1 and 3.6.2 show that an increase in We_L has the same effect on glaze ice shape as an increase in n_0 ; that is, horns move back with an increase in the included horn angle as either n_0 or We_L decrease. Weber numbers with other lengths have been considered in the past, such as one based on drop size and water properties, We_δ :

$$We_\delta = \frac{V^2 \delta \rho_w}{\sigma_{w/a}} \quad (3.70)$$

Before data like those of figures 3.3.6 and 3.3.7 were available, this Weber number seemed to be the logical choice, based on the assumption that drop splashing

plays a role in establishing shapes for glaze ice, and that drop size affects splashing characterization. Anderson and Ruff³⁵, Anderson⁴⁶ and Kind³² have all used the Weber number of equation (3.70). Because in most studies, δ was scaled along with chord, matching We_δ would lead to scale velocities not much different from those obtained from matching We_L ; thus, positive scaling results from these studies do not give us clues about the correct form of Weber number.

From equations (3.68) and (3.69) the scale velocity found from $We_{L,S} = We_{L,R}$ is

$$V_S = V_R \sqrt{\frac{d_R}{d_S}} \quad (3.71)$$

As a practical matter for tests with nearly constant air density, this result is little different from that obtained using constant We_c (eq. (3.66)), but has a stronger basis in experimental evidence. Equation (3.69) provides one potential additional similarity parameter to supplement Ruff's basic scaling method.

The Weber number based on the water film thickness, h_{film} , was proposed by Feo.⁴⁷

$$We_h = \frac{V^2 h_{film} \rho_w}{\sigma_{w/a}} \quad (3.72)$$

Feo and Urdiales⁴⁸ had measured the water film thickness for heavy rain and developed the following correlation:

$$\frac{h_{film}}{d} \propto LWC^{1/2} Re_a^{-1/4} Re_\delta^{15/4} We_\delta^{-9/4} \quad (3.73)$$

Later studies by Feo⁴⁷ were made with LWC 's in the range of 2.6 to 14.5 g/m³. Although still somewhat higher than desired to represent typical icing conditions, these LWC 's were lower than those used in the heavy rain work. From this effort, the correlation

$$\frac{h_{film}}{d} = \left(\frac{LWC}{\rho_w} \right)^{1/2} Re_a^{-1/4} \quad (3.74)$$

was found. Evaluations of the water-film-thickness Weber number in scaling tests using h_{film} from equation (3.74) have been made⁴⁹ and the results compared well with those using the Weber number of equation (3.70). While these results are encouraging, the conclusions of section 3.5.13 that LWC does not have an effect on ice shape independent of freezing fraction are not consistent with a Weber-number length having the form of equation (3.74). It's possible that L may prove to be a water-film thickness of some form, however.

Another approach presented by Feo⁵⁰ involved simultaneously matching the water-film thickness and a Weber number that used the water-film velocity and water-film thickness:

$$We_k = \frac{U_w^2 h_{film} \rho_w}{\sigma_{w/a}} \quad (3.75)$$

where the water-film velocity was found by equating shear stresses at the air-water interface

$$U_w = \left(\frac{h_{film}}{d} \right)^2 V^2 Re_a \quad (3.76)$$

When equation (3.76) is incorporated into equation (3.75) and scale and reference values of h_{film}/d are equated, the scale free-stream velocity for this Feo method is

$$V_S = V_R \left(\frac{d_R}{d_S} \right)^{2/3} \quad (3.77)$$

While this approach provides a simple expression to find scale velocity, there is no fundamental reason that both film thickness and Weber number should simultaneously match. Another approach is to equate only the scale and reference We_k from equation (3.75) without requiring film thickness to match. With water-film velocity again taken from equation (3.76) and water-film thickness from equation (3.74), when the We_k are matched, the scale velocity becomes:

$$V_S = V_R \left(\frac{LWC_R}{LWC_S} \right)^{2/3} \left(\frac{d_R}{d_S} \right)^{5/9} \left(\frac{\rho_{a,R}}{\rho_{a,S}} \right)^{1/9} \left(\frac{\mu_{a,S}}{\mu_{a,R}} \right)^{1/9} \quad (3.78)$$

Kind and coauthors^{30,51,52,53} have also argued for the use of a Weber number based on water-film thickness as a similarity parameter for scaling. They introduced two alternatives, We_w and We_b , given by

$$We_w = \frac{\rho_a V^2 h_{film,A}}{\sigma_{w/a}} \quad (3.79)$$

and

$$We_b = \frac{\rho_a V^2 h_{film,B}}{\sigma_{w/a}} \quad (3.80)$$

where $h_{film,A}$ and $h_{film,B}$ are two forms of analytically derived water-film thickness ($t_{w,a}$ and $t_{w,b}$, respectively, in Kind's nomenclature). Each Weber number is similar to equation (3.72), but uses air density in place of water density. Expressions for Kind's water film thickness were derived by first applying continuity, then develop-

ing two different mean water-film velocity terms. The first, for $h_{film,A}$, was found by assuming the water film velocity was the result of aerodynamic shear stress alone (Couette flow). The resulting water-film thickness was

$$\frac{h_{film,A}}{d} \propto \left(\frac{LWC}{\rho_w} \right)^{1/2} \left(\frac{\mu_w}{\mu_a} \right)^{1/2} Re_a^{-1/2} \quad (3.81)$$

The scale velocity found by matching scale and reference Weber numbers using equations (3.79) and (3.81) was then

$$V_S = V_R \left[\left(\frac{LWC_R}{LWC_S} \right) \left(\frac{d_R}{d_S} \right) \left(\frac{\rho_{a,R}}{\rho_{a,S}} \right) \right]^{1/3} \quad (3.82)$$

As noted for other expressions discussed in this section, existing data supports the view that LWC does not have an effect on ice shape independent of the freezing fraction; therefore, equation (3.82) does not seem to be fully consistent with experimental observations. However, because the effect of LWC on V_S in equation (3.82) is weak ($LWC^{1/3}$), this expression cannot be disregarded.

The mean water-film velocity used by Kind to develop an expression for $h_{film,B}$ came from the additive effect of both shear-, as for $h_{film,A}$, and pressure-gradient- (Poiseuille-flow-) driven contributions. The resulting expression for water-film thickness is not a closed form, but must be solved by iteration:

$$h_{film,B} = \frac{\mu_w LWC V \beta (1-n) \frac{d}{2} \sin \theta}{\rho_w \frac{\rho_a V^2}{2} \left(\frac{C_f}{2} + 0.42 \Delta C_p \frac{h_{film,B}}{d} \right)} \quad (3.83)$$

Kind evaluated this film thickness at an angle of 45° from the stagnation, and ΔC_p was the change in pressure coefficient from stagnation to 45° .

In addition to the various Weber numbers described here, there are several other similarity parameters related to water film. These will be discussed next. It is possible to find a scale velocity by matching scale and reference values of any of the water-film similarity parameters.

3.6.2. Other Water-Film Parameters and Additional Methods to Determine Scale Velocity

Feo^{54,55} suggested that the non-dimensional water film thickness itself might be a critical dimension controlling surface water dynamics. Although no experimental data exist for the actual film thickness in glaze icing encounters, the correlation of equation (3.74) was obtained for cloud conditions not too much different from icing clouds. This form of h_{film} , if considered as a similarity parameter, suggests that LWC should have an

effect on ice shape independent of its effect through n_0 . As noted previously, this conclusion is not consistent with the observed effects of LWC shown in section 3.5.13, where ice shapes were seen to be invariant with changing LWC as long as n_0 was fixed. Nevertheless, the correlation of equation (3.73) was used in two recent studies^{35,46} as a possible description of h_{film}/d . Scale velocities calculated by matching scale and reference values of h_{film} from equation (3.73) were lower than the reference and gave glaze ice shapes that did not match the reference. The general conclusion of references 35 and 46 from looking at a range of scale-to-reference velocity ratios was that scale velocities needed to be higher than the reference for good simulation of glaze ice shapes when the scale model size was less than the reference.

When scale and reference values of water-film thickness were equated to find V_S using equation (3.74), the scale velocity values were typically close to those determined with the average- V method discussed next and provided generally good matches of scale and reference ice shapes.⁴⁹

Equation (3.73) suggests that the water-film thickness depends on both the Re_a and We_δ . Anderson and Ruff³⁵ and Anderson⁴⁶ used a scale velocity that was the average of those found by matching We_δ and by matching Re_a . This average velocity is

$$V_S = \frac{V_R}{2} \left(\frac{d_R}{d_S} \frac{\rho_{a,R}}{\rho_{a,S}} \frac{\mu_{a,S}}{\mu_{a,R}} + \sqrt{\frac{\delta_R}{\delta_S}} \right) \quad (3.84)$$

Excellent scaling results were typically obtained in references 35 and 46 using this average-velocity method of finding scale velocity.

Finally, the capillary number, Ca , is the ratio of viscous forces to surface-tension forces. This parameter has been used by Kind, et al^{31,32} to describe the phenomena in the surface water on glaze ice. The capillary number is

$$Ca = \frac{\mu_w V}{\sigma_{w/a}} \quad (3.85)$$

For practical scaling, the scale test will use water with viscosity and surface tension that match the reference values; thus, matching of the capillary number is equivalent to matching the scale and reference velocity. As noted previously, studies of the effect of velocity on sub-scale ice shapes^{35,46} showed the best match of reference ice shapes occurred when the scale velocity was higher than the reference. Thus, the capillary number by itself is not likely to be a useful similarity parameter. However, Kind noted that when the We_w (eq. (3.79)) is

matched, the capillary number is coincidentally matched as well.

Section 5.3.4 compares the scale velocity that results from using each of the parameters presented in sections 3.6.1 and 3.6.2 when scaling model size. Section 5.3.7 gives recommendations for how best to determine the scale test conditions, including velocity, when model size is scaled.

3.7. Other Phenomena

The physical models for icing on which the similitude parameters have been based have not been fully verified and probably do not include all phenomena that may have some effect on the ice accretion process. Close-up studies of water impact and freezing on surfaces were made by Olsen and Walker.¹⁰ They believed that shedding of water from the surface is a significant part of the ice-accretion process. Such shedding is most likely to occur from the tips of the horns. Whether such shed water is subsequently re-entrained and deposited aft of the main ice shape is not known at this time. However, water shed from the horns would not impact the accretion process at the leading edge, and therefore does not affect the analytical expression for freezing fraction at stagnation or the n_e found from the measured ice thickness there. In addition to water shedding, ice shedding is a major consideration for situations involving high speeds, rotorcraft and deicing systems. Olsen and Newton¹³ and Ruff⁷ discuss the similitude requirements for ice shedding.

Both of these shedding phenomena take place away from stagnation where the scaling analyses are focused. Thus, the present approach to scaling cannot easily incorporate such effects. Furthermore, until high-speed, close-up studies can better identify the processes taking place, shedding events will not be included in scaling methods. For typical Appendix C conditions, reasonable success with scaling has been demonstrated without including shedding.

3.8. Summary of Potential Scaling Parameters

For convenience, all the similarity parameters discussed above that appear to have the most influence on ice accretion and are therefore most likely to form the basis of a scaling method will be listed here again. All are dimensionless except for the water-energy and air-energy transfer terms (ϕ and θ) which have dimensions of temperature.

- Reynolds number, Re_a (eq. (3.1))
- Modified inertia parameter, K_0 (eq. (3.8))
- Stagnation collection efficiency, β_0 (eq. (3.13))
- Accumulation parameter, A_c (eq. (3.26))

- Relative heat factor, b (eq. (3.55))
- Water-energy transfer parameter, ϕ (eq. (3.56))
- Air-energy transfer parameter, θ (eq. (3.57))
- Freezing fraction, n_0 (eq. (3.59))
- Weber number, for example: We_c , We_L , We_δ , We_h , We_w or We_t (eqs. (3.66) (3.69), (3.70), (3.72), (3.79) or (3.80))
- Water film thickness, h_{film}/d , (eq. (3.74))

Note that in place of the modified inertia parameter, K_0 , the collection efficiency at the leading edge, β_0 , can be used. β_0 is a more sensitive parameter than K_0 . These two parameters are directly related by equation (3.13).

4. Experimental Evaluation of Scaling Methods: Studies at NASA

Many of the test results cited in this manual were obtained in the NASA Glenn Icing Research Tunnel (IRT). This facility and the experimental procedures used in testing scaling methods will be described here. In addition, facility effects on scaling results will be discussed.

4.1. NASA Glenn Icing Research Tunnel

The NASA Glenn (formerly NASA Lewis) Icing Research Tunnel (IRT) has been updated and improved several times in the last 10 years. Several of these modifications occurred over the period of time the data presented in this manual were taken. Consequently, only a general description of the tunnel will be given here. For more information, the reader is directed to the relevant IRT publications^{56,57,58,59} and references to individual scaling studies.

The IRT has a test section width of 9 ft and a height of 6 ft. The current refrigeration system and heat exchanger allows accurate control of the test-section total temperature from approximately -20 to +40°F.

A water spray system with ten spray bars simulates the conditions in a natural icing cloud. The test-section cloud drop MVD, δ , and liquid-water content, LWC , depend on spray-bar air and water pressures. The relationships among these pressures, the tunnel airspeed and the cloud properties are established periodically by a series of tunnel calibration tests.^{60,61,62} For Appendix C icing the cloud has been calibrated over a range of test-section airspeeds from 50 to 350 mph and drop median volume diameters from 14 to 50 μm . Two sets of spray nozzles, the Mod-1 and Standard nozzles, are used to provide different ranges of liquid-water content. Depending on the nozzle set, the airspeed and the drop diameter, the test-section liquid-water content can be controlled from less than 0.2 to over 5 g/m³.

Figure 4.1.1 gives the IRT Appendix-C cloud calibration envelope for both nozzle sets for a test-section velocity of 200 mph. The *LWC* range increases for lower velocities and shrinks for higher velocities. The solid line indicates the limiting envelope for the Mod-1 nozzles and the dashed line that for the Standard nozzle set. These envelopes illustrate the limitations that can be placed on available test conditions in the IRT. For example, test conditions that include a velocity of 200 mph, a drop MVD of 30 μm and an *LWC* of 0.4 g/m^3 can be seen from figure 4.1.1 to be unavailable. Similar limitations apply to all facilities, although the specific boundaries of operation may be different from those illustrated. Scaling methods can be used to determine appropriate conditions within the envelope that will simulate the results of tests at conditions outside the calibrated envelope. These methods will be discussed in section 5.2, and sample calculations will be presented in Appendix B.

4.2. Tunnel Effects

In addition to the limits inherent in the cloud calibration, several tunnel effects need to be recognized when performing scaling studies or evaluating results of scaling tests. These effects are common to all facilities, although some facilities may be more susceptible than others.

LWC is typically determined without the test model in place. Anything that changes the flow in the tunnel, such as blockage that's not centered or models that generate lift, will shift the position of the cloud. Because the cloud in an icing tunnel may only be uniform to within $\pm 20\%$, movement of the cloud will alter the centerline

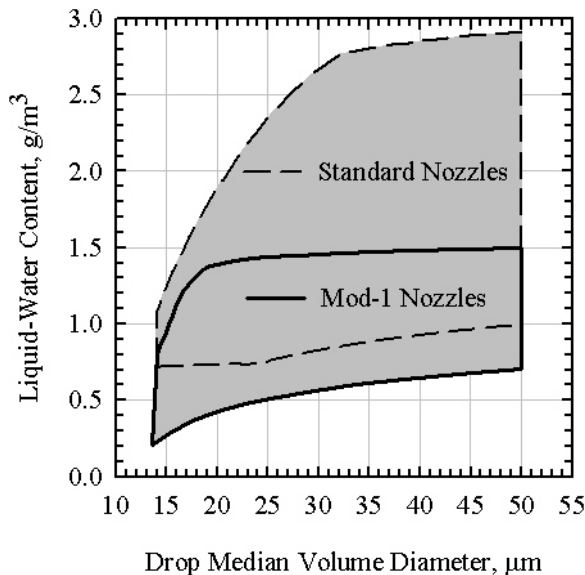


Figure 4.1.1.—IRT Calibrated Envelope for 200 mph (89 m/s).

LWC from the calibrated value. Furthermore, cloud size and *LWC* uniformity may vary with airspeed. Clearly, a non-intrusive method is needed to measure *LWC* at the test section with the model installed at the desired angle of attack. Until such a method is available users need to assure themselves of the calibration validity for their model and test conditions. Some ways to do this are outlined in the following paragraphs.

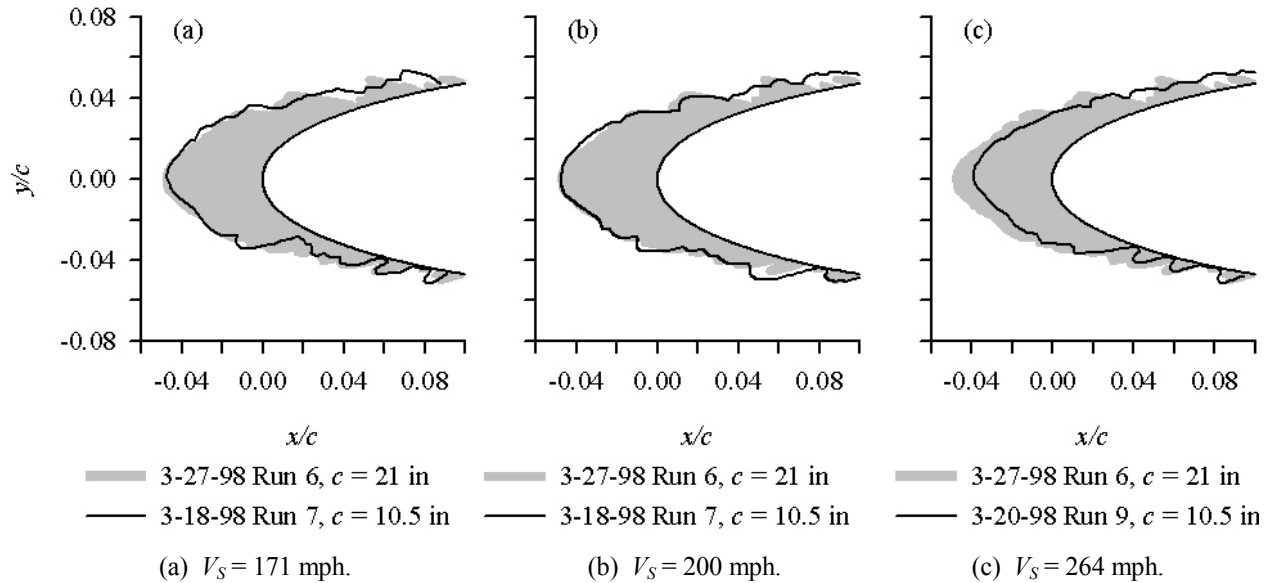
The consistency of the cloud calibration over a range of conditions should be checked with the model installed. This can be done by testing at rime conditions where proper scaling can be assured simply to matching A_c and β_0 between a reference and scale test, with both sets of conditions satisfying $n_0 = 1$. The non-dimensional ice shapes from both tests should match if the tunnel calibration is consistent for the two model sizes and sets of conditions.

For example, figure 4.2.1 reproduces rime test results from reference 35. The ice shapes recorded for three scale tests (solid lines) are compared individually with the same reference test shape (shaded). The spray-bar conditions for these tests were chosen to produce the desired *LWC* based on the tunnel calibration. The A_c reported in the table accompanying the figure was based on this calibrated value of *LWC*. The three portions of the figure show scale tests performed at three velocities: figure 4.2.1 (a) shows results for $V_S = 171$ mph, (b) for 200 mph, and (c) for 264 mph.

Good consistency of the *LWC* calibration was seen for reference and scale test conditions in figure 4.2.1 (a) and (b), but the smaller scale ice shape for part (c) indicated that at the relatively high velocity for that test, the true *LWC* was apparently lower than indicated by the tunnel calibration. Testing with *LWC*'s significantly different from assumed values affects both the quantity of ice accreted and, for glaze ice, the freezing fraction. The resulting ice shapes can lead to incorrect interpretations of scale test results.

The actual *LWC* for each test shown in figure 4.2.1 could have been determined by measuring the leading-edge thickness for each ice shape and applying equations (3.29) and (3.26) with the known value of β_0 and $n_0 = 1$.

Another tunnel effect which can affect ice accretion and influence scale test results is the possibility that water drops have frozen before impact on the model. For the IRT this can be avoided by insuring that the temperatures of the air and water in the spray bars are high enough. Tests of ice accretion with varying spray-bar temperatures have been used to establish proper operating temperatures. A related problem is the failure of water drop temperatures to reach the air temperature. This is a



Date/Run	c , in	t_{st} , °F	V , mph	δ , μm	LWC , g/m ³	τ , min	β_0 , %	A_c	n_0	b	ϕ , °F	θ , °F	Re_{δ} , 10 ⁴	We_{δ} , 10 ³	We_c , 10 ³	We_L , 10 ⁶
(a) 3-27-98/6	21.0	-5	200	40	0.51	10.0	87.6	1.75	1.00	0.36	35.3	45.0	12.07	4.93	2.67	2.08
3-18-98/7	10.5	-4	171	28	0.81	3.7	87.8	1.78	1.00	0.37	35.1	46.2	5.20	2.50	0.98	0.75
(b) 3-27-98/6	21.0	-5	200	40	0.51	10.0	87.6	1.75	1.00	0.36	35.3	45.0	12.07	4.93	2.67	2.08
3-19-98/9	10.5	-5	200	26	0.72	3.5	87.4	1.75	1.00	0.36	35.2	44.9	6.01	3.13	1.33	1.04
(c) 3-27-98/6	21.0	-5	200	40	0.51	10.0	87.6	1.75	1.00	0.36	35.3	45.0	12.07	4.93	2.67	2.08
3-20-98/9	10.5	-6	264	23	0.56	3.3	87.7	1.68	1.00	0.33	35.2	41.4	7.61	4.95	2.21	1.80

Figure 4.2.1.—Rime Scaling Tests to Check Tunnel LWC Calibration Consistency.³⁵ NACA 0012 Airfoils at 0°AOA.

particular concern in small tunnels for which drop residence time may be too short for ambient temperatures to be reached.

All of these effects need to be carefully checked; otherwise, it's difficult to know if a poor scaling result demonstrates the inadequacy of the scaling method under evaluation or a tunnel effect.

When performing scaling tests, it is always wise to perform the scale and reference tests during the same test entry whenever possible. In addition, the evaluation of a particular scaling method should be based on a large number of tests including both repeated conditions as well as a range of reference test conditions. These procedures avoid unwarranted conclusions due to random tunnel repeatability differences and help to define types of situations for which a scaling method may or may not be valid.

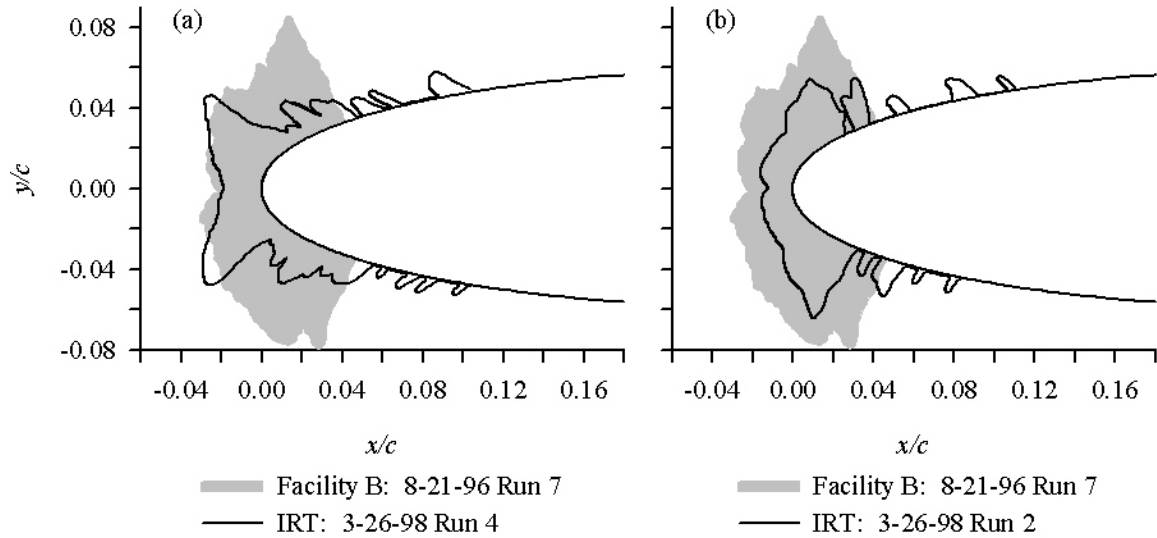
4.3. Tunnel Comparisons

Phenomena such as water-drop freeze-out or failure to reach ambient temperature can affect ice shapes. These effects can differ from one facility to another. Some of

these phenomena are influenced by the physical size and features of a tunnel. In addition, the calibrations of LWC and δ are not presently subject to any standard methods and are not based on absolute reference values. Consequently, ice shapes generated for a given set of nominal conditions cannot be expected to reproduce from one tunnel to another. Illustrations of how shapes can differ due to calibration differences will be given in this section.

In 1996, Anderson and Ruff ran a series of NACA 0012 icing tests in the IRT.³⁵ The indicated test conditions were repeated with the same models in a second tunnel. These “facility-B” test results have not been published previously. Recently, results of tests at a third icing tunnel (“facility C”) were published,³⁰ and these used nominal conditions close enough to previous IRT test conditions to provide additional data for facility comparison.. Facilities B and C both had a smaller test section than the IRT.

Figures 4.3.1 and 4.3.2 compare the ice shapes from each of the facilities. The facility-B-IRT comparisons are given in figure 4.3.1, and the facility-C-IRT comparisons



(a) Same Nominal Conditions for Both Facilities.

(b) IRT Tests at Higher Temperature than Facility B.

Fac.	Date/Run	c_s , in.	t_{stb} , °F	V , mph	δ , μm	LWC , g/m ³	τ , min	n_0
B	8-21-96/7	21	17	150	40	0.65	11.2	0.47
IRT	3-26-98/4	21	17	150	40	0.61	11.2	0.48

Fac.	Date/Run	c_s , in.	t_{stb} , °F	V , mph	δ , μm	LWC , g/m ³	τ , min	n_0
B	8-21-96/7	21	17	150	40	0.65	11.2	0.47
IRT	3-26-98/2	21	22	150	40	0.61	11.2	0.30

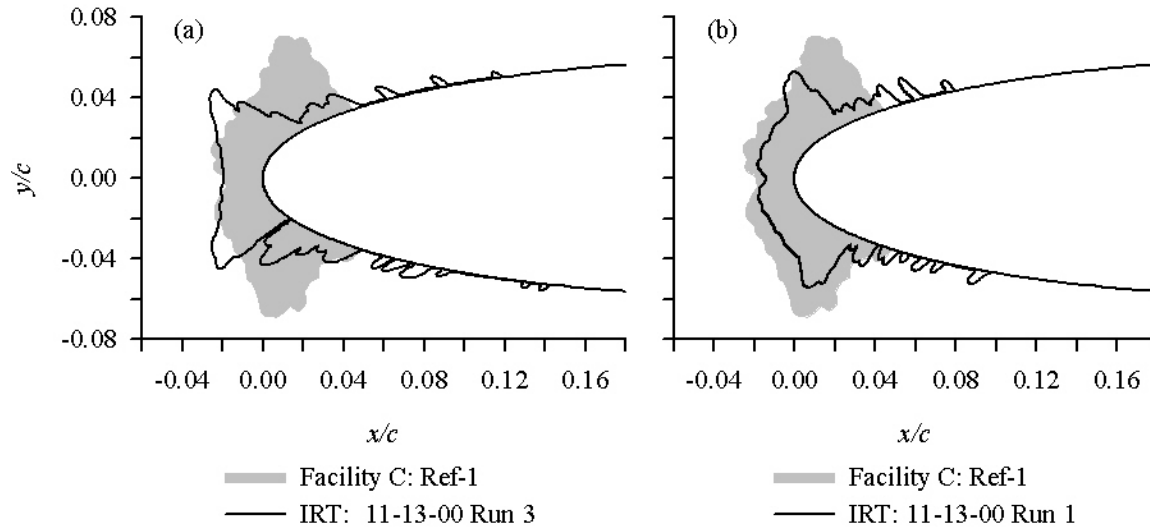
Figure 4.3.1.—Comparison of Ice Shapes Accreted in Facility B and IRT.³⁵ All Tests with NACA 0012 at 0°AOA; β_0 ; 86%; A_c , 1.90.

in 4.3.2. The shaded shapes in the two figures represent those obtained in facility B or C, respectively, and the shape with the solid line in each portion of the figures was recorded in the IRT. The shapes in figure 4.3.1 (a) were obtained with the same nominal test conditions in both tunnels. The calculated freezing fraction, based on the indicated test conditions, was 0.47 for each. The facility B accretion is significantly larger than that from the IRT and has an overall shape that is characteristic of a lower freezing fraction. Both the increased size relative to the IRT accretion and a lower freezing fraction would result from a higher LWC compared with the IRT value.

Figure 4.3.1 (b) compares the same facility B shape with one from the IRT at a reduced freezing fraction. For this illustration, the IRT freezing fraction was decreased by increasing the static temperature by 5°F (3°C) rather than by increasing LWC ; however, section 3.5.13 demonstrated that the effects of LWC changes on ice shape characteristics can also be produced by changing temperature when the freezing fraction is constant. Although the quantity of ice is still much greater for the facility-B accretion, the features of the two test results corresponded well. These results indicate that the LWC calibration for facility B gave a significantly higher LWC than that for the IRT.

Similar results were obtained when IRT shapes were compared with those from facility C in figure 4.3.2. Again, the nominal conditions in 4.3.2 (a) were the same for both facility C and the IRT. As for the facility-B shape, the facility-C shape was not only larger than that from the IRT, but had the characteristics suggestive of a lower freezing fraction. In 4.3.2 (b) the facility-C shape is compared with one from the IRT obtained at a lower freezing fraction (higher temperature), and the features, but not the size, of the two accretions were remarkably similar. Apparently, the true LWC for facility C, as for B, was significantly higher than that of the IRT for the same reported cloud conditions.

It is clear from these comparisons that the cloud LWC calibrations cannot be the same in all three facilities. Because of the differences, different conclusions will be drawn about what shape will be achieved with a particular freezing fraction. However, if these calibrations differ simply by a constant factor such that the LWC is consistent over the full range of conditions, evaluations of scaling tests should be valid in any of the facilities. Nevertheless, the true LWC must be validated for each facility to insure that users obtain realistic ice shapes and quantities. Presently, each facility is calibrated by methods used traditionally by personnel in that establishment. Standardized calibration instrumentation and methods



(a) Nominal IRT and Facility C Conditions Almost Same.

(b) IRT Tests at Higher Temperature than Facility C.

Fac.	Run	c , in.	t_{st} , °F	V , mph	δ , μm	LWC , g/m ³	τ , min	n_0
C	Ref-1	19.7	14	150	30	1.00	7.3	0.44
IRT	11-13-00/3	21.0	14	149	38	1.00	7.3	0.40

Fac.	Run	c , in.	t_{st} , °F	V , mph	δ , μm	LWC , g/m ³	τ , min	n_0
C	Ref-1	19.7	14	150	30	1.00	7.3	0.44
IRT	11-13-00/1	21.0	19	149	38	1.00	7.3	0.28

Figure 4.3.2.—Comparison of Ice Shapes Accreted in Facility C³⁰ and in IRT.³⁵ NACA 0012 Airfoil at 0° AOA for all Tests; β_0 ; 86%; A_c , 1.90.

need to be established, and the resulting calibrations must be checked against rime ice shapes as described in section 4.2. Documentation of the effects of tunnel flow (angularity and turbulence) and blockage on local cloud is also needed.

Efforts are being made to understand tunnel differences and improve calibration standards among facilities through the SAE AC-9C Icing Subcommittee.⁶³ Recent re-calibrations of the facilities compared in figures 4.3.1 and 4.3.2 could significantly change the relative shapes and sizes of the accretions shown in those figures.

4.4. Repeatability

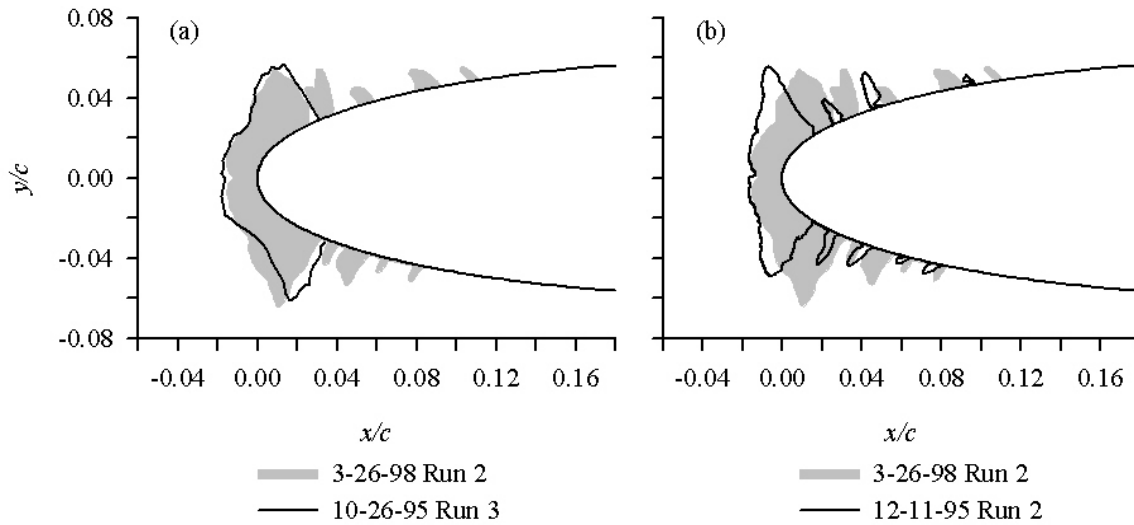
There is a random aspect to ice accretion. Each cloud of a given δ and LWC includes a distribution of drop sizes. The size of a water drop hitting a particular spot on the model at a specific time into the spray may be different for each repeated test run. Small variations in local temperature, δ and LWC in the cloud occur with position and with time. At the same time, there is some (usually small) variability in the test conditions from run to run. Because of the random nature and test variability, some differences in accreted ice shape from one run to another and from one test entry to another can be expected.

Testing of scaling methods requires comparing ice shapes recorded during separate tunnel tests, one using a reference model with reference test conditions and one

using the scale model with scale conditions. It is necessary, then, to document the extent of the shape variation from run to run to determine how closely scaled shapes can be expected to agree. Whenever tunnel physical features or spray-bar characteristics are changed, the tunnel should be re-calibrated. The new calibration should permit the V , δ and LWC at the test-section center to reproduce values previously obtained such that tests performed with the new calibration will give ice shapes in reasonable agreement with those found up to that time.

Figure 4.4.1 compares ice shapes taken from 1995 through 1998 in the NASA Glenn IRT using the same model and the same test conditions each time. In figure 4.4.1 (a) a March 1998 shape (shaded) is compared with one taken in October 1995. The gross features, including the leading-edge thickness, the horn size and the horn positions, of the main ice shape repeated well with only minor differences. Apparently, the feathers were not traced in the October 1995 test. In general, this comparison shows very good repeatability of the shapes. Good repeatability of shapes in the IRT is typical. It suggests that the random aspects of icing cited earlier have only a small effect on the major features of ice accretions.

Occasionally, ice shapes do not repeat well from one entry to another, however, and the reasons are not well understood. This situation is shown in figure 4.4.1 (b) where a December 1995 test produced significant



(a) October 1995 Compared with March 1998.

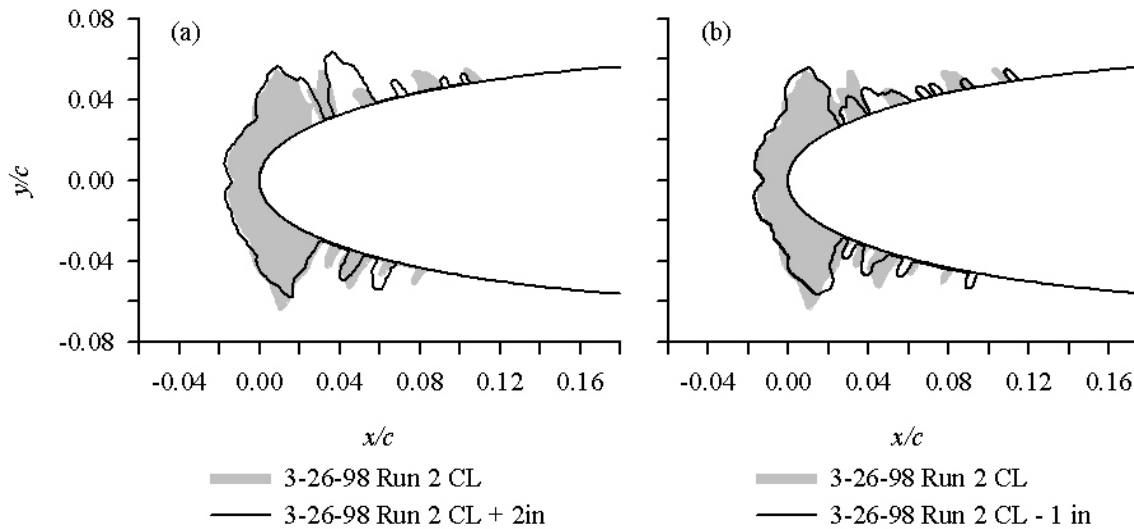
(b) December 1995 Compared with March 1998.

Figure 4.4.1.—Ice Shape Repeatability in IRT. 21-in- (53.3-cm-) Chord NACA 0012 Airfoil at 0°AOA Tested with same Conditions on Three Entries. t_{st} , 22°F (-6°C); V , 150 mph (67 m/s); δ , 40 μ m; LWC , 0.65 g/m³; τ , 11.2 min.

differences from that of March 1998. While the leading-edge thickness matched, the horn size and angle were different for the two shapes. If the accretions in figure 4.4.1 (b) had been produced from a test of a particular scaling method, the conclusion might well be that the shapes did not agree sufficiently well to validate that method. When evaluating scaling methods, it is important to repeat tests several times with multiple tunnel entries to avoid mistaken conclusions.

Another issue that arises with respect to comparing

shapes recorded by hand tracing is the variability of the recorded shape due to the inaccuracy of the method. Figure 4.4.2 is a comparison of the mid-span tracing of an ice accretion with tracings made 2 in (5 cm) above mid-span (fig. 4.4.2 (a)) and with one made 1 in (2.5 cm) below mid-span (fig. 4.4.2 (b)). The March 1998 ice shape from figure 4.4.1 (mid-span position) has been used again for this illustration. For all three tracing sites the leading-edge thickness and most of the features of the main ice shape were reproduced very consistently. The horn tips varied somewhat from one tracing to another;



(a) Tracings at Mid-Span (CL) and 2 in Above.

(b) Tracings at Mid-Span (CL) and 1 in Below.

Figure 4.4.2.—Comparison of Tracings at Different Span-wise Locations in IRT. 21-in- (53.3-cm-) Chord NACA 0012 Airfoil at 0°AOA; t_{st} , 22°F (-6°C); V , 150 mph (67 m/s); δ , 40 μ m; LWC , 0.65 g/m³; τ , 11.2 min.

some of this variation may have been due to actual differences over the span of the model and some to the pencil tracing technique itself. The feather size and location show the greatest diversity, which reflects the reality that feather formation is generally the result of random impacts of drops or possibly of water shed from the tips of the horns. Thus their size and density vary randomly along the span, and it is not realistic to expect scaling methods to precisely reproduce the specific location of feathers from a reference test, although the approximate feather size in a general location on the model should be simulated.

4.5. IRT Scaling Models

Scaling studies in the IRT have used cylinders, GLC 305 airfoils and NACA 0012 airfoils made from aluminum, fiberglass and wood. Airfoil chords have ranged from 5 to 36 in. All models were mounted vertically in the center of the IRT test section. Figure 4.5.1 shows typical NACA 0012 models in the IRT test section. In figure 4.5.1 (a) a 6-ft-span, 36-in-chord fiberglass airfoil section can be seen, and 4.5.1 (b) shows a 2-ft-span, 21-in-chord



(a) 91.4-cm-Chord NACA 0012 Model Installed in IRT Test Section.

Figure 4.5.1.—NACA 0012 Airfoil Models in IRT Test Section.



(b) 21-in- (53.3-cm-) Chord NACA 0012 Model Installed in IRT Test Section.

Figure 4.5.1.—concluded.

aluminum model. The shorter-span models were placed between end plates. The models' mid spans were located on the tunnel centerline (midway between floor and ceiling of the test section). Three to five horizontal lines were typically marked around the leading edge of each airfoil to indicate the mid-span and of positions 1 and 2 in above and below mid-span for locating ice-tracing templates. Shapes were recorded by hand tracing.

4.6. IRT Scaling Test Procedures

The typical procedure involved setting the temperature, airspeed and spray-bar air and water pressures for the test. Once these pressures stabilized, the water valves were opened to initiate the spray, and the spray timer was started. Before 1997, once the water valves were opened, water and air pressures sometimes took a minute or more to stabilize. Because spray duration is timed from the opening of the valves, when testing with the earlier system it was necessary either to shield the model until the spray had stabilized or to add time to correct for the ramp-up period. This correction was typically 20 sec. Spray times reported for pre-1997 tests were the desired exposure times before this spray extension was added. For icing exposures of about 10 minutes or more, errors in the correction applied to the spray time could be on the order of 30 sec without having any noticeable effect on the total quantity of ice accreted. A correction to the spray time was applied by Olsen and Newton¹³ in their

scaling tests in the 1980's and by Bilanin and Anderson⁴² and Anderson^{33,34,64,65} for models of 21-in chord and larger in scaling tests before 1996.

IRT scaling tests in 1995 employed a metal shield in front of models smaller than 21-in chord. When the cloud had stabilized, the shield was raised and the spray timing initiated. A complete description of this technique is given in references 34 and 65. Although the spray conditions were steady throughout the test using this shield, the test-section blockage changed when the shield was raised, and some transients in the airspeed were experienced.

An improved shield system was used for tests in 1996. A fabric patch was attached to the front of the model using Velcro strips. This shield was large enough to cover the leading-edge region of the model back to at least 20% chord and 16 in of the span around the centerline of the tunnel. Because the shield conformed to the shape of the model, it did not change the tunnel blockage as the metal shield had done. A rope was attached to the shield and passed through a port in the ceiling of the tunnel. When the cloud was stabilized, the shield was manually pulled free from the model and through the port.

The IRT spray system was rebuilt in 1997.⁵⁸ The 10-bar spray system now recirculates water to permit the stabilization of air and water pressures prior to opening the water valve at each nozzle. This feature virtually eliminates start-up transients. Consequently, for tests made after this upgrade neither shielding nor corrections to the spray time have been needed. Comparisons of ice shapes obtained before and after the new spray-bar system was installed showed good repeatability. These comparisons tend to validate the methods used to account for spray-bar transients with the old system.

At the completion of the icing spray time, the spray was turned off and the tunnel fan was stopped. Personnel then entered the test section, and a thin heated plate was used to cut horizontal slices into the accreted ice at the desired span-wise locations. The ice shape cross-sections were traced onto cardboard templates and later digitized for computer storage. Finally, the model was cleaned and the procedure repeated for the next test.

5. Description and Evaluation of Scaling Methods

The evaluation of scaling methods involves choosing a series of reference test conditions, applying either size scaling or test-parameter scaling to develop corresponding scale conditions and performing both the reference and scale tests in an icing wind tunnel. Ice shapes are recorded for both reference and scale tests and compared.

At the present time, quantification of these ice shapes has not progressed sufficiently to permit objective, numerical comparison of ice shapes, although some approaches have been proposed and evaluated.⁶⁶ Consequently, it is necessary to plot ice shapes and visually match them to make subjective judgments of whether two tests have produced the same shape. In this section, scaling studies will be reviewed and ice shapes compared from a number of studies. The purpose of these comparisons is to assess the effectiveness of scaling methods and, when possible, to deduce how significant each of the scaling parameters identified in section 3 is to determining the ice shape. This kind of sensitivity analysis is important to developing improved scaling methods, but it can also lead to a better understanding of the basic physics of ice accretion. The insight gained can be used to refine ice-accretion prediction codes as well.

5.1. Basic Approach to Scaling Method Development

Section 3 gave the definition and derivation of several similarity parameters. The matching of scale and reference values of each similarity parameter provides one of a set of equations that can be solved for the scale test conditions. For sea-level tunnels, after the scale model size has been chosen, five scaled test conditions (temperature, airspeed, drop size, cloud liquid-water content and exposure time) need to be determined. For altitude tunnels, the scale pressure adds a sixth variable. Thus, a system of only five or six equations is needed, and a choice must be made of those similarity parameters most likely to affect ice shape for the conditions of interest. For some scaling methods, various test conditions themselves are matched to the reference values so that even fewer similarity parameters are used. In some cases, it is not possible or practical to match certain parameters; for example, in section 3.2, it was noted that Re_a and M_a cannot both be matched if scale model size differs from the full scale.

The scale test is defined first by the model size, which is selected by the test designer. For test-condition scaling, the model size is equal to the reference. For both test-condition and size scaling the scale model geometry and AOA must be the same as the reference. Two test parameters can be found by applying similarity of drop trajectories and water catch. The remaining parameters can be computed from the equations formed by matching various terms in the energy balance and expressions related to surface phenomena. The scaling methods that have been proposed differ primarily in which of these energy terms or surface parameters are matched.

Table I compares scaling methods that have been evaluated by various studies in the past 30 years. Earlier methods described by Sibley and Smith,¹⁶ Dodson,¹⁷ and

Table I.—Comparison of Some Published Scaling Methods

Method	Test Conditions							Similarity Parameters										
	d	t_{st}	p_{st}	V	δ	LWC	τ	K_0	A_c	n_0	b	r_A	ϕ	θ	Ca	Re_a	We_δ	M_a
$LWC \times \text{time}^{68}$	M	M	M	M	M	s	calc	(m)	M				(m)	(m)	(m)	(m)	(m)	(m)
Olsen ^{33,68}	M	calc	M	M	M	s	calc	(m)	M	M					(m)	(m)	(m)	(m)
Ingelman-Sundberg ⁷³	s	M	a	s	calc	M	calc	M	M									
ONERA ^{14,15}	s	a	a	calc	calc	calc	calc	M	M	M	M							
Ruff ⁷ - 1	s	M	M	s	calc	s	calc	M	M									
Ruff ⁷ - 2	s	calc	M	s	calc	s	calc	M	M	M								
Ruff ⁷ - 3	s	calc	M	s	calc	calc	calc	M	M	M	M							
Ruff ⁷ - 4*	s	calc	calc	s ¹	calc	calc	calc	M	M	M	(m)		M	M				
Mod. Ruff ⁶⁸	s	calc	a	s ¹	calc	calc	calc	M	M	M			M					
Kind ³² - 1	s	M	a	calc	calc	calc	calc	M	M			M					M	
Kind ³² - 2	s	M	a	(m)	calc	calc	calc	M	M			M	(m)		M			(m)

* AEDC Method

- M matched to reference value
- (m) coincidentally matched to reference value
- s specified by user
- s¹ one of the test conditions t_{st} , p_{st} , V , δ or LWC can be selected
- a determined by ambient conditions and test parameters
- calc calculated from matched parameters

Hauger and Engler⁶⁷ will not be discussed here. Methods proposed in the past few years that involve similarity parameters other than those in the table have not been included but will be discussed in section 5.3. Ruff⁷ evaluated four approaches to scaling, and all four are listed in the table. The “modified-Ruff method” shown is an adaptation of his method 4 for sea-level facilities—that is, facilities with no ability to control test-section pressure. Because this facility limitation exists for the IRT as well as many other facilities, the “modified-Ruff method” will be simply called the “Ruff method” in the remainder of this manual.

Table I includes examples of both test-condition and size-scaling methods, indicating the similarity parameters that are matched between scale and reference. The general way scale test conditions are determined is shown: whether they are matched to the reference, calculated by matching scaling parameters or determined by ambient conditions. For example, in the ONERA method the user first specifies the scale model size, d . Then the test conditions t_{st} , V , δ , LWC and τ are calculated by matching the similarity parameters K_0 , A_c , n_0 and b . Because the

ONERA tunnel at Modane, for which this method was developed, has no control of pressure or temperature, the static values of these conditions are determined by the environment. In this way, all the conditions for the scale test are established.

Note that the Ruff method 2 reduces to the Olsen method if the scale model size, velocity and drop size are chosen to be the same as the respective reference values. Both the ONERA and Ruff methods will be described in more detail in section 5.3.

5.2. Methods to Scale Test Conditions

In section 4.1 it was noted that the calibrated envelope of an icing facility can leave some combinations of MVD and LWC unobtainable. Facilities are also limited with respect to the velocity which can be tested. Furthermore, substitutions for temperature or pressure are sometimes necessary. By applying test-conditions scaling, alternatives for each of these test conditions can often be found that fall within the facility capability yet provide an ice shape that simulates that of the reference (desired) conditions. Test-condition scaling methods will be discussed here.

5.2.1. LWC

5.2.1.1. LWC × Time = Constant

The simplest scaling method is used for *LWC* scaling⁶⁸ and explicitly satisfies only water-catch similarity (matching the accumulation parameter.) For this application, scale model size, temperature, pressure, airspeed and drop size are matched to the corresponding reference values:

$$c_S = c_R \quad (5.1)$$

$$t_{st,S} = t_{st,R} \quad (5.2)$$

$$p_{st,S} = p_{st,R} \quad (5.3)$$

$$V_S = V_R \quad (5.4)$$

$$\delta_S = \delta_R \quad (5.5)$$

It is understood, of course, that scale model geometry and AOA are the same as the reference. When the scale and reference values for the accumulation parameter, equation (3.26), are equated and constants cancelled, the product of the liquid-water content and time is seen to match:

$$LWC_S \tau_S = LWC_R \tau_R \quad (5.6)$$

The user chooses the scale *LWC* and from equation (5.6), the scale accretion time can be found. The leading-edge heat balance is assumed to be satisfied simply by matching the static temperature. The modified inertia parameter, K_θ , is matched because the model size, velocity, cloud drop size and ambient pressure have been matched. The effect of liquid-water content on the heat balance is ignored.

In addition, because the model size, airspeed and drop size are maintained at reference values, Re_a , M_d and various Weber numbers also match coincidentally. From equations (3.56) and (3.57) it is apparent that equating the scale and reference static temperatures, pressures and velocities insures that scale and reference values of both ϕ and θ will also be equal. Thus, this method satisfies equality of most of the parameters listed in section 3.8; the scale values of only n_θ , b , r_A , and h_{film}/d differ from the reference values.

Evaluations of the ‘*LWC* × time = constant’ method have been made in the NASA-Glenn IRT^{33,34,64} using both cylinders and a 21-in- (53.3-cm-) chord NACA 0012.

More details about the models and test procedures were given in the references. Figure 3.5.2 (a) and (b) showed one set of results for which the *LWC* was decreased from 1.4 to 1.0 then to 0.8 g/m³ with the time increased to satisfy equation (5.6) and all other test conditions constant. Although the total quantity of ice accreted appeared to be constant, the increasing freezing fraction caused a decrease in the horn angle. The leading-edge ice thickness would also tend to increase with decreasing *LWC* (increasing n_θ). For rime conditions, this method would be effective providing the temperature was low enough that rime was maintained for all *LWC*’s. For glaze ice at very small accumulation parameters (very short accretion times), the change in horn angle might not be noticed. But in general, figure 3.5.2 shows that this method fails because it does not maintain freezing fraction constant.

The ‘*LWC* × time = constant’ scaling method is simple to apply and convenient to use when data are needed at liquid-water contents not available in flight or not achievable in an icing tunnel. Unfortunately, as figure 3.5.2 demonstrates, simply matching static temperatures is not an adequate way to account for the leading-edge energy balance.

5.2.1.2. Olsen Method

A refinement of the ‘*LWC* × τ = constant’ method was suggested by Olsen and Newton.^{13,68} As with the previous method, the user selects the scale *LWC*, while maintaining chord, velocity and drop size unchanged (i.e., equations (5.1), (5.4), and (5.5) are satisfied.) Since model size, airspeed and water drop size are unchanged from the reference values, $K_{\theta,S} = K_{\theta,R}$. The scale icing time is once more found from equation (5.6) to insure that $A_{c,S} = A_{c,R}$. But, in the Olsen method, the freezing fraction is matched instead of the static temperature. The scale static temperature is then calculated from the scale freezing fraction. This constraint of calculating a static temperature to insure a specific freezing fraction makes the Olsen method less convenient to use than the ‘*LWC* × τ = constant’ method, but gives more confidence that the scale ice shape will simulate the shape which would have accreted if the desired conditions could have been tested.

Olsen and Newton proposed the Olsen method for use in size scaling as well as test-condition scaling. However, we have subsequently learned that when size is scaled, the scale and reference velocity cannot match if surface-water phenomena are properly simulated. Therefore, the Olsen method can only be applied when the model size of scale and reference cases is the same.

Experimental evaluations of this method have been reported in references 33 and 34. The scale results were compared with the same reference cases as used in the

NASA Glenn ' $LWC \times \text{time} = \text{constant}$ ' study discussed above. Typical results were shown in figure 3.5.3. It is apparent from that figure that the scale ice shapes using the Olsen method are significantly better simulations of the reference shapes than were those from the ' $LWC \times \text{time} = \text{constant}$ ' method (fig. 3.5.2). The Olsen method results in the correct size, location and angle of glaze horns, and the feathers aft of the horns also appear to be well matched in size to those on the reference accretion.

Ruff's⁷ method 2 was identical to the Olsen method. However, in his tests he found that "...the size and locations of the glaze horns are not adequately reproduced." He concluded that this method can only be used to simulate the type of ice but not the shape. It is possible that Ruff's tests failed to give the good match of shapes demonstrated in the IRT because of problems with his facility LWC calibration. This speculation is also consistent with Bilanin's³⁹ inability to calculate experimental freezing fractions from Ruff's ice shapes that were consistent with analytical values (see section 3.5.14).

The success of the Olsen method over the ' $LWC \times \tau = \text{constant}$ ' method in simulating the reference ice-shape features is a result of requiring that the scale freezing fraction match the reference. Glaze ice shapes appear to be more sensitive to changes in n_0 than to variations in the other heat-balance parameters, b , ϕ , θ or r_A . The Olsen-method results show once again that the freezing fraction is one of the fundamental similarity parameters that must be matched for good scaling. The Olsen method is based on a fundamentally sound approach, but has been experimentally validated over only a specific range of test conditions. Therefore, some caution may be warranted for application to other conditions.

5.2.2. Temperature

Figures 3.5.4 and 3.5.5 showed that when the total temperature is higher than about 27°F ice shape characteristics can be quite different from those at lower temperatures. The size-scaling method recommended below in section 5.3.7 will give scale total temperatures higher than the reference, and it is possible for some sets of conditions for the resulting scale total to exceed the 27°F limit. If the original reference total temperature was below 27°F, the scale temperature should be scaled to a value below this limit as well.

With model, velocity and drop size fixed, temperature scaling can be accomplished using the Olsen method described in section 5.2.1.2. The premise of the Olsen method is that with c , V and δ constant, scale and reference ice shapes will match if the scale n_0 matches the reference. To apply the Olsen method for temperature scaling, one first selects a scale static temperature so that

the scale total temperature will be below 27°F. Then the scale LWC is calculated so that scale freezing fraction is the same as the reference value. Finally, the accretion time is determined by matching scale and reference A_c .

5.2.3. Drop Size

Figures 3.3.6 and 3.3.7 showed that drop size variations from 15 to 20, from 25 to 40 and from 20 to 55 μm had no apparent effect on the main ice shape for the conditions and models tested. These observations imply that for Appendix-C conditions, if a test is needed with a value of δ outside the tunnel capability, it should be possible to substitute a value within the tunnel operating map to simulate the desired ice shape. With model size and velocity unchanged from the reference, temperature would have to be adjusted to maintain n_0 because δ influences n_0 through β_0 . Time would also need to be set so that the product $\beta_0 A_c$ was maintained the same as for the reference conditions.

There are some limitations to this approach, however. First, very small drops cannot be used to simulate accretions with larger drops. The discussion following equation (3.8) noted that when the inertia parameter, K , is less than 1/8, drops will not impinge on the model. Therefore, there must be a lower limit of drop MVD, dependent on model size and velocity, below which ice shapes will differ from those produced with larger drops. Furthermore, the lack of effect of MVD on ice shape has not been tested for drop sizes below 15 μm , and it cannot be assumed that the conclusions of figures 3.3.6 and 3.3.7 apply to drops smaller than 15 μm .

Second, changes to δ also affect the impingement limit. The impingement limit is dependent on β_0 ; thus, it should be possible to establish that limit experimentally with any combination of velocity and drop size that produced the reference β_0 for the given model. For any test, it is always desirable to determine test conditions such that the β_0 is as close a match to that for the conditions to be simulated as possible.

The insensitivity of ice shapes to drop size as shown in figures 3.3.6 and 3.3.7 were for Appendix-C conditions and cannot be expected to be valid in general for SLD conditions. Even within Appendix C the observation that drop size has little effect on ice shape comes from only limited testing. Tests over a range of speed, model size and cloud conditions are needed before a method of drop-size substitution can be recommended with any confidence. Some such tests are currently being conducted at the NASA Glenn IRT for both Appendix C and SLD conditions to try to define the limits of conditions for which an available MVD can be used in an icing test to simulate results with another.

5.2.4. Airspeed

If a test is required to simulate airspeed outside the available range for a facility, the user would start by selecting a more suitable value. Typically, the desired (reference) velocity would be higher than the facility permits, so the scale velocity will be lower than the reference. No studies have been made specifically to evaluate ways to scale airspeed. However, based on knowledge of what similarity parameters are most important to ice accretion, it is possible to propose a method.

At the present time, We_L appears to be one of the leading candidates of similarity parameter related to surface-water effects. In order to match scale and reference We_L , equation (3.71) shows that scale model size must be greater than the reference if $V_S < V_R$. This fact will limit the usefulness of this method. For situations for which this approach can be applied, however, LWC_S can be chosen arbitrarily. Then by setting $K_{0,S} = K_{0,R}$, $A_{c,S} = A_{c,R}$ and $n_{0,S} = n_{0,R}$, the scale δ , τ and t_{st} can be found, respectively. Additional testing is needed to verify this approach, so it should be used with caution.

For very short accretion times, for which features like horns have not yet developed, it should be possible to ignore We_L , match the model size and choose the scale velocity arbitrarily, but the limits of this approach have not been defined.

5.2.5. Pressure (Altitude)

Many icing wind tunnels do not have the capability to simulate altitude by controlling test-section pressure. The scaling method evaluations shown in this manual were obtained primarily in the IRT, which is a sea-level facility. Yet, aircraft are flown in icing conditions at altitudes of 20,000 ft (6000 m) and more, and it is often necessary to simulate the altitude ice accretion in sea-level facilities. Thus, the question of what effect pressure has on ice shapes is an important one and deserves review in some detail.

This issue has been discussed by Bartlett.^{43,44,69} In reference 44 he reported, "The data base at AEDC indicates that pressure changes have an almost insignificant effect upon the formation of ice." He also presented⁶⁹ limited ice shape data taken on a 2-in-diameter cylinder in the AEDC Icing Research Test Cell. The data were for temperatures of 4 and 23°F, a velocity of 250 ft/sec, MVD of 28 μm , an LWC of 0.8 g/m^3 and spray times of 18 and 19 min. The static pressures were 8, 10, 12 and 14 psia for each of the two sets of tests (one set at each temperature). Within the tunnel ice-shape repeatability, there was no effect of pressure. Bartlett concluded, "The effects of pressure (altitude) on icing similitude in the range studied herein are negligible..."

The National Research Council, Canada and the Centro Italiano Ricerche Aerospaziali (CIRA) jointly conducted a series of tests at the NRC Altitude Icing Wind Tunnel. Oleskiw, et al.⁴⁵ reported that when test conditions were repeated with only pressure varied, pressure produced "only relatively small changes" in the main ice shape. The published ice shapes showed differences no greater than those typically observed when tests were repeated.

De Gregorio, et al.^{70,71} reported more of the results from the same NRC/CIRA test series. Within ice-shape repeatability, pressures of 14.7, 12.7 and 8.2 psia (101, 87 and 56 kPa) had no effect on ice shape at a temperature of 14°F (-10°C), V of 212 mph (95 m/s), δ of 23 μm , LWC of 0.85 g/m^3 and spray time of 10 min. All but one of the other sets of data comparing accretions at high and low pressure showed evidence of drop freeze out for the low-pressure test, so no conclusions about the effect of pressure could be reached.

These experimental results lead to the conclusion that to scale altitude test conditions for a sea-level tunnel test, the correct ice shapes can be achieved by simply matching the desired model size and temperature, velocity, drop size, liquid-water content and spray time while using the available tunnel pressure.

The observed lack of a pressure effect on ice shapes was also cited in section 3.6 to help deduce the importance of some of the scaling parameters with regard to their role in ice-accretion physics. We can deduce that parameters that are strongly affected by pressure cannot have a major effect on ice shape, while those parameters that most strongly influence the ice shape must be independent of pressure or have only a weak dependence.

Table II is a compilation of the calculated effects of pressure on each of the similarity parameters. The pressure-altitude relation is from the U.S. Standard Atmosphere.⁷² The values were based on an NACA 0012 with a chord of 21 in. The parameters K_0 , β_0 , A_c , n_0 , ϕ , We_δ , We_L , Ca and r_A do not vary with pressure, or the change is less than 10% over the pressure range shown. The lack of an experimental effect of pressure on ice shape is thus consistent with what has already been assumed or shown about the importance of K_0 (β_0), A_c and n_0 on ice shape. Even for a chord of 72 in, the effect of pressure on β_0 , over the range of pressure shown and for the velocity given, is less than 10%. For higher velocities, the variation of β_0 with pressure is even less than that shown. The matching of K_0 between scale and reference cases insures matching of β_0 , but K_0 in Table II increased by 30% as pressure dropped over the range given; thus, while size-scaling methods commonly include this parameter, its change with pressure suggests that it does not need to be matched rigorously. Although drop MVD (and therefore

Table II.

Effect of Pressure (Altitude) on Similarity Parameters
 c , 21 in; t_{st} , 20°F; t_{tot} , 24°F; V , 150 mph; δ , 30 μ m; LWC , 1 g/m³; time, 7.3 min. NACA 0012 Airfoil. Pressures from *U.S. Standard Atmosphere, 1976*.⁷²

p_{st} , psia	14.7	12.2	10.1	8.3	6.8
Altitude, ft	0	5000	10000	15000	20000
K_0	3.58	3.84	4.13	4.43	4.78
β_0 , %	80.0	80.8	81.8	82.7	83.6
A_c	1.90	1.90	1.90	1.90	1.90
n_0	0.27	0.27	0.27	0.27	0.27
b	0.54	0.60	0.66	0.74	0.83
ϕ , °F	11.0	11.0	11.0	11.0	11.0
θ , °F	14.8	16.1	17.9	20.0	22.8
r_A	0.24	0.24	0.25	0.25	0.26
Re_a , 10 ⁴	8.95	7.45	6.16	5.05	4.11
We_δ , 10 ³	2.07	2.07	2.07	2.07	2.07
We_c , 10 ³	1.54	1.28	1.06	0.87	0.71
We_L , 10 ⁶	1.16	1.16	1.16	1.16	1.16
M_a	0.20	0.20	0.20	0.20	0.20
Ca	1.84	1.84	1.84	1.84	1.84

K_0 or β_0) are important for determining impingement limits, figures 3.3.6 and 3.3.7 demonstrated that it does not have a significant effect on the main ice shape. The studies of the effects of pressure cited above concentrated on main ice shape effects.

Both θ and b change significantly with pressure; therefore, neither of these parameters can have a strong independent effect on ice shape.

Since pressure has little or no discernible effect on ice shape, if the Weber number does affect ice shape, it must be in a form that is independent of pressure. Because of the change in air density, We_c (based on model size and air density) decreases to about half its sea-level value when pressure is reduced to simulate a 6000-m altitude. Thus, it would seem that the appropriate Weber number must be one dependent on the density of water, rather than air; for example, We_δ or We_L (eqs. (3.70) or (3.69)).

The effect of pressure on air density also reduces Re_a to about half its sea-level value when pressure is reduced to the 20,000-ft-altitude level. This result suggests that if Re_a has any effect on ice shape, it is likely to be a weak one.

Thus, all the evidence indicates that pressure effects can be ignored when altitude ice accretion is to be simulated in sea-level tunnels. However, a rigorous pressure-scaling method can be devised based on matching those

similarity parameters that have been shown to be important. This scaling method has not been tested, and it needs to be validated in a pressure-controlled tunnel before it can be recommended. With model size, velocity and LWC matched and the reference and scale pressures defined, the scale drop size is calculated so that the scale and reference K_0 match. The resulting scale drop size could differ from the reference by 15 to 20%. Because drop size has a minor effect on freezing fraction, a new temperature should be calculated such that the scale freezing fraction matches the reference. The scale temperature will differ from the reference by only a small amount, perhaps on the order of 1°F. Because d , V and LWC were all matched to the reference, the accumulation parameter will match, and the scale and reference icing time will be the same.

5.2.6 Summary of Methods to Scale Test Parameters

Table III summarizes the methods discussed above for scaling test parameters. The Olsen method is recommended for scaling either LWC or t_{st} , using the approaches described in sections 5.2.1.2 and 5.2.2 and outlined in Table III. Methods to scale drop size, air-speed and pressure are proposed, based on matching the similarity parameters of importance to scaling ice shapes. These proposed methods for scaling δ , V and p_{st} have not been tested, and thorough testing is required before those methods can be recommended.

5.3. Methods to Scale Model Size

A common application of scaling is for testing situations in which the facility restricts the size of model that can be used. Scaling methods are applied to find test conditions for the subscale model that will produce ice shapes similar to those that would accrete on a full-sized, or reference, model. A number of methods have been developed through the years but only three will be discussed here to illustrate some of the different approaches which have been used. The recommended method to scale size will be given in section 5.3.7.

Table IV compares the way the scaled test parameters are determined in the three scaling methods. For all three, with scale model geometry and AOA the same as the reference, the user selects the scale model size. The test conditions are then found by different strategies. In the following sections, these approaches to finding the appropriate scale conditions will be discussed further.

5.3.1. Ingelman-Sundberg

The Swedish-Soviet Working Group on Aircraft Safety described a size-scaling method⁷³ that relied on matching only the similarity parameters K_0 and A_c and test conditions t_{st} and LWC (see Table I.) The user specifies the

Table III.—Methods for Scaling Test Conditions

Test Condition to be Scaled	Test Conditions							Similarity Parameters									
	<i>d</i>	<i>t_{st}</i>	<i>p_{st}</i>	<i>V</i>	δ	<i>LWC</i>	τ	<i>K₀</i>	<i>A_c</i>	<i>n₀</i>	<i>b</i>	ϕ	θ	<i>Re_a</i>	<i>We_δ</i>	<i>We_L</i>	<i>M_a</i>
<i>LWC</i> *	M	calc	M	M	M	s	calc	(m)	M	M				(m)	(m)	(m)	(m)
<i>t_{st}</i> *	M	s	M	M	M	calc	calc	(m)	M	M					(m)	(m)	
δ	M	calc	a	calc	s	M	calc	M	M	M							
<i>V</i>	calc	calc	a	s	calc	M	calc	M	M	M						M	
<i>p_{st}</i>	M	calc	s	M	calc	M	M	M	(m)	M						(m)	

* Olsen method

M	matched to reference value	a	determined by ambient conditions and test parameters
(m)	coincidentally matched to reference value	calc	calculated from matched parameters
s	specified by user		

scale model size and velocity. With model size and velocity given, the drop size can be determined by matching scale and reference *K₀*, and, with *LWC_S* and *V_S* known, icing time can be found by matching *A_c*. If scale and reference velocities are the same, the freezing fractions will also match, but, other than for this special case, this method does not recognize the importance of the freezing fraction. Furthermore, as we now know, velocity has too great an effect on ice shape to be chosen arbitrarily. Tests in reference 64 showed that this method is inadequate in general to provide a good simulation of glaze ice shapes. However, for rime ice or for very short accretion times, for which glaze features have not yet formed, the Ingelman-Sundberg method should be adequate.

Table IV.

Methods to Determine Scale Test Conditions For Size Scaling

Test Parameter	Ingelman-Sundberg ⁷³	ONERA ^{14,15}	Ruff ⁷
<i>c_S</i>	user selects	user selects	user selects
<i>t_{st,S}</i>	= <i>t_{st,R}</i>	<i>t_{tot,S}</i> known	$\phi_S = \phi_R$
<i>V_S</i>	user selects	<i>n_{0,S}</i> = <i>n_{0,R}</i>	user selects (typical)
<i>MVD_S</i>	<i>K_{0,S}</i> = <i>K_{0,R}</i>	<i>K_{0,S}</i> = <i>K_{0,R}</i>	<i>K_{0,S}</i> = <i>K_{0,R}</i>
<i>LWC_S</i>	= <i>LWC_R</i>	<i>b_S</i> = <i>b_R</i>	<i>n_{0,S}</i> = <i>n_{0,R}</i>
τ_S	<i>A_{c,S}</i> = <i>A_{c,R}</i>	<i>A_{c,S}</i> = <i>A_{c,R}</i>	<i>A_{c,S}</i> = <i>A_{c,R}</i>
<i>p_{st,S}</i>	<i>p_{tot,S}</i> = <i>p_{tot,R}</i>	<i>p_{tot,S}</i> known	$\theta_S = \theta_R$

5.3.2. ONERA

Charpin and coworkers^{14,15} of ONERA described a scaling technique in which the parameters *K₀* and *A_c* and two terms from the energy balance, the freezing fraction, *n₀*, and the relative heat factor, *b*, were matched to the reference values. If the surface temperature is assumed to be at the freezing point of water (*t_s* = *t_f* = 0°C), and the properties of air and water are substituted into equation (3.54), the resulting equation is ONERA’s form of the energy equation:

$$\frac{1.058 \times 10^6 \frac{\text{K nt}}{\text{m}^2}}{p_{st}} = t_{st} (1 + b) + (1732 \text{ K}) \frac{p_w}{p_{st}} + 79.7 \frac{\text{cal}}{\text{g}} n_0 b + (3.6458 + b) \frac{V^2}{8373 \frac{\text{m}^2}{\text{s}^2 \text{ K}}} \tag{5.7}$$

To develop equation (5.7), the following properties of air and water at 0°C have been used: *h_G/h_c* = 2.9 gK/cal, *A_v* = 597.3 cal/g, *p_{ww}* = 610.8 nt/m², *A_f* = 79.7 cal/g, *c_{p,ws}* = 1 cal/gK, *r* = .875, and *c_p* = .24 cal/gK. Note that the K appearing in equation (5.7) is the absolute temperature unit, Kelvin, not the inertia parameter.

The procedure to find scale test conditions is as follows: Knowing the reference test conditions, *b_R* can be calculated from equation (3.55), then equation (5.7) is solved for *n_{0,R}*. *b_S* and *n_{0,S}* can now be set equal to these respective reference values. Substituting these into equation (5.7) gives the energy equation for the scale case, which now relates four of the scale test conditions: velocity, static temperature, static pressure, and vapor pressure. The Modane tunnel, for which the ONERA method was

developed, does not permit control of either static temperature or static pressure. The total temperature and pressure in the settling chamber can be measured (they are, of course, the ambient temperature and pressure at the time of the test.) The static temperature in the test section is a function of velocity and the known total temperature. Likewise, static pressure is a function of velocity and total pressure. Finally, the vapor pressure in the test section is a function only of static temperature.

Thus, including equation (5.7), we have a system of four equations that involve only the unknowns, V_S , $t_{st,S}$, $p_{st,S}$ and $p_{w,S}$. These equations can be solved by using a simple iterative approach. For example, one could start by assuming a value for V_S , perhaps setting $V_S = V_R$ as a first guess. Then $t_{st,S}$ and $p_{st,S}$ can be calculated, and, knowing $t_{st,S}$, $p_{w,S}$ can be determined. Finally, equation (5.7) can be solved for a new estimate of V_S . The process is repeated until the test conditions found in successive iterations match. With V_S , $t_{st,S}$ and $p_{st,S}$ thus established, the scale drop size can be found from equation (3.18). Finally, LWC_S is calculated by matching the expressions for b_S and b_R , using the definition in equation (3.55), along with definitions of β_0 from equation (3.13) and h_c from equation (3.32).

As discussed following equation (3.32), Charpin and coworkers used $Nu_a \propto Re_a^{0.8}$ to determine h_c rather than $Nu_a \propto Re_a^{0.5}$ (eq. (3.33)). The 0.8 exponent is not consistent with measured heat-transfer coefficients in the IRT, but it may reflect the situation in the Modane tunnel. It is not recommended for other facilities without further study of heat transfer coefficients in those tunnels.

The ONERA method was evaluated in the Modane tunnel with scales of 1/6 and 1/12, and it was reported that this approach was effective.^{14,15} Tests of a modified form of this method were reported in references 33 and 64, but rather than calculating the scale velocity as specified in references 14 and 15, a value was chosen arbitrarily. With $b_S = b_R$ and $n_{0,S} = n_{0,R}$, the scale temperature was then determined from the energy balance, equation (5.7). This approach did not adequately match scale and reference ice shape features for size-scaled tests. Tests reported in reference 33 using a convective heat-transfer film coefficient dependency of $Re_a^{0.5}$ instead of $Re_a^{0.8}$ seemed to improve the ability of the method to scale the ice shapes somewhat, but features still did not compare as well as one would want. None of the tests of references 33 and 64, however, applied the ONERA method as used in the Modane tunnel; therefore, these assessments only apply to a method for which the same similarity parameters were matched.

The ONERA method typically results in scale velocities less than the reference. We now know that scale velocities need to be higher than the reference for good simulation of reference ice shapes using sub-scale models. Thus, the ONERA method would almost certainly be improved by replacing b with We_L in the list of four similarity parameters to be matched, then modifying the procedure as follows: First find the scale velocity by matching the We_L , then static temperature and pressure can be determined from the totals, vapor pressure can be calculated from static temperature, and the energy equation solved for b_S with scale and reference freezing fraction matched. Next, determine scale LWC from b_S . The remaining test conditions would be found as they are in the present ONERA method. Such an approach needs to be evaluated before it can be recommended, however. To date, no such evaluation has been performed.

5.3.3. Ruff (AEDC)

Ruff⁷ was the first to systematically evaluate scaling using various combinations of the similarity parameters, K_0 , A_c , n_0 , b , ϕ and θ . He tested four methods (see Table I.) The first matched only K_0 and A_c , the second K_0 , A_c and n_0 , the third, K_0 , A_c , n_0 and b , and finally, the fourth matched K_0 , A_c , n_0 , ϕ and θ . Note that Ruff's third method involved the same similarity parameters as the ONERA method, but unlike that approach, Ruff assigned a scale velocity and calculated a scale static temperature by matching freezing fraction. Ruff also used equation (3.33) for the Nusselt number.

Ruff achieved the best agreement of scale and reference ice shapes when K_0 , A_c , n_0 , ϕ and θ were matched. It can be seen from equation (3.59) that when these last three parameters are matched, so too is b . This approach has been widely adopted, and is often referred to as the AEDC Method. It applies to tunnels with altitude-simulation capability, because it permits determining the value of the static pressure. The matching of five similarity parameters gives five equations that are solved for five of the six scale test conditions t_{st} , p_{st} , V , δ , LWC and τ (see Table IV). This method permits the user to arbitrarily assign a value to one of the test conditions. Typically, V_S would be selected, and this is the way Ruff conducted his tests. For facilities with limited airspeed capability, setting a value for scale velocity seems reasonable, even necessary; however, it totally ignores the physics behind the large effect that velocity has on ice shape (see figure 3.6.1). The effect of velocity, demonstrated in references 18, 35 and 46, was not appreciated until the late 1990's.

In Ruff's method 4 with model size selected, suppose a value for V_S is arbitrarily picked. Then $t_{st,S}$ and $p_{st,S}$ can be determined by solving the two equations formed by

matching ϕ_S and θ_S to their respective reference values. $K_{0,S} = K_{0,R}$ can now be solved for δ_S , and LWC_S found by matching $n_{0,S}$ with $n_{0,R}$. Finally, τ_S is established by matching scale and reference A_c .

For tunnels that cannot control the test-section pressure, a modified Ruff Method has been used (refs. 33 and 34) in which, typically, the air-energy transfer parameter is ignored and a value for scale velocity can again be selected. For a tunnel like the IRT, for which the settling chamber upstream of the test section is vented to atmosphere, the total pressure is the ambient pressure. Then, the scale test-section static pressure is determined from this total pressure and the scale velocity. The static temperature is found from matching ϕ_S to ϕ_R , as shown in Table IV. The scale drop size is established by matching scale and reference K_θ , scale LWC by matching n_0 and scale icing time by matching A_c .

A variation of the modified Ruff method⁴⁶ for sea-level tunnels is to determine scale temperature by matching θ while ignoring ϕ . This approach results typically in lower temperatures than by using constant ϕ . Reference 46 concluded from limited testing that it made no difference to the ice shape whether temperature was found by matching ϕ or θ . Reference 49 also showed scale ice shapes that matched the reference when temperature was found by applying constant θ with ϕ unmatched. These results are not surprising since neither ϕ nor θ has been shown to have an effect on ice shape independent of the freezing fraction. Thus, it is highly probable that the scale temperature (or, alternatively, LWC) can be chosen arbitrarily with the LWC (or temperature) determined by matching scale and reference n_0 . Anderson and Tsao⁷⁴ demonstrated good matches of scale and reference shapes for conditions for which neither ϕ nor θ matched reference values. Additional testing is needed to confirm this result, but if validated, it would provide useful flexibility in the definition of scale test conditions.

5.3.4. Methods to Choose Scale Velocity

The Ingelman-Sundberg size-scaling method discussed in section 5.3.1 left the choice of scale velocity to the user, as though any velocity would be equally appropriate. The Ruff method, too, permits the user to arbitrarily select a scale velocity. The ONERA method calculates V_S by matching freezing fraction; this approach gives scale velocities that are typically lower than the reference. In this section we shall look at alternate ways to select scale velocity and see how their choice affects ice shape. A recommended method will be given.

The simplest way to select the scale velocity is to equate it to the reference value, but when high airspeeds need to be simulated, facility limitations may make it tempting to

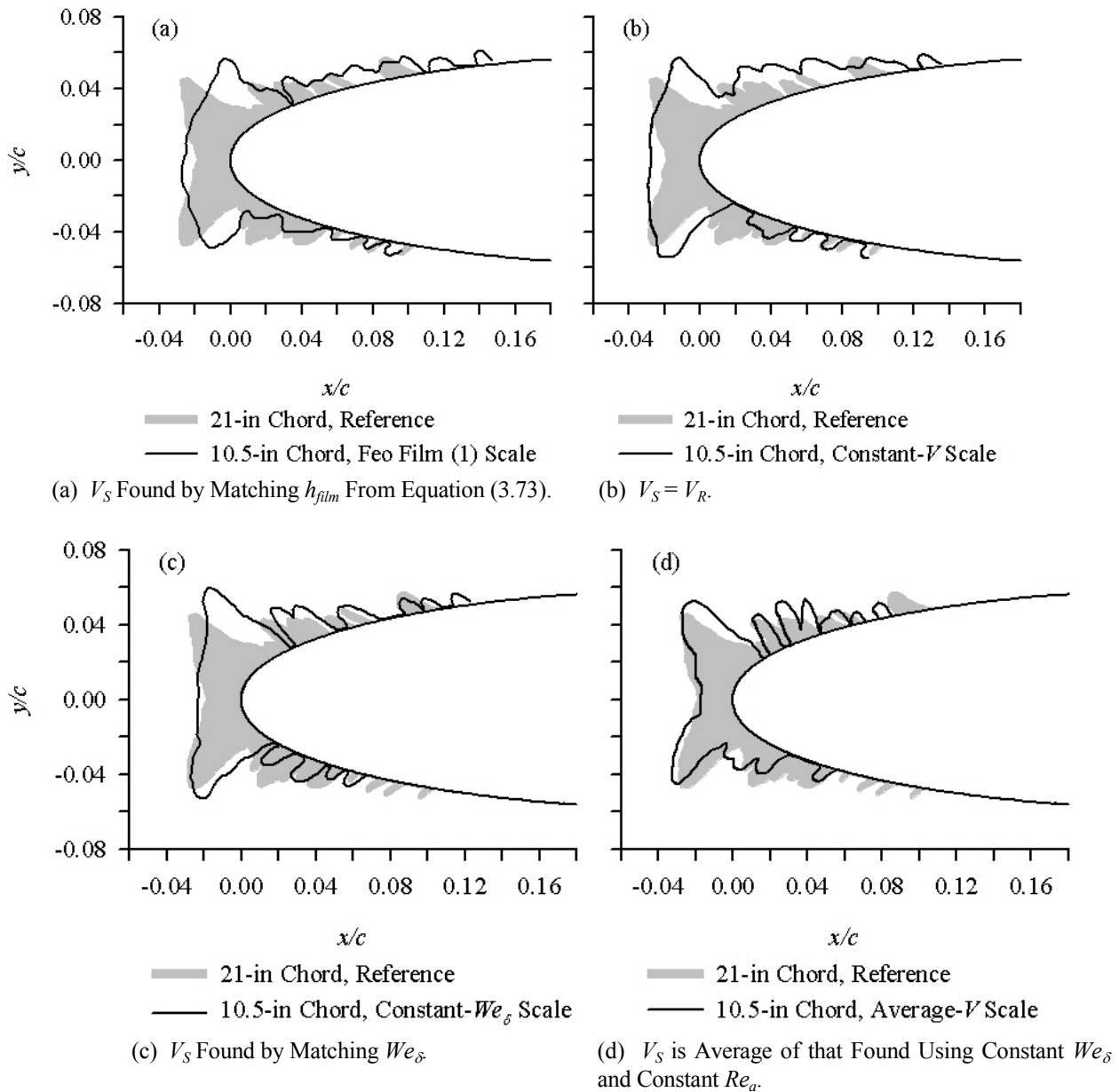
use a scale velocity that is less than the reference. Matching velocities is also equivalent to approximately equating the scale and reference Mach numbers, so if M_a could be shown to be important in the physics of icing, this is a valid approach. However, most icing encounters take place at low Mach numbers where compressibility is not important, and reference 35, in limited testing, found no effect of Mach number up to $M_a = 0.5$.

If M_a does not have to match and, as we have seen, velocity has a significant effect on ice shape independent of the parameters K_θ , A_c , n_0 , b , ϕ and θ , it is important to determine the velocity that gives the most faithful simulation of reference ice shapes. Tests to evaluate a variety of ways to choose scale velocities were reported in references 35 and 46. Figure 5.3.1 reproduces results from reference 35 at a nominal freezing fraction of 0.5. The figure shows how scale ice shapes vary with different scale velocities. In each part of the figure the shaded shape is the reference, recorded on a 21-in-chord NACA 0012 airfoil with a velocity of 150 mph. The solid line is the 10.5-in (26.7-cm) scale result. The changes in horn angle as the scale velocity increased is entirely consistent with what was shown earlier in figure 3.6.1.

The scale velocity was calculated using different methods for each portion of the figure. Figure 5.3.1 (a) gives the scale ice shape for a velocity of 127 mph (57 m/s), just 81% of the reference value. This velocity resulted from matching the scale and reference film thickness from equation (3.73). While the reference horns projected slightly forward, the scale horns were swept back, comparing poorly with the reference. Note that this correlation for h_{film} was based on heavy-rain studies rather than Appendix-C icing conditions. A later study by Feo produced equation (3.74). When this latter water-film thickness was matched between scale and reference, the resulting V_S was significantly higher than V_R , and the resulting scale ice shapes were a better match to the reference⁴⁹ than that shown in figure 5.3.1 (a). Results from tests using this similarity parameter will be discussed later in this section.

When the scale velocity was increased to match the reference, 150 mph (67 m/s), the scale shape in figure 5.3.1 (b) resulted. While the horns moved forward slightly, the change was not sufficient to provide a good match of the reference shape.

For figure 5.3.1 (c) the scale velocity was increased to 195 mph (87 m/s), or 30% higher than the reference. This velocity was that obtained by matching the scale We_δ to the reference value. Although the scale horn angle did not precisely match the reference, the shapes probably agreed within typical repeatability.



Date/Run	c , in	t_{st} , °F	V , mph	δ , μm	LWC , g/m ³	τ , min	β_0 , %	A_c	n_0	b	ϕ , °F	θ , °F	Re_a , 10 ⁴	We_δ , 10 ³	We_L , 10 ⁶	h_{film}/d , relative
(Ref) 3-26-98/4	21.0	17	150	40	0.61	11.2	0.858	1.77	0.48	0.36	14.1	19.6	8.54	2.76	1.16	1.00
(a) 3-18-98/3	10.5	17	127	27	0.96	4.2	0.853	1.77	0.48	0.37	14.0	20.3	3.64	1.34	1.42	0.98
(b) 3-19-98/6	10.5	17	150	26	0.86	4.0	0.860	1.78	0.48	0.36	14.1	19.7	4.27	1.82	1.58	0.75
(c) 3-19-98/4	10.5	16	195	24	0.68	3.7	0.859	1.73	0.47	0.33	13.9	17.4	5.45	2.76	0.99	0.44
(d) 3-20-98/2	10.5	15	263	21	0.50	3.8	0.859	1.71	0.45	0.28	14.1	14.1	7.04	4.40	1.79	0.23

Figure 5.3.1.—Effect of Scale Velocity on Scaling of a Reference Ice Shape³⁵. Reference Test, 3-26-98 Run 4. h_{film}/d From Equation (3.73); Values for h_{film}/d are Relative to Reference.

Test results for one more incremental increase in scale velocity are shown figure 5.3.1 (d). This velocity was the average of that determined by matching We_δ and that from matching Re_a . For the tests reported in reference 35, the best scaling resulted using this average-velocity approach.

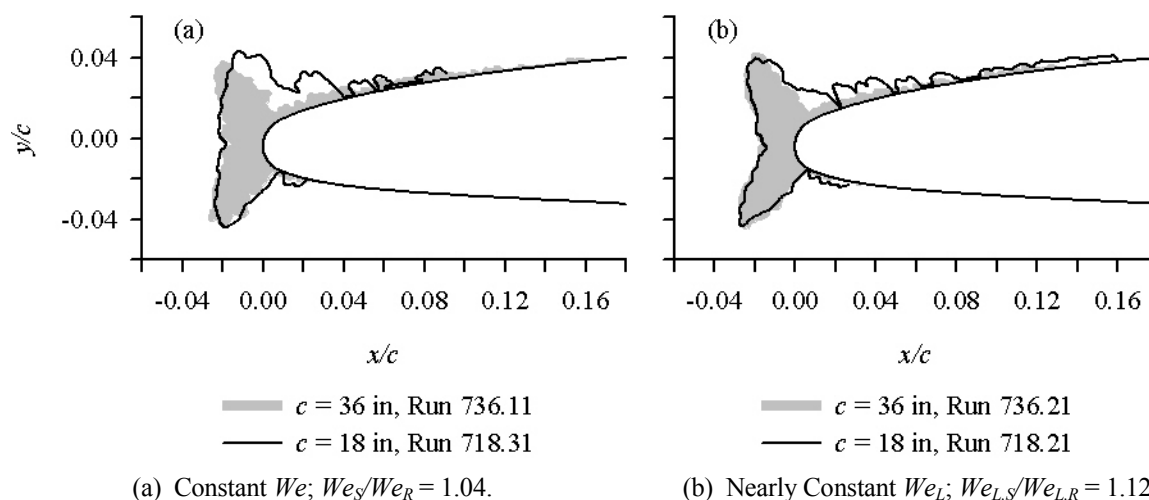
Although not shown in figure 5.3.1, tests reported in reference 35 were also made with a scale velocity found by matching scale and reference Re_a . This scale velocity was 2.1 times the reference. The angle between the horns for the scale shape was more acute than that of the reference shape; therefore, this scale velocity appeared to be higher than necessary for good simulation of the reference shape.

The results shown in figure 5.3.1 are for a freezing fraction of about 0.5. Tests in references 35 and 46 were for either 1/2- or 2/3-size scaling and were conducted at additional nominal freezing fractions of 0.3, 0.6 and 0.8; the general conclusion of all these tests was that the average- V method of choosing scale velocity gave the best match of scale and reference ice shapes. This success of the average- V method was interpreted to be an indication that both We_δ and Re_a are important to the glaze icing process, and this conclusion is consistent with the belief that water-film phenomena play some part in determining ice shapes.

Feo⁴⁷ proposed matching the water-film thickness of equation (3.74) to find the scale velocity. This thickness expression included terms only for LWC and Re_a , omitting the Weber number. Thus, it seemed to ignore some of the physical dependencies known from earlier tests to be important (see figure 3.6.1 and associated discussion). Nevertheless, 1/2-size scaling tests were conducted⁴⁹ for which the film thickness of equation (3.74) was included as a similarity parameter to supplement the Ruff method. Freezing fractions of 0.3, 0.4, 0.5, 0.8 and 1.0 were tested. The resulting scale velocities were close to those of the average- V method; thus, it was not surprising that scale ice shapes were again a good match for the reference. Water-film parameters other than h_{film}/d have also been used^{49,51} to find scale velocity. These include Weber numbers based on water-film thickness using either free-stream or water-film-edge velocities.

Additional examples of scaling with different scale velocities comes from IRT tests by Chen¹⁸ with GLC 305 airfoils. Figure 5.3.2 gives two sets of comparisons for a freezing fraction of 0.3. The reference shape for each pair is shown shaded and the scale is represented with a solid line. The reference models had a chord of 36 in and the scale, 18 in.

The scale test in figure 5.3.2 (a) used a scale velocity that permitted a near match of the Weber number based on drop size, We_δ . The resulting scale shape agreed with the reference within normal ice-shape repeatability. Even



Run	c , in	t_{st} , °F	V , mph	δ , μm	LWC , g/m^3	τ , min	β_0 , %	A_c	n_0	b	ϕ , °F	θ , °F	Re_a , 10^4	We_δ , 10^3	We_c , 10^3	We_L , 10^6
(a) 736.11	36	16	148	50	1.07	13.8	85.4	2.61	0.30	0.75	14.8	20.6	12.4	3.35	2.10	1.64
718.31	18	14	198	29	1.34	4.0	85.5	2.55	0.30	0.78	16.3	20.5	8.2	3.49	1.86	1.48
(b) 736.21	36	16	158	50	1.01	13.5	85.9	2.58	0.30	0.74	14.7	20.1	13.3	3.84	2.40	1.88
718.21	18	12	237	27	1.35	3.3	85.6	2.53	0.29	0.86	17.8	20.5	9.7	4.65	2.61	2.11

Figure 5.3.2.—Scaling Results with Alternate Scale Velocities. GLC 305 Airfoil at 0°AOA. Ice-Shape Data from March 1998 IRT Tests by Chen.¹⁸

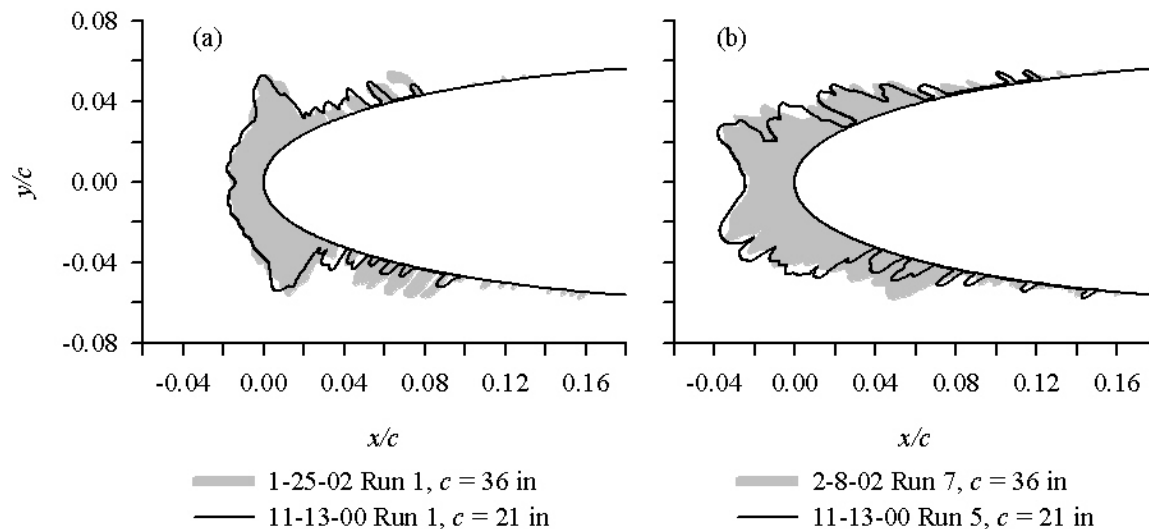
better agreement of shapes was evident in figure 5.3.2 (b), for which a higher scale velocity was tested. For all the tests represented in figure 5.3.2, scale and reference We_L matched within about $\pm 10\%$.

Limited evaluation of scaling with matched We_L using NACA 0012 airfoils has been published⁷⁴ recently. These tests were made using SLD reference conditions. Figure 5.3.3 gives results for freezing fractions of 0.3 (fig. 5.3.3 (a)) and 0.5 (fig. 5.3.3 (b)) for a scale-to-reference size ratio of 1:1.7. Excellent agreement between scale and reference shapes is evident. The experimental results of figures 5.3.2 and 5.3.3 are consistent with the evidence in section 3.6 that suggested that We_L is an important similarity parameter. However, as we have seen, other methods discussed in section 3.6 to find scale velocity have also been used with good experimental results.

The reason that a number of methods of finding scale velocity give similar scaling results is that the resulting scale velocities are not significantly different. Table V shows sample scale velocities found by various methods for a reference velocity of 150 mph and for scale-to-reference size ratios of 1/2 and 1/3. For this reference velocity, for the 1/3-scale case, no solution could be

found for some of the methods; these situations are indicated with asterisks. For half-size scaling, several methods give scale velocities in the range between that given by constant We_δ and that from the average- V approach. Within this range of scale velocities, it is difficult to discern significant differences in ice shape. Thus icing tests cannot help us identify the most important water-film similarity parameter.

Figure 5.3.4 graphs some of the information in Table V along with additional data. Here, the scale-to-reference velocity ratio is given as a function of the reference-to-scale size ratio for a range of size ratios from 1.7 to 4. The shaded band represents scale velocity ratios in the range of $\pm 15\%$. The velocity ratio for most of the methods was calculated for a reference velocity of 150 mph. At this reference velocity, however, the routines used to calculate scale velocity failed for the average-velocity and constant- We_k methods at scale ratios greater than 2; therefore, to obtain values over the complete range of scale ratios, the reference velocity used for these methods was 115 mph. It is evident that even with a scale ratio as high as 4 there are a number of methods whose scale velocities differ by no more than $\pm 15\%$. This is not a sufficient difference to produce significant variations in ice shape.



(a) Scaling for a Freezing Fraction of 0.3

(b) Scaling for a Freezing Fraction of 0.5

Date/Run	c , in	t_{st} , °F	V , mph	δ , μm	LWC , g/m ³	τ , min	β_0 , %	A_c	n_0	b	ϕ , °F	θ , °F	Re_a , 10 ⁴	We_δ , 10 ³	We_c , 10 ³	We_L , 10 ⁶
(a) 1-25-02/1	36	12	115	160	1.50	9.7	95.4	1.70	0.30	1.26	19.9	28.7	11.6	6.50	1.52	1.17
11-13-00/1	21	19	149	38	1.00	7.3	84.9	1.88	0.28	0.58	11.8	16.2	8.6	2.61	1.47	1.15
(b) 2-8-02/7	36	-3	115	160	1.50	9.7	95.4	1.70	0.50	1.25	34.0	46.7	12.4	6.54	1.58	1.18
11-13-00/5	21	9	150	38	0.99	7.3	84.9	1.88	0.52	0.58	21.6	29.9	8.9	2.62	1.51	1.16

Figure 5.3.3. Examples of Scaling for which Scale Velocity was Found by Matching We_L . NACA 0012 Airfoils at 0°AOA.⁷⁴

Table V.

Scale Velocity for Different Methods.
 NACA 0012 Airfoil; $t_{sl,R}$, 6°F; δ_R , 40 μm ; LWC_R , 1.0 g/m^3 .

Method	c , in	V , mph
Reference	36	150
Constant V	18	150
Constant We_w	18	175
Constant We_h	18	193
Constant We_δ	18	197
Constant We_k	18	212
Constant We_L	18	212
Constant We_t	18	218
Constant $We_h + \text{Const. } h_{film}/d$	18	238
Constant h_{film}/d (eq. (3.74))	18	253
Average V	18	265
Constant Re_a	18	332
Constant V	12	150
Constant We_w	12	191
Constant We_h	12	224
Constant We_δ	12	230
Constant We_k	12	*
Constant We_L	12	260
Constant We_t	12	274
Constant $We_h + \text{Const. } h_{film}/d$	12	312
Constant h_{film}/d (eq. (3.74))	12	318
Average V	12	*
Constant Re_a	12	*

* No solution

As Table V and figure 5.3.4 show, for half-size scaling, the scale velocity resulting from matching We_L falls in the range between constant We_δ and average V that has shown reasonable scaling results in past studies. At this time, We_L seems to have greater experimental justification than other similarity parameters. The practical advantage of using constant We_L is that the scale velocity-to-reference velocity ratio is simply the square root of the size ratio (eq. (3.71)). Furthermore, it leads to a more

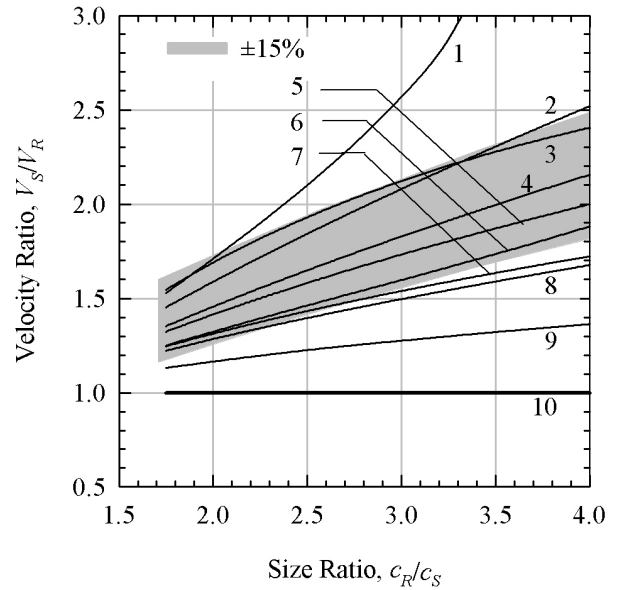


Figure 5.3.4. Comparison of Velocity Ratio for Ten Methods to Find Scale Velocity. NACA 0012; c_R , 36 in; $t_{sl,R}$, 6°F; δ_R , 40 μm ; LWC_R , 1.0 g/m^3 .

Method	eq.	V_R , mph
1.	Average-Velocity (3.84)	115*
2.	Const.- $We_h + \text{Const. } h_{film}/d$ (3.77)	150
3.	Constant- h_{film}/d (3.74)	150
4.	Constant- We_t (3.80) with (3.83)	150
5.	Constant- We_L (3.69)	150
6.	Constant- We_k (3.78)	115*
7.	Constant- We_δ (3.70)	150
8.	Constant- We_h (3.72)	150
9.	Constant- We_w (3.82)	150
10.	Constant-Velocity ($V_S = V_R$)	150

* No solution for some scale ratios with $V_R = 150$ mph

moderate scale velocity than some of the similarity parameters that might be used.

5.3.5. Size Scaling for Intercycle Ice Studies

It is clear from the results of figure 5.3.1 (b) that for $1/2$ -size scaling, the scale velocity cannot be set equal to the reference for adequate simulation of the horn angle or position for glaze ice. However, these conclusions apply to significant ice-accretion times. For short accretion times, for which horns or other features have insufficient time to develop, constant- V determination of the scale velocity may be entirely adequate. Such is the case for intercycle-ice accretion, as one example.

Intercycle ice is the ice that forms between cycles of an impulse deicing ice-protection system. The most common form of impulse system is the pneumatic-boot deicer in which pneumatic tubes inflate and deflate rapidly

at prescribed intervals to break ice from the leading-edge region of airfoils, tailplanes, or other critical surfaces. Aerodynamic forces then cause the ice to shed. Typically, in such a process all the ice does not shed, and the surface will be left with some residual ice. After the boot deflates, ice will begin to form both on the clean portions of the surface and on the residual ice. The accretion that has formed by the next boot inflation cycle is termed the intercycle ice.

Intercycle ice represents significant roughness on critical surfaces, and it is important to determine the aerodynamic effects of the roughness. Wind-tunnel testing is a relatively inexpensive and safe way to record intercycle ice shapes. If the desired wing section is too large for an icing tunnel, it is possible to perform a scale test to establish the intercycle ice sizes and shapes. As for other icing situations, shapes recorded by molding or by pencil tracing can be transformed into castings to be applied to wing sections for aerodynamic testing.

In 2000 a preliminary study⁷⁵ was made in the Goodrich Icing Wind Tunnel (IWT) to determine if the size-scaling methods discussed in preceding sections of this manual could be applied to intercycle ice accretion. Intercycle ice shapes were recorded for a reference model and compared with shapes from a 1/2-size scale test. The desired reference model was a 72-in-chord NACA 23012 airfoil section, and the scale was a 36-in-chord 23012. Because the full 72-in-chord model would have been too large for the IWT, a hybrid-scaled^{2,3} model was used in its place for the reference tests. The hybrid model consisted of a nose section with 72-in-chord NACA 23012 coordinates and a truncated afterbody. The resulting chord was 36 in. The afterbody was designed so that the resulting hybrid airfoil would have the same collection-efficiency curve at 2° AOA as the full 72-in-chord NACA 23012. This objective was met. The hybrid airfoil included a trailing-edge flap that was adjusted to correct the β -curve for off-design angles of attack. Drop-trajectory and flowfield-analysis codes were used to determine the afterbody coordinates at 2° AOA and to establish appropriate flap deflections for other angles of attack.

The pneumatic deicer was mounted flush with the nose section of both models. It consisted of two 1.25-in-wide inflatable tubes at the leading edge of each model and one-in-wide tubes immediately aft on the upper and lower surfaces. The hybrid (reference) model used three 1-in tubes on the upper surface and five on the lower surface, while the scale model had only one 1-in tube on the upper surface and two on the lower. The active portion of the deicers extended to the same non-dimensional chord-wise extent on both models. Thus, while the over-

all active portions of the deicers were geometrically scaled, the individual inflatable tubes were not.

Test conditions for the scale model were determined from the reference conditions using the Ruff method, described in section 5.3.3, with scale and reference velocities equated. The ratios of scale-to-reference boot cycle times were the same as the scale-to-reference total icing time.

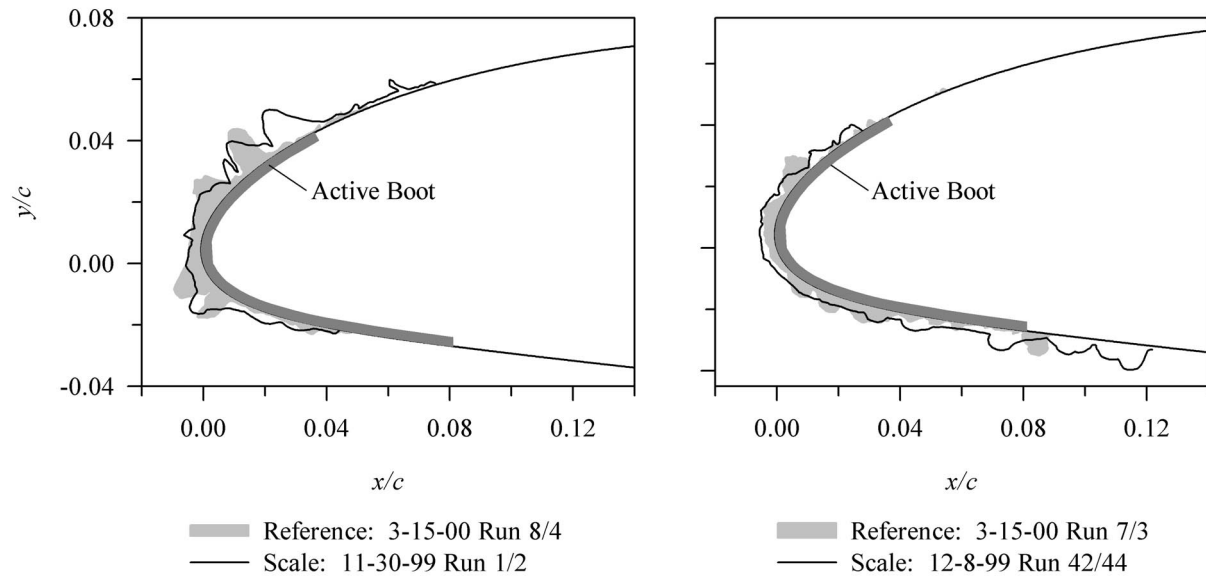
Two examples of the intercycle-ice scaling results from reference 75 are given in figure 5.3.5. In general, the scale tests reproduced the non-dimensional ice thickness of the reference tests at and near the leading-edge region. The non-dimensional size of ridges and features aft of the leading edge were also determined accurately by the scale tests. However, the chord-wise positions of these aft features were not well simulated. These features tended to form along the boot stitching; therefore, the authors' speculated that if the pneumatic tubes for the deicers had been geometrically scaled, there might have been better agreement between the non-dimensional scale and reference locations of these features. Although further study and testing of scaling for intercycle ice accretion is needed, the results demonstrate how constant-velocity scaling can be applied effectively when ice accretion times are short.

5.3.6. Acceptable Parameter Variations

Even for glaze ice, the similarity parameters may not always need to be matched precisely between scale and reference to insure good scale ice shapes. In fact, in practice, uncertainties in test conditions make it impossible to specify precisely the scale parameter values. Thus, it is helpful to know what tolerances are acceptable. This topic was reviewed in reference 19. There it was recommended that uncertainties in test parameters should be minimized such that the scale-reference match of n_0 and of A_c should be within $\pm 10\%$. If scale and reference β_0 do not match, the product $\beta_0 A_c$ should match within $\pm 10\%$. Ice shape is not as sensitive to changes in velocity as to those in n_0 and A_c , as shown in section 5.3.4. It is recommended, however, that $We_{L,S}$, the similarity parameter from which scale velocity is found, be maintained within $\pm 15\%$ of $We_{L,R}$. Additional testing of the effects of variations in this parameter on ice shape is needed to better establish acceptable variations in We_L .

5.3.7. Recommended Method to Scale Size

The Ruff method reviewed in section 5.3.3, supplemented with the constant- We_L approach (section 5.3.4) to calculate scale velocity, is recommended for simulating the main ice shape with a model scaled in size. This method requires matching scale and reference model non-dimensional geometry and AOA, as well as scale



(a) Freezing Fraction, 0.6; Angle of Attack, 0°.

(b) Freezing Fraction, 0.2; Angle of Attack, 4°.

Date	Run	c , in	t_{st} , °F	V , mph	δ , μm	LWC , g/m^3	τ , min	Cycle Time, sec	β_0 , %	A_c	n_0	b	ϕ , °F	θ , °F	Re_a , 10^4	We_δ , 10^3	We_c , 10^3	We_L , 10^6
(a) 3-15-00	8/4	72	14	200	31	0.32	34.5	509	63.1	0.27	0.60	0.30	16.3	20.5	39.2	3.81	8.93	7.10
11-30-99	1/2	36	14	200	20	0.45	12.2	180	63.0	0.27	0.60	0.30	16.3	20.5	19.6	2.46	4.46	3.55
(b) 3-15-00	7/3	72	14	200	31	1.38	8.6	170	63.1	0.40	0.23	1.29	16.3	20.5	39.2	3.81	8.93	7.10
12-8-99	42/44	36	14	200	20	1.95	3.1	60	63.0	0.39	0.23	1.29	16.3	20.5	19.6	2.46	4.46	3.55

Figure 5.3.5. Results of Size-Scaling Tests for Intercycle Ice.⁷⁵ Reference Model: 36-in-Chord Hybrid with 72-in-Chord NACA 23012 Nose Section and Truncated Trailing Edge; Scale Model: 36-in-Chord NACA 23012.

and reference values of the similarity parameters K_0 , A_c , n_0 , ϕ , θ and We_L for tunnels with altitude capability or K_0 , A_c , n_0 , We_L and the choice of either ϕ or θ for sea-level tunnels. At this time, matching of We_L appears to have the strongest analytical basis for finding scale velocity. The velocity resulting from use of this method is of the same magnitude as several other proposed approaches listed in Table V, and experimental evaluation of this method seems to validate it. As greater understanding of water-film effects is gained, this recommendation may change.

Scale drop size can be found either from equation (3.18) or by matching K_0 from equation (3.8). For simulating the main ice shape, a great deal of flexibility is possible in choosing scale drop size, because, as shown in figures 3.3.6 and 3.3.7, for the conditions investigated to date, K_0 has no measurable effect on main ice shape. Nevertheless, it is recommended that K_0 be matched whenever possible, because it does affect the impingement limit. If scale and reference K_0 can not be matched, instead of simply matching A_c , the product $\beta_0 A_c$ should be matched as closely as possible. Furthermore, if K_0 is not matched

and impingement limits are important additional tests should be performed at the reference β_0 , A_c and n_0 to determine these limits. For scaled impingement-limit tests, the parameters ϕ (or θ) and We_L , necessary for faithful scaling of main ice shapes, can be ignored.

For scaling tests to determine main ice shape, there is a high probability that the parameters ϕ and θ do not have to be matched to the reference values, but additional testing is required to confirm that this simplification is valid. Until such testing is completed, it is recommended that these parameters continue to be used.

In some cases, the scale total temperature found by matching either ϕ or θ is above freezing. References 35 and 46 showed that when total temperatures exceeded 27°F (-3°C) ice shapes are distorted enough that a good match of the reference is not possible. Thus, when scale total temperature is greater than 27°F, ϕ and θ must be abandoned and a scale temperature selected such that the total temperature is below 27°F (-3°C). LWC must then also be adjusted to maintain constant n_0 .

For very short accretion times for which ice features do not have time to form, simplifications to the above recommendations are possible. For example, a constant-velocity approach can be substituted for constant- We_L , as discussed in section 5.3.5. For short times (small values of A_c) the primary concern should be to match scale and reference $\beta_0 A_c$.

The matching of all the parameters required to find scale test conditions necessitates solving several equations simultaneously. The programming of solutions to this system of equations is not difficult, and is simplified by the use of mathematical software such as Mathcad® or Mathematica®.

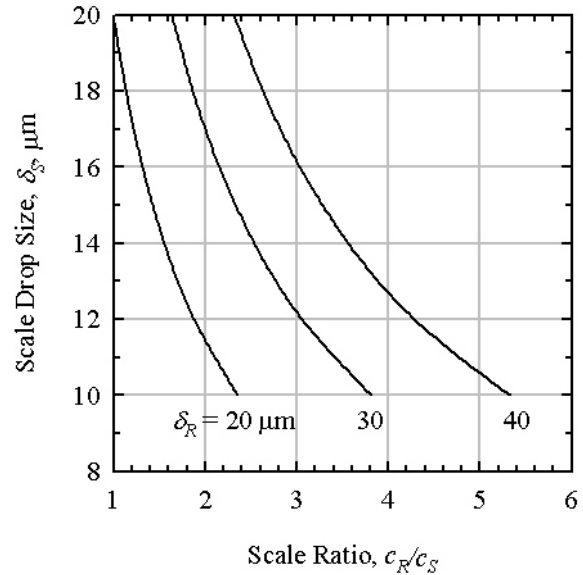
5.3.8. Practical Limitations to Size Scaling

This section reviews the practical constraints to size scaling imposed by facility restrictions as well as by natural physical limitations. Both types of restriction impose an upper limit on the reference-to-scale model size ratio. Restrictions on test-condition scaling have not been explored sufficiently to define those limits; therefore, this discussion will concentrate on size-scaling limits.

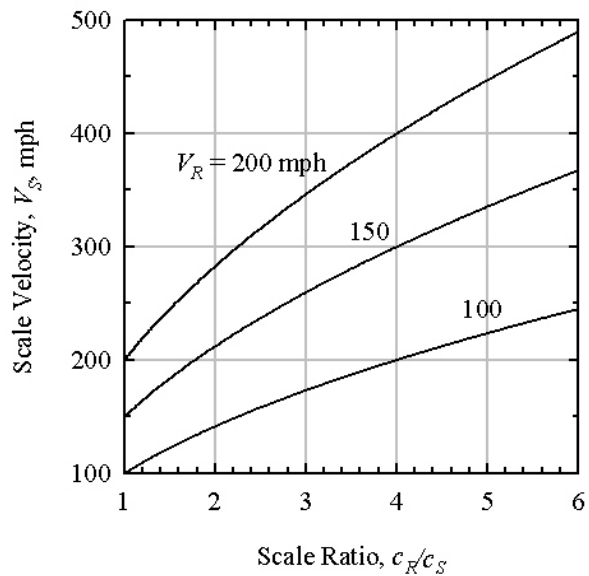
Figure 5.3.6 shows the relationships between scale conditions and scale ratio. The values in this figure were calculated by applying the method recommended in this manual; that is, the Ruff method supplemented with constant We_L to determine scale velocity. The validity of this method has not been tested at scale ratios greater than 3.4, but there does not appear to be any fundamental reason that it can't be applied to higher scale ratios. Testing scaling methods at higher scale ratios is difficult because, to perform such tests, both the reference and scale conditions have to fall within the tunnel calibrated operating map.

Figure 5.3.6. (a) gives the effect of scale ratio on scale drop size for reference drop sizes of 20, 30 and 40 μm . The calculations were made for a reference velocity of 150 mph, but the effect of velocity on scale drop size is not significant. It can be seen from the figure that for a facility with a minimum calibrated drop size of 14 μm , the maximum scale ratio is about 3.5 for a reference drop size of 40 μm . For reference drop sizes of 30 and 20 μm , the maximum scale ratio is 2.5 and 1.5, respectively. If the facility calibration is extended down to an MVD of 10 μm , scale ratios of close to 5.5 could be tested with the 40- μm reference drop size.

Figure 5.3.6. (b) shows the effect of scale ratio on scale velocity for reference velocities of 100, 150 and 200 mph. For this illustration, the constant- We_L method of finding scale velocity was used. If the reference velocity is 200 mph and the maximum test-section velocity is 350 mph, scale ratios only as high as 3 can be tested. Obvi-



(a) Effect on Scale Drop Size. V_R , 150 mph.



(b) Effect on Scale Velocity.

Figure 5.3.6. Effect of Scale Size Ratio on Scale Test Conditions. Scaling using Ruff Method with Constant We_L . c_R , 72 in; T_R , 490 R.

ously, lower reference velocities permit higher scale ratios for the same maximum test-section velocity. For a facility with a maximum test-section velocity of 200 mph, the scale ratio is limited to approximately 2 when simulating a reference velocity of 150 mph and 4 for a reference velocity of 100 mph.

There may be other physical limitations. The minimum-MVD problem might be eased somewhat by extending the calibration of spray systems to smaller drop sizes.

Such calibration depends on accurately measuring small drops, which cannot yet be done with certainty. However, even if possible, this approach is limited by the minimum drop size that will impinge on a model (see figure 3.3.2.) For smaller and smaller cloud MVD's it is more and more likely that the smallest portions of the cloud will fall into the regime in which no impingement occurs. This situation makes it questionable whether a very small-MVD cloud can be used reliably to simulate a cloud with a larger MVD. Testing to determine practical minimum MVD's has not been done and such testing is needed if large reference-to-scale model size ratios are desired.

Velocities are limited by physical constraints, as well. As the velocity increases, the risk of aerodynamic damage to the scale ice shape during accretion increases. Frequent shedding of feathers and even of small portions of glaze horns has been observed in tests with velocities over 300 mph. Furthermore, as velocities increase above 350 mph compressibility effects may need to be considered, and the scaling assumptions that Mach number can be ignored may no longer be valid. Thus, it appears that a velocity somewhere around 350 mph is probably a practical maximum for scaling applications, even if the facility is capable of higher speeds.

In summary, then, because of both facility and fundamental physical constraints, scale model sizes cannot be much smaller than to $\frac{1}{2}$ to $\frac{1}{4}$ that of the reference, depending on reference conditions and facility capabilities.

6. Recommended Future Studies in Scaling

This manual concentrated on scaling for simple geometries and two-dimensional wing sections. Future studies need to address such applications as swept wings, rotorcraft and scaling for ice-protection systems. For small sweep angles, swept-wing accretions may be close enough to unswept that the scaling methods in this manual might be applicable. Testing is required to verify this approach, however, and to date none has been done.

For rotorcraft, it may be possible to divide the rotor into several radial regions according to rotating speed. Determination of the local ice shape would come from tests performed at various speeds to represent each radial location. Near the tip, speeds will be too high for icing facilities, and lower speeds could be found by matching a similarity parameter such as We_L . Matching any of the Weber numbers to simulate a high speed with a lower speed necessitates the use of a larger chord. Therefore, this approach has practical limits. Furthermore, simulation of high-speed shedding is not addressed by this approach. Finally, the Mach number may need to be included in the scaling methodology for regions at and near the tip.

In addition to ice shedding caused by aerodynamic forces, shedding due to centrifugal forces can have a significant effect on ice shape for rotating blades. A shedding analysis needs to include issues such as varying adhesion of ice to the surface and local stresses on the ice for different conditions.

Scaling for thermal ice-protection systems will require the addition of terms to the energy balance equation of section 3.5 to represent the ice-protection system. For such applications of scaling, there is no ice shape to be concerned about, so, in addition to thermal similarity parameters, it is only necessary to match the product $\beta_0 A_c$ to insure the correct water catch is simulated. This is not difficult to do, but scaling methods for thermal ice protection need to be evaluated.

Intercycle-ice scaling studies, initiated in the work of reference 75, need to be continued. Future experiments in this area should consider the effects of pneumatic-tube size relative to airfoil size, inflation-deflation schedules and inflation pressure. Reference 75 used a hybrid-scaled model as equivalent to the full-size reference; in future studies, if possible, a model with the full-size chord and geometry should be used for clear-cut comparisons with the scale results.

Appendix A Resources for Scaling Calculations

This Appendix contains a listing of all the properties and relationships needed to find the scaled test conditions that will simulate an icing encounter with given reference conditions. A sample size-scaling case will be solved step by step using the Ruff method with constant We_L , and the solution to an LWC -scaling case using the Olsen method will also be demonstrated. Finally tables of sample reference and scale test conditions will be given for both types of scaling.

A.1. Properties of Air, Water and Ice and General Relationships

This section gives the constants or expressions used to find the properties of air and water. These property values are those used in scaling calculations at NASA Glenn. They will be listed alphabetically. Values or equations will be given in pairs, with the first of each pair in English units and the second in S.I. All symbols used here appear in the Nomenclature list, Section 1 of the Manual. References for this Appendix appear at the end of the Appendix.

$c_{p,a}$ Specific Heat at Constant Pressure The specific heat of air at a pressure of 14.5 psia over the range -40°F to 40°F is given by NIST⁷⁶ as

$$\begin{aligned} c_{p,a} &= .240 \frac{\text{Btu}}{\text{lbm R}} \\ &= .240 \frac{\text{cal}}{\text{g K}} \end{aligned} \quad (\text{A.1})$$

At this pressure, $c_{p,a}$ varies with temperature only in the 5th decimal place. The variation with pressure for these temperatures is less than .2% over the range 6 – 14.5 psia. Therefore, a constant value for $c_{p,a}$ can be used for all icing scaling situations.

The ratio, γ , of the constant-pressure specific heat to the constant-volume specific heat for air will be discussed below.

Data for the specific heat of water over the range -40°F to 40°F were given by Pruppacher and Klett.²⁹ A fit to their data gives the expression used for water on the surface of the model:

$$\begin{aligned} c_{p,ws} &= 1.0074 \frac{\text{Btu}}{\text{lbm R}} + \\ & 2.559 \times 10^{-5} \frac{\text{Btu}}{\text{lbm R}^3} (T_s - 491.67 \text{ R})^2 \\ &= 1.0074 \frac{\text{cal}}{\text{g K}} + \\ & 8.29 \times 10^{-5} \frac{\text{cal}}{\text{g K}^3} (T_s - 273.15 \text{ K})^2 \end{aligned} \quad (\text{A.2})$$

Note that for the first form of equation (A.2) the absolute surface temperature, T_s , is in Rankine degrees, while in the second it must be in Kelvin.

k_a Thermal Conductivity of Air A fit to the NIST air thermal conductivity data⁷⁶ at a pressure of 14.5 psia for the range of temperature from -40 to 40°F is

$$\begin{aligned} k_a &= -.008529 \frac{\text{Btu}}{\text{hr ft R}} + .001016 \frac{\text{Btu}}{\text{hr ft R}^{1.5}} \sqrt{T_{film}} \\ &= -12.69 \frac{\text{cal}}{\text{hr m K}} + 2.029 \frac{\text{cal}}{\text{hr m K}^{1.5}} \sqrt{T_{film}} \end{aligned} \quad (\text{A.3})$$

For this temperature range k_a varies with pressure only by approximately .1% for pressures from 6 to 14.5 psia. Therefore, equation (A.3) can be used without regard for pressure for icing scaling calculations. As the units in equation (A.3) indicate, the absolute temperature must be in Rankine or Kelvin, respectively. As indicated, the thermal conductivity of air is evaluated at the film temperature, defined by equation (A.13), when calculating the convective heat-transfer coefficient from equation (A.33).

D_v Diffusivity of Water vapor The water-vapor diffusivity in air was given by the following expression in Pruppacher and Klett.²⁹

$$\begin{aligned} D_v &= 2.271 \times 10^{-4} \frac{\text{ft}^2}{\text{s}} \left(\frac{T_{film}}{491.67 \text{ R}} \right)^{1.94} \left(\frac{14.696}{p_{st}} \right) \\ &= .211 \frac{\text{cm}^2}{\text{s}} \left(\frac{T_{film}}{273.15 \text{ K}} \right)^{1.94} \left(\frac{1.0132 \times 10^5 \text{ Pa}}{p_{st}} \right) \end{aligned} \quad (\text{A.4})$$

Note that the diffusivity is evaluated at the film temperature, equation (A.13).

p Air Pressure For the IRT the settling chamber is vented to atmosphere, so the total pressure everywhere in

the tunnel is approximately atmospheric. For the altitude in Cleveland, Ohio, a typical value for atmospheric pressure is 14.5 psia. Thus, for scaling calculations,

$$\begin{aligned} p_{tot} &= 14.5 \text{ psia} \\ &= 9.997 \times 10^4 \text{ Pa} \end{aligned} \quad (\text{A.5})$$

is used for IRT testing for both scale and reference conditions.

The static pressure in the absence of compressibility is

$$p_{st} = \frac{p_{tot}}{\left(1 + \frac{V^2}{2R_a T_{st}}\right)} \quad (\text{A.6})$$

The compressible form of equation (A.6) is

$$p_{st} = \frac{p_{tot}}{\left(1 + \frac{\gamma - 1}{2} M^2\right)^{\frac{\gamma}{\gamma - 1}}} \quad (\text{A.7})$$

The static pressures found from equations (A.6) and (A.7) differ by approximately 1.5% at an airspeed of 400 mph. At 350 mph, a practical maximum airspeed for the IRT, the difference is less than 1%, and it continues to decrease with speed. Thus, for typical icing conditions, equation (A.6) provides an adequate approximation.

For some tunnels, the test section, rather than the settling chamber, is vented to the atmosphere. In that situation, the test-section static pressure is the ambient pressure and the total pressure is calculated from equation (A.6).

p_w , Vapor Pressure of Water Pruppacher and Klett gave a curve fit for the saturation pressure of vapor over water for the range of -58°F to 32°F (-50°C to 0°C). It is:

$$p_w = a_0 + \Delta T \left(a_1 + \Delta T \left(a_2 + \Delta T \left(\Delta T \left(a_3 + \Delta T \left(\Delta T \left(a_4 + \Delta T \left(\Delta T \left(a_5 + \Delta T a_6 \right) \right) \right) \right) \right) \right) \right) \right) \quad (\text{A.8})$$

where

$$\begin{aligned} \Delta T &= T - 491.67\text{R} \\ &= T - 273.15\text{K} \end{aligned} \quad (\text{A.9})$$

with coefficients:

$$\begin{aligned} a_0 &= .088586 \text{ psi} &= 610.78 \text{ Pa} \\ a_1 &= 3.5748 \times 10^{-3} \text{ psi/R} &= 44.365 \text{ Pa/K} \\ a_2 &= 6.3964 \times 10^{-5} \text{ psi/R}^2 &= 1.4289 \text{ Pa/K}^2 \end{aligned}$$

$$\begin{aligned} a_3 &= 6.5919 \times 10^{-7} \text{ psi/R}^3 &= 2.6506 \times 10^{-2} \text{ Pa/K}^3 \\ a_4 &= 4.1880 \times 10^{-9} \text{ psi/R}^4 &= 3.0312 \times 10^{-4} \text{ Pa/K}^4 \\ a_5 &= 1.5613 \times 10^{-11} \text{ psi/R}^5 &= 2.0341 \times 10^{-6} \text{ Pa/K}^5 \\ a_6 &= 2.6169 \times 10^{-14} \text{ psi/R}^6 &= 6.1368 \times 10^{-9} \text{ Pa/K}^6 \end{aligned}$$

Equation (A.8) can be used to find both the vapor pressure at the surface, p_{ww} , and that in the atmosphere, p_w , by substituting the appropriate absolute temperature, T , in equation (A.9). For glaze ice the surface is at the freezing temperature of water, so ΔT in either system of units is 0, and $p_{ww} = a_0$. To determine the atmospheric vapor pressure the ambient static temperature, T_{st} , in Rankine or Kelvin units, respectively, should be used.

In section 3.5 sublimation was neglected in the energy balance because it is small compared with the evaporation term. However, for completeness, it will be discussed briefly here. The driving force for sublimation is the difference between the partial pressure of vapor at the surface and that in the atmosphere. The atmospheric vapor pressure can be determined from equations (A.8), (A.9) and the coefficients a_0 to a_6 . At the surface, the partial pressure of vapor is the saturation pressure of water vapor over ice. Pruppacher and Klett's fit for the saturation pressure of vapor over ice for the range -58°F to 32°F (-50°C to 0°C) is:

$$p_{wi} = b_0 + \Delta T \left(b_1 + \Delta T \left(b_2 + \Delta T \left(\Delta T \left(b_3 + \Delta T \left(\Delta T \left(b_4 + \Delta T \left(\Delta T \left(b_5 + \Delta T b_6 \right) \right) \right) \right) \right) \right) \right) \right) \quad (\text{A.10})$$

with ΔT given by equation (A.9) and coefficients

$$\begin{aligned} b_0 &= .088606 \text{ psia} &= 610.92 \text{ nt/m}^2 \\ b_1 &= 4.0568 \times 10^{-3} \text{ psia/R} &= 50.347 \text{ Pa/K} \\ b_2 &= 8.4426 \times 10^{-5} \text{ psia/R}^2 &= 1.8860 \text{ Pa/K}^2 \\ b_3 &= 1.0386 \times 10^{-6} \text{ psia/R}^3 &= 4.1762 \times 10^{-2} \text{ Pa/K}^3 \\ b_4 &= 8.0476 \times 10^{-9} \text{ psia/R}^4 &= 5.8247 \times 10^{-4} \text{ Pa/K}^4 \\ b_5 &= 3.7141 \times 10^{-11} \text{ psia/R}^5 &= 4.8388 \times 10^{-6} \text{ Pa/K}^5 \\ b_6 &= 7.8412 \times 10^{-14} \text{ psia/R}^6 &= 1.8388 \times 10^{-8} \text{ Pa/K}^6 \end{aligned}$$

R_a , Gas Constant for Air The air gas constant is

$$\begin{aligned} R_a &= 53.34 \frac{\text{lb ft}}{\text{lbm R}} \\ &= .287 \frac{\text{nt m}}{\text{g K}} \end{aligned} \quad (\text{A.11})$$

T. Absolute Temperature Absolute temperatures were calculated from the temperatures in °F and °C in the standard way:

$$T = t + 459.67R = t + 273.15K \quad (\text{A.12})$$

By convention, the degree symbol, °, is omitted from Kelvin unit,⁷⁷ K. To be consistent with this practice, the degree symbol is omitted from the Rankine unit, R, as well.

T_{film}, Film Temperature The film temperature is used to evaluate air properties for convective heat transfer parameters and for diffusivity. The film temperature is the average of the free-stream static temperature and the surface temperature:

$$T_{film} = \frac{1}{2}(T_s + T_{st}) \quad (\text{A.13})$$

This temperature can be interpreted as approximately the mean temperature of the boundary layer.

t_s, Surface Temperature For glaze ice the existence of liquid water on the surface requires the surface temperature to be the freezing temperature of water. Thus,

$$\begin{aligned} t_s &= 32^\circ\text{F} \\ &= 0^\circ\text{C} \end{aligned} \quad (\text{A.14})$$

and

$$\begin{aligned} T_s &= 491.67R \\ &= 273.15K \end{aligned} \quad (\text{A.15})$$

T_{tot}, Total Temperature The total temperature is related to the static temperature for incompressible flow by the following expression:

$$T_{tot} = T_{st} + \frac{V^2}{2c_{p,a}} \quad (\text{A.16})$$

where $c_{p,a}$ is the specific heat of air, equation (A.1). For compressible flow, the relation is

$$T_{tot} = T_{st} \left(1 + \frac{\gamma - 1}{2} M^2 \right) \quad (\text{A.17})$$

However, there is less than .01% difference between the results obtained from equations (A.16) and (A.17) for speeds up to 400 mph. Note that equation (A.16) can be applied to either absolute or ordinary temperatures, while equation (A.17), in the form given, can only be used with absolute temperatures.

γ, Ratio of Specific Heats for Air The ratio of specific heats is

$$\begin{aligned} \gamma &= \frac{c_{p,a}}{c_{v,a}} \\ &= 1.40 \end{aligned} \quad (\text{A.18})$$

From reference 76 at -40°F γ varies from 1.402 to 1.404 as pressure varies from 6 to 14.5 psia. At 6 psia γ decreases from 1.402 to 1.401 as temperature increases from -40 to 40°F. At 14.5 psia γ decreases from 1.404 to 1.402 for the same temperature increase. All can be rounded off to 1.40. Therefore, the value in equation (A.18) is representative of γ for the range of temperatures and pressures of interest to icing.

Δ, Latent Heat From Pruppacher and Klett, the latent heat released when water freezes is

$$\begin{aligned} A_f &= 143.46 \frac{\text{Btu}}{\text{lbm}} + .485 \frac{\text{Btu}}{\text{lbm R}} (T - 491.67R) - \\ &1.39 \times 10^{-3} \frac{\text{Btu}}{\text{lbm R}^2} (T - 491.67R)^2 \\ &= 79.7 \frac{\text{cal}}{\text{g}} + .485 \frac{\text{cal}}{\text{g K}} (T - 273.15K) - \\ &2.5 \times 10^{-3} \frac{\text{cal}}{\text{g K}^2} (T - 273.15K)^2 \end{aligned} \quad (\text{A.19})$$

For scaling calculations, the temperature in this expression is the surface temperature in absolute units. Thus, incorporating equation (A.15) results in

$$A_f = 143.46 \frac{\text{Btu}}{\text{lbm}} = 79.7 \frac{\text{cal}}{\text{g}} \quad (\text{A.20})$$

for glaze ice.

Pruppacher and Klett give the following expression for the latent heat of vaporization:

$$\begin{aligned} A_v &= 1075 \frac{\text{Btu}}{\text{lbm}} \left(\frac{491.67R}{T} \right)^E \\ &= 597.3 \frac{\text{cal}}{\text{g}} \left(\frac{273.15K}{T} \right)^E \end{aligned} \quad (\text{A.21})$$

Where the exponent E is also a function of temperature:

$$\begin{aligned} E &= .167 + 2.039 \times 10^{-4} \frac{T}{R} \\ &= .167 + 3.670 \times 10^{-4} \frac{T}{K} \end{aligned} \quad (\text{A.22})$$

As in the evaluation of A_f the temperature to be used in these expressions is the surface temperature. Thus, for glaze ice

$$A_v = 1075 \frac{\text{Btu}}{\text{lbm}} = 597.3 \frac{\text{cal}}{\text{g}} \quad (\text{A.23})$$

Because the heat balance equations, in which A_f and A_v appear, are only of interest for glaze ice, equations (A.20) and (A.23) are not needed for rime scaling calculations.

μ . Viscosity The viscosity of air as a function of temperature can be obtained from reference 76. Over the range -40°F to 40°F these values were fit to the following expression:

$$\begin{aligned} \mu_a &= \frac{10^{-5}}{.18995 + 333.18 \left(\frac{R}{T} \right)} \frac{\text{lbm}}{\text{ft s}} \\ &= \frac{10^{-4}}{.12764 + 124.38 \left(\frac{K}{T} \right)} \frac{\text{g}}{\text{cm s}} \end{aligned} \quad (\text{A.24})$$

The air viscosity varies by less than .1% over the pressure range of 6 – 14.5 psia for the given temperature range, so the effect of pressure has been ignored. Depending on the application the temperature T may be either the free-stream static, T_{st} , or the film temperature from equation (A.13).

The viscosity of water used in these calculations was the value at the freezing point of water:

$$\mu_w = 1.20 \times 10^{-3} \frac{\text{lbm}}{\text{ft s}} = .01786 \frac{\text{g}}{\text{cm s}} \quad (\text{A.25})$$

ρ . Density The density of air as a function of temperature and pressure was found using the gas-law expression

$$\rho_a = \frac{P_{st}}{R_a T_{st}} \quad (\text{A.26})$$

where p_{st} and T_{st} are the static pressure and temperature of the airflow.

Ice density varies depending on the type of ice. For the scaling calculations a fixed value was assumed:

$$\rho_i = 57.2 \frac{\text{lbm}}{\text{ft}^3} = .917 \frac{\text{g}}{\text{cm}^3} \quad (\text{A.27})$$

There is an uncertainty of perhaps as much as 10% on this value, but as long as the same value is used for both reference and scale calculations, the scaling results should be insensitive to this uncertainty.

The density of water at the freezing point was used. It is

$$\rho_w = 62.4 \frac{\text{lbm}}{\text{ft}^3} = 1.0 \frac{\text{g}}{\text{cm}^3} \quad (\text{A.28})$$

σ_{wa} . Surface Tension The surface tension of water against air for the IRT demineralized water was measured

using a standard technique on three occasions using different samples.⁴² The value that has been used consistently in scaling calculations for the IRT is

$$\sigma_{wa} = 4.45 \times 10^{-3} \frac{\text{lb f}}{\text{ft}} = 65 \frac{\text{dyne}}{\text{cm}} \quad (\text{A.29})$$

The two other values reported in reference 42 were $3.33 \times 10^{-3} \text{lb f/ft}$ and $4.10 \times 10^{-3} \text{lb f/ft}$ (48.6 and 59.8 dyne/cm).

Surface tension changes when surfactant is added to the water. Reference 42 reported surface tensions of water measured with the addition of two surfactants at various concentrations. For all combinations, surface tension varied only from $1.94 \times 10^{-3} \text{lb f/ft}$ to $2.07 \times 10^{-3} \text{lb f/ft}$. For calculations of Weber numbers for IRT tests with surfactant addition, $2.06 \times 10^{-3} \text{lb f/ft}$ (30 dyne/cm) was selected as representative, and this value has been used consistently.

A.2. Similarity Parameters and Other Terms

The definitions of the similarity parameters and other formulations needed to perform icing scaling calculations will be repeated here from the main text; they are listed alphabetically.

$$A_c = \frac{LWC V \tau}{\rho_i d} \quad (\text{A.30})$$

$$b = \frac{LWC V \beta_0 c_{p,ws}}{h_c} \quad (\text{A.31})$$

$$d = 2r_{ie} \quad (\text{A.32})$$

$$h_c = \frac{k_a Nu_a}{d} \quad (\text{A.33})$$

$$\frac{h_{film}}{d} = \left(\frac{LWC}{\rho_w} \right)^{1/2} Re_a^{-1/4} \quad (\text{A.34})$$

$$h_G = \frac{h_c}{c_{p,a}} \left(\frac{Pr_a}{Sc_a} \right)^{0.67} \quad (\text{A.35})$$

When computing the values of h_c and h_G from equations (A.33) and (A.35) the film temperature, equation (A.13), should be used to evaluate k_a , Nu_a , Pr_a and Sc_a .

$$K = \frac{\rho_w \delta^2 V}{18d \mu_a} \quad (\text{A.36})$$

$$K_0 = \frac{1}{8} + \frac{\lambda}{\lambda_{Stokes}} \left(K - \frac{1}{8} \right) \quad (\text{A.37})$$

$$M_a = \frac{V}{\sqrt{\gamma R_a T_{st}}} \quad (\text{A.38})$$

$$n_0 = \left(\frac{c_{p,ws}}{\Lambda_f} \right) \left(\phi + \frac{\theta}{b} \right) \quad (\text{A.39})$$

$$Ca = \frac{\mu_w V}{\sigma_{wa}} \quad (\text{A.40})$$

$$Nu_a = 1.14 Pr_a^{0.4} Re_a^{0.5} \quad (\text{A.41})$$

$$Pr_a = \frac{c_{p,a} \mu_a}{k_a} \quad (\text{A.42})$$

$$r_A = \frac{\left(1 + \frac{q_c}{q_c} \right) h_c (T_s - T_{st})}{LWC V \Lambda_f} \quad (\text{A.43})$$

$$Re_a = \frac{V d \rho_a}{\mu_a} \quad (\text{A.44})$$

Note that when computing the value of Re_a for use in equation (3.33), the air density, ρ_a , and viscosity, μ_a , should be evaluated at the film temperature, equation (A.13).

$$Re_\delta = \frac{V \delta \rho_a}{\mu_a} \quad (\text{A.45})$$

$$Sc_a = \frac{\mu_a}{\rho_a D_v} \quad (\text{A.46})$$

$$We_\delta = \frac{V^2 \delta \rho_w}{\sigma_{wa}} \quad (\text{A.47})$$

$$We_c = \frac{V^2 d \rho_a}{\sigma_{w/a}} \quad (\text{A.48})$$

$$We_L = \frac{V^2 L \rho_w}{\sigma_{w/a}} \quad (\text{A.49})$$

$$\beta_\theta = \frac{1.40 \left(K_\theta - \frac{1}{8} \right)^{.84}}{1 + 1.40 \left(K_\theta - \frac{1}{8} \right)^{.84}} \quad (\text{A.50})$$

$$\frac{\delta_S}{\delta_R} = \left(\frac{d_S}{d_R} \right)^{.617} \left(\frac{p_S}{p_R} \right)^{.235} \left(\frac{V_S}{V_R} \right)^{-.383} \left(\frac{T_S}{T_R} \right)^{.235} \quad (\text{A.51})$$

Equation (A.51) is based on equation (0.18) of the main text with $\kappa = 3.38$ substituted.

$$\theta = T_s - T_{st} - \frac{V^2}{2c_{p,a}} + \frac{h_G}{h_c} \Lambda_v \left(\frac{\frac{p_{ww}}{T_{st}} - \frac{p_{tot}}{T_{tot}} \frac{p_w}{p_{st}}}{1 - \frac{p_{tot}}{T_{tot}} \frac{p_{ww}}{T_{st}}} \right) \quad (\text{A.52})$$

A tabulation of range parameter as a function of drop Reynolds number was given by Langmuir and Blodgett. A fit to their data has been used in scaling calculations for the IRT. It is

$$\frac{\lambda}{\lambda_{Stokes}} = \frac{1}{0.8388 + 0.001483 Re_\delta + 0.1847 \sqrt{Re_\delta}} \quad (\text{A.53})$$

$$\phi = T_f - T_{st} - \frac{V^2}{2c_{p,ws}} \quad (\text{A.54})$$

Appendix B Sample Scaling Calculations

B.1. Sample Calculations for Size Scaling (Ruff Method with Constant We_L)

An example of calculating the scale test conditions to simulate a given reference icing encounter will be detailed in this section. This illustration uses the Ruff method supplemented with constant We_L to find the scale velocity.

B.1.1. Choose Reference Conditions The following reference conditions will be used for an NACA 0012 airfoil:

$$\begin{aligned} c_R &= 36 \text{ in} && = 91.4 \text{ cm} \\ t_{st,R} &= 5.8 \text{ }^\circ\text{F} && = -14.6 \text{ }^\circ\text{C} \\ p_{tot} &= 14.5 \text{ psia} && = 1.00 \times 10^5 \text{ Pa} \\ V_R &= 150 \text{ mph} && = 67.1 \text{ m/s} \\ \delta_R &= 40 \text{ } \mu\text{m} \\ LWC_R &= 1 \text{ g/m}^3 \\ \tau_R &= 15.1 \text{ min} \end{aligned}$$

B.1.2. Calculate Values for Reference Properties and Parameters The leading-edge radius for the NACA 0012 airfoil is given by Abbott and von Doenhoff⁷⁸ as 1.58% of chord. Thus, with

$$\begin{aligned} d_R &= 0.0316 c_R \\ &= 1.138 \text{ in} && = 2.890 \text{ cm} \end{aligned}$$

From equation (A.12) the reference static temperature is

$$T_{st,R} = 465.47 \text{ R} \quad = 258.6 \text{ K}$$

Substituting V_R and T_R into equation (A.38) gives the reference Mach number,

$$M_{a,R} = 0.2080$$

The total temperature and static pressure can now be determined from equations (A.17), (A.12) and (A.7), respectively:

$$\begin{aligned} T_{tot,R} &= 469.5 \text{ R} && = 260.8 \text{ K} \\ t_{tot,R} &= 9.8 \text{ }^\circ\text{F} && = -12.3 \text{ }^\circ\text{C} \\ p_{st,R} &= 14.07 \text{ psi} && = 9.700 \times 10^4 \text{ Pa} \end{aligned}$$

The accumulation parameter is (eq. (3.26))

$$A_{c,R} = 2.293$$

The properties and parameters needed to determine K_0 will be calculated next, using the static temperature, $T_{st,R}$, for temperature-dependent properties:

$$\rho_{a,R} = 0.08163 \text{ lbm/ft}^3 \quad = 1.308 \text{ g/m}^3$$

$$\mu_{a,R} = 1.104 \times 10^{-5} \text{ lbm/ft s} \quad = 1.643 \times 10^{-4} \text{ g/cm s}$$

$$Re_{\delta,R} = 213.5$$

$$\lambda_R = 0.2592$$

$$\rho_w = 62.43 \text{ lbm/ft}^3 \quad = 1.000 \text{ g/cm}^3$$

$$K_R = 12.56$$

$$K_{\theta,R} = 3.350$$

$$\beta_{0,R} = 0.789$$

Values of the parameters (b , ϕ and θ) needed for the freezing fraction and the freezing fraction itself will now be found.

$$c_{p,wsR} = 1.007 \text{ Btu/lbm R} \quad = 1.007 \text{ cal/g K}$$

$$T_{film,R} = 478.6 \text{ R} \quad = 265.9 \text{ K}$$

$$k_{a,R} = 0.0137 \text{ Btu/hr ft R} \quad = 20.4 \text{ cal/hr m K}$$

$$Pr_{a,R} = 0.712$$

The Prandtl number was evaluated at the film temperature.

$$\rho_{a,R} = 0.0816 \text{ lbm/ft}^3 \quad = 1.308 \times 10^3 \text{ g/m}^3$$

$$Re_{a,R} = 1.542 \times 10^5$$

This is the model Reynolds number based on twice the leading-edge radius of curvature and properties at the free-stream static temperature. The following Reynolds number uses properties evaluated at the film temperature, as does the Nusselt number:

$$Re_{film,R} = 1.468 \times 10^5$$

$$Nu_R = 381.3$$

$$h_{c,R} = 55.10 \text{ Btu/hr ft}^2 \text{ R} \quad = 2.690 \times 10^5 \text{ cal/hr m}^2 \text{ K}$$

$$b_R = 0.7134$$

$$\phi_R = 25.24 \text{ R} \quad = 14.02 \text{ K}$$

$$p_{ww,R} = 0.0886 \text{ psia} \quad = 610.8 \text{ Pa}$$

$$p_{w,R} = 0.0288 \text{ psia} \quad = 198.4 \text{ Pa}$$

$$D_{v,R} = 2.249 \times 10^{-4} \text{ ft}^2/\text{s} \quad = 2.089 \times 10^{-5} \text{ m}^2/\text{s}$$

$$Sc_{a,R} = 0.6316$$

$$h_{G,R} = 0.06909 \text{ lbm/ft}^2 \text{ s} \quad = 337.3 \text{ g/m}^2 \text{ s}$$

$$\theta_R = 34.62 \text{ R} \quad = 19.23 \text{ K}$$

$$A_{f,R} = 143.5 \text{ Btu/lbm} \quad = 79.70 \text{ cal/g}$$

$$n_{0,R} = 0.518$$

$$We_{L,R} = 2.00 \times 10^6$$

B.1.3. Calculate Scale Properties, Parameters and Test Conditions A scale model chord of 10.5 in was chosen for this example.

$$d_s = 0.0316c_s \\ = 0.332 \text{ in} \quad = 0.843 \text{ cm}$$

Matching the We_L between reference and scale gives the simple relationship $V_S = V_R \sqrt{c_R/c_S}$. Then

$$V_S = 277.7 \text{ mph} \quad = 124.2 \text{ m/s}$$

The scale We_L calculated from this velocity is, of course,

$$We_{L,S} = 2.00 \times 10^6$$

The static temperature can be found in terms of ϕ_S by rearranging equation (A.54):

$$T_{st,S} = T_f - \phi_S - V_S^2 / 2c_{p,ws}$$

Because $\phi_S = \phi_R$ is one of the similarity equalities, this equation can be solved to give:

$$T_{st,S} = 463.1 \text{ R} \quad = 257.3 \text{ K}$$

$$t_{st,S} = 3.5 \text{ }^\circ\text{F} \quad = -15.8 \text{ }^\circ\text{C}$$

$$M_{a,S} = 0.386$$

$$T_{tot,S} = 477.0 \text{ R} \quad = 265.0 \text{ K}$$

$$t_{tot,S} = 17.3 \text{ }^\circ\text{F} \quad = -8.2 \text{ }^\circ\text{C}$$

$$p_{st,S} = 13.1 \text{ psia} \quad = 9.02 \times 10^4 \text{ Pa}$$

The scale drop size can now be determined. Equation (A.51) can be used for this purpose, or that equation can provide a first guess of δ_S to try to match $K_{0,S}$ with $K_{0,R}$. Solving equation (A.51) for δ_S gives

$$\delta_S = 14.5 \text{ } \mu\text{m}$$

$K_{0,S}$ can now be calculated to compare with $K_{0,R}$:

$$\rho_{a,S} = 0.0765 \text{ lbm/ft}^3 \quad = 1.23 \times 10^3 \text{ g/m}^3$$

$$\mu_{a,S} = 1.10 \times 10^{-5} \text{ lbm/ft s} \quad = 1.64 \times 10^{-4} \text{ g/cm s}$$

$$Re_{\delta,S} = 134.9$$

$$\lambda/\lambda_{\text{Stokes}} = .314$$

$$K_S = 10.5$$

$$K_{0,S} = 3.39$$

This value of $K_{0,S}$ is within about 1% of the $K_{0,R}$ calculated above. For practical applications, this is close enough. For the purposes of illustration, however, the calculation will be continued with a new estimate for δ_S :

$$\delta_S = (14.5 \text{ } \mu\text{m})(K_{0,R}/K_{0,S}) = 14.3 \text{ } \mu\text{m}$$

$$Re_{\delta,S} = 133.3$$

$$\lambda/\lambda_{\text{Stokes}} = 0.316$$

$$K_S = 10.3$$

$$K_{0,S} = 3.33$$

Finally, linear interpolation between the two previous δ_S and their corresponding $K_{0,S}$ gives a third estimate of drop size:

$$\delta_S = 14.5 \text{ } \mu\text{m} + (14.3 \text{ } \mu\text{m} - 14.5 \text{ } \mu\text{m}) \frac{3.35 - 3.39}{3.33 - 3.39} \\ = 14.4 \text{ } \mu\text{m}$$

$$Re_{\delta,S} = 133.9$$

$$\lambda/\lambda_{\text{Stokes}} = 0.315$$

$$K_S = 10.4$$

$$K_{0,S} = 3.35$$

$$\beta_{0,S} = 0.789$$

The final value of $K_{0,S}$ matches $K_{0,R}$ to two decimal places. Note that the final value of δ_S is only .1 μm less than the original estimate from equation (A.51). This difference is much less than the experimental uncertainty in drop MVD, so it can be seen that equation (A.51) provides entirely adequate values of scale drop size for this example. This adequacy of equation (A.51) has also been observed for a variety of scaling situations and reference test conditions.

The scale LWC can now be determined by matching the scale and reference freezing fraction, n_0 . As with the solution for drop size, an iterative procedure is required. The first guess is to match LWC_S and LWC_R . Thus,

$$LWC_S = 1 \text{ g/m}^3$$

$$c_{p,ws,S} = 1.007 \text{ Btu/lbm R} \quad = 1.007 \text{ cal/g K}$$

$$T_{film,S} = 477.4 \text{ R} \quad = 265.2 \text{ K}$$

$$k_{a,S} = 0.01367 \text{ Btu/hr ft R} \quad = 20.35 \text{ cal/hr m K}$$

$$Pr_{a,S} = 0.7118$$

$$\rho_{a,S} = 0.07626 \text{ lbm/ft}^3 \quad = 1.222 \times 10^3 \text{ g/m}^3$$

$$Re_{a,S} = 7.811 \times 10^4$$

$$Re_{film,S} = 7.421 \times 10^4$$

$$Nu_{a,S} = 271.1$$

$$h_{c,S} = 134.0 \text{ Btu/hr ft}^2 \text{ R} \quad = 6.544 \times 10^5 \text{ cal/hr m}^2 \text{ K}$$

$$b_S = 0.5431$$

$$\phi_S = 25.24 \text{ R} \quad = 14.02 \text{ K}$$

(Recall that the scale value of ϕ was set to the reference value earlier in this section to find the scale static temperature.)

$$p_{ww,S} = .08859 \text{ psia} \quad = 610.8 \text{ Pa}$$

$$\begin{aligned}
p_{w,S} &= .02585 \text{ psia} &= 178.2 \text{ Pa} \\
D_{v,S} &= 2.394 \times 10^{-4} \text{ ft}^2/\text{s} &= 2.224 \times 10^{-5} \text{ m}^2/\text{s} \\
Sc_{a,S} &= 0.6339 \\
h_{G,S} &= 0.1676 \text{ lbm}/\text{ft}^2 \text{ s} &= 818.5 \text{ g}/\text{m}^2 \text{ s} \\
\theta_S &= 27.72 \text{ R} &= 15.42 \text{ K} \\
A_{f,S} &= 143.5 \text{ Btu}/\text{lbm} &= 79.7 \text{ cal}/\text{g} \\
n_{0,S} &= 0.536
\end{aligned}$$

This first-guess value of LWC_S leads to a scale freezing fraction a little higher than the reference value of 0.518, so a second estimate will be made by forming a simple ratio with the desired $n_{0,S}$ of 0.518:

$$LWC_S = 1 \frac{\text{g}}{\text{m}^3} \left(\frac{0.536}{0.518} \right) = 1.035 \frac{\text{g}}{\text{m}^3}$$

Both ϕ and θ as well as the properties needed to calculate n_0 are independent of LWC . Therefore, with the new estimate for LWC it is only necessary to reevaluate b_S :

$$b_S = 0.5621$$

$$n_{0,S} = 0.524$$

As this freezing fraction is still too high, a third estimate of LWC will be made by extrapolating from the two previous results:

$$\begin{aligned}
LWC_S &= 1.000 \frac{\text{g}}{\text{m}^3} + \left(1.037 \frac{\text{g}}{\text{m}^3} - 1.000 \frac{\text{g}}{\text{m}^3} \right) \frac{0.536 - 0.518}{0.536 - 0.524} \\
&= 1.052 \frac{\text{g}}{\text{m}^3}
\end{aligned}$$

This new value of LWC_S then gives the following values of b_S and $n_{0,S}$:

$$b_S = 0.5714$$

$$n_{0,S} = 0.518$$

Thus, with $LWC_S = 1.052 \text{ g}/\text{m}^3$ the scale and reference freezing fractions match. This final value of LWC_S is only about 5% greater than the original estimate, while the experimental uncertainty in LWC is about $\pm 10\%$. Furthermore, for analytical freezing fractions of this magnitude, experimental ice shapes do not show discernable differences for freezing fraction variations less than 10%. Therefore, if the estimated LWC_S results in a scale freezing fraction within about 10% of the reference value, that is usually close enough, and the above sequence of calculations to refine the original estimate of LWC_S would not have been necessary in a practical application.

It only remains to determine the scale icing time. This is found by setting $A_{c,S} = A_{c,R}$ and solving equation (3.26) for the time:

$$\tau_S = 2.26 \text{ min}$$

Table B.I. gives a number of sample reference conditions with the corresponding size scaling test conditions found using the Ruff Method supplemented with constant We_L to find the scale velocity. Reference and scale similarity parameters are also given in the table. Case 1 is the size scaling example presented in section B.1. Numbers in the table were generated with a scaling computer program and were rounded off for presentation.

B.2. Sample Calculations for LWC Scaling (Olsen Method)

The Olsen method maintains scale and reference accumulation parameter and freezing fraction the same for fixed values of model size, velocity and drop size. Scale LWC can be chosen arbitrarily, then scale temperature is calculated to provide a match of freezing fraction, and scale icing time is calculated by matching accumulation parameter.

B.2.1. Choose Reference Conditions The following reference conditions will be used, with, again, an NACA 0012 airfoil:

$$\begin{aligned}
c_R &= 36 \text{ in} &= 91.4 \text{ cm} \\
t_{st,R} &= 19.6 \text{ }^\circ\text{F} &= -6.9 \text{ }^\circ\text{C} \\
p_{tot} &= 14.5 \text{ psia} &= 1.00 \times 10^5 \text{ Pa} \\
V_R &= 200 \text{ mph} &= 89.4 \text{ m/s} \\
\delta_R &= 20 \text{ } \mu\text{m} \\
LWC_R &= 0.25 \text{ g}/\text{m}^3 \\
\tau_R &= 25 \text{ min}
\end{aligned}$$

B.2.2. Calculate Values for Reference Properties and Parameters

The combination of reference velocity, drop MVD and LWC given in section B.2.1 is outside the current range of calibrated conditions for the IRT. Consequently, in order to perform a test, it is necessary to choose a new LWC that falls within the IRT calibrated envelope. Scale model size, velocity and drop size will be set to the same values as the reference; thus, K_θ is already matched between scale and reference. This parameter only needs to be evaluated for the purpose of finding β_0 , which is needed to find n_0 . Freezing fraction and accumulation parameter will be calculated for the reference case.

$$\begin{aligned}
d_R &= 0.0316 c_R \\
&= 1.138 \text{ in} &= 2.890 \text{ cm}
\end{aligned}$$

Table B.I
 Examples of Size Scaling
 Ruff Method with Constant We_L
 NACA 0012 Airfoils

Case	Type	c , in	t_{st} , °F	t_{tot} , °F	V , mph	δ , μm	LWC , g/m ³	τ , min	K_θ	β_0 , %	A_c	n_0	b	ϕ , °F	θ , °F	Re , 10 ⁴	We_L , 10 ⁶	M
1	Ref	36.0	5.8	9.8	150.0	40.0	1.00	15.1	3.35	0.789	2.29	0.518	0.714	25.2	34.6	15.4	2.00	0.208
"	Scale	10.5	3.5	17.3	277.7	14.4	1.05	2.3	3.35	0.789	2.29	0.518	0.572	25.2	27.8	7.8	2.00	0.386
2	Ref	72.0	0.0	4.0	150.0	40.0	1.00	25.0	1.72	0.675	1.90	0.559	0.862	31.0	41.9	31.5	4.00	0.209
"	Scale	36.0	-1.0	7.1	212.1	22.5	1.09	8.1	1.72	0.675	1.90	0.559	0.804	31.0	39.0	21.7	4.00	0.296
3	Ref	72.0	0.0	4.0	150.0	30.0	1.00	25.0	1.12	0.583	1.90	0.613	0.745	31.0	41.9	31.5	4.00	0.209
"	Scale	36.0	-1.0	7.1	212.1	17.0	1.09	8.1	1.12	0.583	1.90	0.613	0.695	31.0	39.0	21.7	4.00	0.296
4	Ref	72.0	0.0	4.0	150.0	20.0	1.00	25.0	0.62	0.438	1.90	0.743	0.560	31.0	41.9	31.5	4.00	0.209
"	Scale	36.0	-1.0	7.1	212.1	11.4	1.09	8.1	0.62	0.438	1.90	0.743	0.522	31.0	39.0	21.7	4.00	0.296
5	Ref	72.0	0.0	7.2	200.0	40.0	1.00	25.0	2.03	0.706	2.53	0.471	1.054	30.3	38.8	41.0	7.10	0.279
"	Scale	36.0	-1.7	12.6	282.8	22.3	1.01	8.8	2.03	0.706	2.53	0.471	0.917	30.3	33.7	27.7	7.10	0.395
6	Ref	72.0	0.0	7.2	200.0	30.0	1.00	25.0	1.33	0.620	2.53	0.507	0.926	30.3	38.8	41.0	7.10	0.279
"	Scale	36.0	-1.7	12.6	282.8	16.8	1.01	8.8	1.33	0.620	2.53	0.507	0.805	30.3	33.7	27.7	7.10	0.395
7	Ref	72.0	0.0	7.2	200.0	20.0	1.00	25.0	0.74	0.481	2.53	0.592	0.718	30.3	38.8	41.0	7.10	0.279
"	Scale	36.0	-1.7	12.6	282.8	11.3	1.01	8.8	0.74	0.481	2.53	0.592	0.624	30.3	33.7	27.7	7.10	0.395
8	Ref	72.0	0.0	4.0	150.0	40.0	1.00	25.0	1.72	0.675	1.90	0.559	0.862	31.0	41.9	31.5	4.00	0.209
"	Scale	24.0	-1.9	10.2	259.8	16.1	1.10	4.4	1.72	0.675	1.90	0.559	0.745	31.0	36.2	17.3	4.00	0.363
9	Ref	72.0	0.0	4.0	150.0	30.0	1.00	25.0	1.12	0.583	1.90	0.613	0.745	31.0	41.9	31.5	4.00	0.209
"	Scale	24.0	-1.9	10.2	259.8	12.2	1.10	4.4	1.12	0.583	1.90	0.613	0.644	31.0	36.2	17.3	4.00	0.363
10	Ref	72.0	0.0	4.0	150.0	20.0	1.00	25.0	0.62	0.438	1.90	0.743	0.560	31.0	41.9	31.5	4.00	0.209
"	Scale	24.0	-1.9	10.2	259.8	8.2	1.10	4.4	0.62	0.438	1.90	0.743	0.484	31.0	36.2	17.3	4.00	0.363
11	Ref	72.0	0.0	7.2	200.0	40.0	1.00	25.0	2.03	0.706	2.53	0.471	1.054	30.3	38.8	41.0	7.10	0.279
"	Scale	24.0	-3.4	18.1	346.4	15.8	0.92	5.2	2.03	0.706	2.53	0.471	0.779	30.3	28.6	21.6	7.10	0.485
12	Ref	72.0	0.0	7.2	200.0	30.0	1.00	25.0	1.33	0.620	2.53	0.507	0.926	30.3	38.8	41.0	7.10	0.279
"	Scale	24.0	-3.4	18.1	346.4	11.9	0.92	5.2	1.33	0.620	2.53	0.507	0.684	30.3	28.6	21.6	7.10	0.485
13	Ref	72.0	0.0	7.2	200.0	20.0	1.00	25.0	0.74	0.481	2.53	0.592	0.718	30.3	38.8	41.0	7.10	0.279
"	Scale	24.0	-3.4	18.1	346.4	8.1	0.92	5.2	0.74	0.481	2.53	0.592	0.530	30.3	28.6	21.6	7.10	0.485
14	Ref	72.0	10.0	17.2	200.0	40.0	1.00	25.0	2.03	0.706	2.53	0.315	1.055	20.3	26.0	39.6	7.10	0.276
"	Scale	24.0	6.6	28.1	346.4	15.8	0.77	6.3	2.03	0.706	2.53	0.315	0.647	20.3	15.9	20.8	7.10	0.480
15	Ref	72.0	10.0	17.2	200.0	30.0	1.00	25.0	1.32	0.620	2.53	0.339	0.926	20.3	26.0	39.5	7.10	0.276
"	Scale	24.0	6.6	28.1	346.4	12.0	0.77	6.3	1.32	0.620	2.53	0.339	0.569	20.3	15.9	20.8	7.10	0.480
16	Ref	72.0	10.0	17.2	200.0	20.0	1.00	25.0	0.74	0.480	2.53	0.397	0.717	20.3	26.0	39.5	7.10	0.276
"	Scale	24.0	6.6	28.1	346.4	8.1	0.77	6.3	0.74	0.480	2.53	0.397	0.440	20.3	15.9	20.8	7.10	0.480
17	Ref	72.0	15.0	22.2	200.0	30.0	1.00	25.0	1.32	0.620	2.53	0.252	0.926	15.3	19.1	38.8	7.10	0.275
"	Scale	24.0	11.6	33.1	346.4	12.0	0.60	8.0	1.32	0.620	2.53	0.252	0.443	15.3	9.1	20.5	7.10	0.477

$$T_{st,R} = 479.3 \text{ R} = 266.3 \text{ K}$$

Substituting V_R and T_R into equation (A.38) gives the reference Mach number,

$$M_{a,R} = 0.2734$$

$$T_{tot,R} = 486.4 \text{ R} = 270.2 \text{ K}$$

$$t_{tot,R} = 26.8^\circ\text{F} = -2.9^\circ\text{C}$$

$$p_{st,R} = 13.77 \text{ psi} = 9.492 \times 10^4 \text{ Pa}$$

$$A_{c,R} = 1.265$$

$$\rho_{a,R} = 0.07754 \text{ lbm/ft}^3 = 1.242 \text{ g/m}^3$$

$$\mu_{a,R} = 1.130 \times 10^{-5} \text{ lbm/ft s} = 1.681 \times 10^{-4} \text{ g/cm s}$$

$$Re_{\delta,R} = 132.1$$

$$\lambda_R = 0.3167$$

$$\rho_w = 62.43 \text{ lbm/ft}^3 = 1.000 \text{ g/cm}^3$$

$$K_R = 4.09$$

$$K_{\theta,R} = 1.381$$

$$\beta_{\theta,R} = 0.629$$

Values of the parameters b , ϕ and θ used in the freezing fraction expression and the freezing fraction itself will next be determined.

$$c_{p,ws,R} = 1.007 \text{ Btu/lbm R} = 1.007 \text{ cal/g K}$$

$$T_{film,R} = 485.5 \text{ R} = 269.7 \text{ K}$$

$$k_{a,R} = 0.01386 \text{ Btu/hr ft R} = 20.62 \text{ cal/hr m K}$$

$$Pr_{a,R} = 0.7115$$

$$Re_{a,R} = 1.909 \times 10^5$$

$$Re_{film,R} = 1.867 \times 10^5$$

$$Nu_{a,R} = 429.8$$

$$h_{c,R} = 62.84 \text{ Btu/hr ft}^2 \text{ R} = 3.068 \times 10^5 \text{ cal/hr m}^2 \text{ K}$$

$$b_R = 0.1662$$

$$\phi_R = 10.69 \text{ R} = 5.94 \text{ K}$$

$$p_{ww,R} = 0.08859 \text{ psia} = 610.8 \text{ Pa}$$

$$p_{w,R} = 0.05293 \text{ psia} = 365.0 \text{ Pa}$$

$$D_{v,R} = 2.362 \times 10^{-4} \text{ ft}^2/\text{s} = 2.194 \times 10^{-5} \text{ m}^2/\text{s}$$

$$Sc_{a,R} = 0.6308$$

$$h_{G,R} = 0.07884 \text{ lbm/ft}^2 \text{ s} = 384.9 \text{ g/m}^2 \text{ s}$$

$$\theta_R = 12.38 \text{ R} = 6.88 \text{ K}$$

$$A_{f,R} = 143.5 \text{ Btu/lbm} = 79.70 \text{ cal/g}$$

$$n_{\theta,R} = 0.598$$

B.2.3. Choose Scale Conditions All scale conditions are the same as the reference except for the scale liquid-water content, temperature and time. LWC_S was selected to fall within the IRT calibrated envelope.

$$c_S = 36 \text{ in} = 91.4 \text{ cm}$$

$$p_{tot} = 14.5 \text{ psia} = 1.00 \times 10^5 \text{ Pa}$$

$$V_S = 200 \text{ mph} = 89.4 \text{ m/s}$$

$$\delta_S = 20 \text{ }\mu\text{m}$$

$$LWC_S = 0.60 \text{ g/m}^3$$

B.2.4. Calculate Scale Properties, Parameters and Test Conditions The strategy in the Olsen method is to adjust temperature so that the scale and reference freezing fractions match for the given d , V , δ and LWC .

Because conditions affecting the modified inertia parameter are the same as for the reference situation, the leading-edge collection efficiency will have the same value as the reference. Therefore,

$$\beta_{\theta,S} = 0.629$$

$$c_{p,ws,S} = 1.007 \text{ Btu/lbm R} = 1.007 \text{ cal/g K}$$

An initial guess for the value of scale temperature can be made by setting it equal to the reference value:

$$T_{st,S} = 479.3 \text{ R} = 266.3 \text{ K}$$

$$M_{a,S} = 0.2734$$

$$T_{tot,S} = 486.4 \text{ R} = 270.2 \text{ K}$$

$$p_{st,S} = 13.77 \text{ psi} = 9.492 \times 10^4 \text{ Pa}$$

$$T_{film,S} = 485.5 \text{ R} = 269.7 \text{ K}$$

$$k_{a,S} = 0.01386 \text{ Btu/hr ft R} = 20.62 \text{ cal/hr m K}$$

$$Pr_{a,S} = 0.7115$$

$$\rho_{a,S} = 0.07754 \text{ lbm/ft}^3 = 1.242 \times 10^3 \text{ g/m}^3$$

$$Re_{a,S} = 1.909 \times 10^5$$

$$Re_{film,S} = 1.867 \times 10^5$$

$$Nu_{a,S} = 429.8$$

$$h_{c,S} = 62.84 \text{ Btu/hr ft}^2 \text{ R} = 3.068 \times 10^5 \text{ cal/hr m}^2 \text{ K}$$

$$b_S = 0.3988$$

$$\phi_S = 10.69 \text{ R} = 5.94 \text{ K}$$

$$p_{ww,S} = 0.08859 \text{ psia} = 610.8 \text{ Pa}$$

$$p_{w,S} = 0.05293 \text{ psia} = 365.0 \text{ Pa}$$

$$D_{v,S} = 2.362 \times 10^{-4} \text{ ft}^2/\text{s} = 2.194 \times 10^{-5} \text{ m}^2/\text{s}$$

$$\begin{aligned}
Sc_{a,S} &= 0.6308 \\
h_{G,S} &= 0.07884 \text{ lbm/ft}^2 \text{ s} = 384.9 \text{ g/m}^2 \text{ s} \\
\theta_S &= 12.38 \text{ R} = 6.877 \text{ K} \\
A_{f,S} &= 143.5 \text{ Btu/lbm} = 79.7 \text{ cal/g} \\
n_{0,S} &= 0.2931
\end{aligned}$$

Because this scale freezing fraction is lower than the reference value of 0.598, the estimated scale temperature was too high. It will be arbitrarily decreased by 5 R and the calculations repeated:

$$\begin{aligned}
T_{st,S} &= 474.3 \text{ R} = 263.5 \text{ K} \\
M_{a,S} &= 0.2748 \\
T_{tot,S} &= 481.4 \text{ R} = 267.5 \text{ K} \\
p_{st,S} &= 13.76 \text{ psi} = 9.486 \times 10^4 \text{ Pa} \\
T_{film,S} &= 483.0 \text{ R} = 268.3 \text{ K} \\
k_{a,S} &= 0.01380 \text{ Btu/hr ft R} = 20.54 \text{ cal/hr m K} \\
Pr_{a,S} &= 0.7116 \\
\rho_{a,S} &= 0.07832 \text{ lbm/ft}^3 = 1.255 \times 10^3 \text{ g/m}^3 \\
Re_{a,S} &= 1.944 \times 10^5 \\
Re_{film,S} &= 1.883 \times 10^5 \\
Nu_{a,S} &= 431.8 \\
h_{c,S} &= 62.86 \text{ Btu/hr ft}^2 \text{ R} = 3.069 \times 10^5 \text{ cal/hr m}^2 \text{ K} \\
b_S &= 0.3987 \\
\phi_S &= 15.69 \text{ R} = 8.72 \text{ K} \\
p_{ww,S} &= 0.08859 \text{ psia} = 610.8 \text{ Pa} \\
p_{w,S} &= 0.04264 \text{ psia} = 294.0 \text{ Pa} \\
D_{v,S} &= 2.339 \times 10^{-4} \text{ ft}^2/\text{s} = 2.173 \times 10^{-5} \text{ m}^2/\text{s} \\
Sc_{a,S} &= 0.6313 \\
h_{G,S} &= 0.07883 \text{ lbm/ft}^2 \text{ s} = 384.9 \text{ g/m}^2 \text{ s} \\
\theta_S &= 19.64 \text{ R} = 10.91 \text{ K} \\
A_{f,S} &= 143.5 \text{ Btu/lbm} = 79.7 \text{ cal/g} \\
n_{0,S} &= 0.4560
\end{aligned}$$

Note that many of the values changed inconsequentially when the temperature was changed from the initial estimate. The calculations can be simplified if desired by approximating the parameter b_S with

$$b_S = b_R \frac{LWC_S}{LWC_R}$$

Using this constant value for b_S for all the iterations, only ϕ_S and θ_S need to be re-evaluated for each new temperature estimate. However, for this sample calculation, the complete set of evaluations will be shown.

The next temperature estimate can be found by a linear extrapolation of the two previous temperatures with their corresponding freezing fractions:

$$T_{st,S} = T_{st,S1} + \frac{n_{0,R} - n_{0,S1}}{n_{0,S2} - n_{0,S1}} (T_{st,S2} - T_{st,S1})$$

$$\begin{aligned}
T_S &= 469.9 \text{ R} = 261.1 \text{ K} \\
M_{a,S} &= 0.2761 \\
T_{tot,S} &= 477.1 \text{ R} = 265.1 \text{ K} \\
t_{st,R} &= 10.24 \text{ }^\circ\text{F} = -12.09 \text{ }^\circ\text{C} \\
t_{tot,R} &= 17.40 \text{ }^\circ\text{F} = -8.11 \text{ }^\circ\text{C} \\
p_{st,S} &= 13.75 \text{ psi} = 9.481 \times 10^4 \text{ Pa} \\
T_{film,S} &= 480.8 \text{ R} = 267.1 \text{ K} \\
k_{a,S} &= 0.01375 \text{ Btu/hr ft R} = 20.46 \text{ cal/hr m K} \\
Pr_{a,S} &= 0.7116 \\
\rho_{a,S} &= 0.07901 \text{ lbm/ft}^3 = 1.266 \times 10^3 \text{ g/m}^3 \\
Re_{a,S} &= 1.975 \times 10^5 \\
Re_{film,S} &= 1.898 \times 10^5 \\
Nu_{a,S} &= 433.5 \\
h_{c,S} &= 62.88 \text{ Btu/hr ft}^2 \text{ R} = 3.070 \times 10^5 \text{ cal/hr m}^2 \text{ K} \\
b_S &= 0.3989 \\
\phi_S &= 20.06 \text{ R} = 11.14 \text{ K} \\
p_{ww,S} &= 0.08859 \text{ psia} = 610.8 \text{ Pa} \\
p_{w,S} &= 0.03515 \text{ psia} = 242.4 \text{ Pa} \\
D_{v,S} &= 2.319 \times 10^{-4} \text{ ft}^2/\text{s} = 2.154 \times 10^{-5} \text{ m}^2/\text{s} \\
Sc_{a,S} &= 0.6317 \\
h_{G,S} &= 0.07882 \text{ lbm/ft}^2 \text{ s} = 384.8 \text{ g/m}^2 \text{ s} \\
\theta_S &= 25.65 \text{ R} = 14.25 \text{ K} \\
A_{f,S} &= 143.5 \text{ Btu/lbm} = 79.7 \text{ cal/g} \\
n_{0,S} &= 0.5927
\end{aligned}$$

This value of freezing fraction is within 1% of the reference value of 0.5982; consequently, $T_{st,S} = 469.9 \text{ R}$ (261.1 K) will be accepted as the scale temperature.

Finally, spray time is found by matching scale and reference accumulation parameter:

$$A_{c,S} = A_{c,R} = 1.265$$

$$\tau_S = A_{c,S} \frac{d_S \rho_i}{LWC_S V_S} = 10.4 \text{ min}$$

Table B.II gives the reference and scale information for several LWC scaling cases using the Olsen method. The detailed sample calculations offered in section B.2. were for case 1 of the table.

B.3. Procedures for Scaling Drop Size and Temperature

B.3.1. Drop-Size The calibrated envelope of Appendix C cloud conditions for the IRT currently covers a range of drop sizes from 14 to 50 μm MVD. Figure 4.1.1. showed the Mod-1 and Standard nozzle calibrated LWC -vs- δ envelopes for an airspeed of 200 mph (89 m/s). In section 4.1 some of the facility limitations were discussed. In this section, examples will be given for scaling drop size when desired conditions fall outside the capability of the facility to test them. These desired conditions may themselves be the result of a size-scaling calculation. For example, in Table B.I the scale drop

sizes calculated for cases 4, 7, 9, 10, 12, 13, 15, 16 and 17 are all below the 14- μm minimum calibrated drop size for the IRT. However, in section 3.3.3 it was demonstrated that the main ice shape was unaffected by a change in drop size from 20 to 55 μm . If this insensitivity to drop size holds true for smaller drops, it should be possible to make at least small changes to the scale drop size and still obtain scale ice shapes that adequately represent the reference shape. Using case 4 in Table B.I as an example, the procedure is:

- (1) Increase δ_S from 11.4 to 15 μm without changing c_S , V_S or LWC_S . The scale cloud conditions now fall within the IRT envelope.
- (2) Calculate the new $\beta_{0,S}$. Note that this parameter will no longer match the reference value, and impingement limits will therefore be different for scale and reference accretions. For this example $\beta_{0,S}$ increases from 0.438 to 0.540.
- (3) Calculate the new scale icing time that will produce a match between the scale and reference products $\beta_{0,S} A_{c,S}$ and $\beta_{0,R} A_{c,R}$.
- (4) Calculate a new scale temperature such that $n_{0,S}$ matches the reference value. This step is necessary because the increase in $\beta_{0,S}$ would otherwise decrease the

Table B.II
Examples of LWC Scaling
Olsen Method
NACA 0012 Airfoils

Case	Type	c , in	t_{st} , °F	t_{tot} , °F	V , mph	δ , μm	LWC , g/m^3	τ , min	K_0	β_0 , %	A_c	n_0	b	ϕ , °F	θ , °F	Re , 10^4	We_L , 10^6	M
1	Ref	36.0	19.6	26.8	200.0	20.0	0.25	25.0	1.38	0.629	1.26	0.598	0.166	10.7	12.4	1.91	3.55	0.273
"	Scale	36.0	10.0	17.2	200.0	20.0	0.60	10.4	1.38	0.629	1.26	0.598	0.399	20.3	25.9	1.98	3.55	0.276
2	Ref	36.0	23.7	27.7	150.0	20.0	0.25	25.0	1.16	0.590	0.95	0.548	0.134	7.4	9.4	1.44	2.00	0.204
"	Scale	36.0	17.4	21.4	150.0	20.0	0.55	11.4	1.16	0.590	0.95	0.548	0.294	13.7	18.9	1.48	2.00	0.205
3	Ref	36.0	21.8	25.9	150.0	40.0	0.25	25.0	3.35	0.789	0.95	0.548	0.179	9.2	12.3	1.45	2.00	0.205
"	Scale	36.0	7.8	11.8	150.0	40.0	0.82	7.6	3.35	0.789	0.95	0.548	0.586	23.3	32.1	1.53	2.00	0.208
4	Ref	36.0	20.3	27.5	200.0	20.0	0.25	25.0	1.38	0.629	1.26	0.548	0.166	10.0	11.3	1.90	3.55	0.273
"	Scale	36.0	15.2	22.3	200.0	20.0	0.45	13.9	1.38	0.629	1.26	0.548	0.299	15.1	18.8	1.94	3.55	0.275
5	Ref	36.0	18.4	25.5	200.0	40.0	0.25	25.0	3.96	0.812	1.26	0.548	0.215	11.9	14.2	1.92	3.55	0.274
"	Scale	36.0	5.4	12.6	200.0	40.0	0.70	8.9	3.96	0.812	1.26	0.548	0.601	24.9	32.0	2.01	3.55	0.277
6	Ref	36.0	16.4	27.6	250.0	20.0	0.25	25.0	1.59	0.658	1.58	0.548	0.197	12.9	12.8	2.34	5.55	0.343
"	Scale	36.0	12.6	23.7	250.0	20.0	0.38	16.4	1.59	0.658	1.58	0.548	0.300	16.8	18.4	2.38	5.55	0.344
7	Ref	36.0	14.5	25.6	250.0	40.0	0.25	25.0	4.52	0.829	1.58	0.548	0.249	14.9	15.7	2.36	5.55	0.344
"	Scale	36.0	4.5	15.7	250.0	40.0	0.55	11.4	4.52	0.829	1.58	0.548	0.547	24.8	29.1	2.45	5.55	0.347
8	Ref	36.0	12.0	28.1	300.0	20.0	0.25	25.0	1.78	0.681	1.90	0.548	0.228	16.1	14.1	2.76	7.99	0.413
"	Scale	36.0	8.7	24.8	300.0	20.0	0.35	17.9	1.78	0.682	1.90	0.548	0.319	19.5	18.6	2.79	7.99	0.415
9	Ref	36.0	10.0	26.1	300.0	40.0	0.25	25.0	5.05	0.842	1.90	0.548	0.281	18.2	16.8	2.78	7.99	0.414
"	Scale	36.0	1.6	17.8	300.0	40.0	0.48	13.0	5.05	0.842	1.90	0.548	0.540	26.5	27.8	2.86	7.99	0.418

scale freezing fraction. For case 4, $t_{st,S}$ has to be reduced from -1°F to -5.9°F to give an $n_{0,S}$ of 0.743, the reference value.

Figure B.1. illustrates this example, showing a map of calibrated cloud conditions for the IRT and the specific LWC -MVD combination for this example. Because the IRT undergoes improvements from time to time the cloud calibration is updated periodically. Consequently, the envelopes shown here may not be the same as the current calibration for the IRT. Figure B.1. (a) shows the cloud envelope for the reference velocity of 150 mph (67 m/s). The portion of the map obtained with mod-1 nozzles is given with a solid line and for the standard nozzles with a dashed line. The solid point on the figure represents the reference drop size and liquid water content.

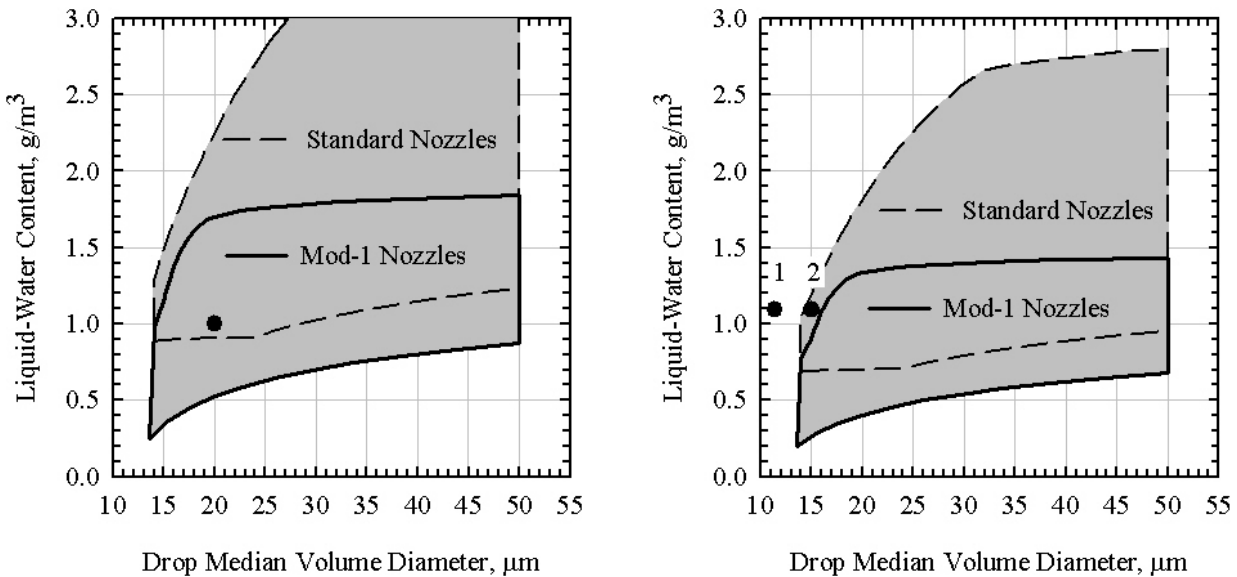
For the scale velocity of 212 mph (95 m/s) the tunnel calibrated cloud contracts to that of figure B.1. (b). The solid circle marked '1' indicates the scale drop size and LWC as given in Table B.I. This condition fell outside the nozzle range for the facility, and therefore could not be tested without special calibration. The second symbol gives the final solution, with δ_S increased to place the condition within the calibrated envelope.

This example involved a relatively small change in δ_S and was therefore simple to adjust to the facility envelope. This is not always the case. For example, for the $\frac{1}{3}$ -scale case 10 in Table B.I δ_S was $8.2\ \mu\text{m}$. While a value within the facility envelope can be found and the possibility exists that substituting such a value may be valid, tests of the effect of such a large change in MVD for this magnitude of drop size have not been made;

therefore, such substitutions carry an unknown level of risk.

Alternately, for situations like case 10, it is possible in principle to modify the original set of reference conditions by using test-condition scaling. We know from figures 3.3.6 and 3.3.7 that an encounter with a cloud MVD of $40\ \mu\text{m}$ should give the same ice shape as one with a drop size of $20\ \mu\text{m}$. Therefore, the reference conditions for case 10 can be replaced by a set of conditions with the same model size, temperature, velocity and liquid-water content as shown in Table B.I, but with $\delta = 40\ \mu\text{m}$ instead of 20. Because β_0 will now be different from that shown in Table B.I for case 10, the scale time must be altered to provide the same $\beta_0 A_c$ as that for the case-10 reference. This new set of reference conditions is now scaled to reduce the model size to $\frac{1}{3}$ of the reference using size scaling. Scaling by this model size ratio from a drop size of $40\ \mu\text{m}$ gives a scale drop size of $16.1\ \mu\text{m}$, which is within the tunnel cloud envelope. This approach can only be used to simulate main ice shapes, and additional tests with matched β_0 are needed if impingement limit information is desired. Drop-size substitution has not yet been fully tested but appears to be promising based on the results shown in figures 3.3.6 and 3.3.7. However, until further validation is obtained, this method should be used cautiously.

Although not illustrated by any of the cases in Table B.I, it is also possible that scale LWC may fall above or below the calibrated envelope of the facility. However, this situation is easily remedied by applying the Olsen method to scale LWC to a value within the nozzle array



(a) Envelope for $V = 150$ mph (67 m/s) (Reference).

(b) Envelope for $V = 212$ mph (95 m/s) (1/2-Scale).

Figure B.1. IRT Cloud Envelope with Conditions for Scaling Case 4, Table B.I.

operating map. An example of this approach was given in section B.1.

B.3.2. Temperature Cases 14 – 17 of Table B.I all had scale total temperatures in excess of 27°F. It was noted in section 3.5.13 that scale temperatures higher than this have been observed to produce ice shapes that do not match the reference shapes well. Therefore, for each of these cases it would be necessary to find a temperature below 27°F for testing. The following examples illustrate the process.

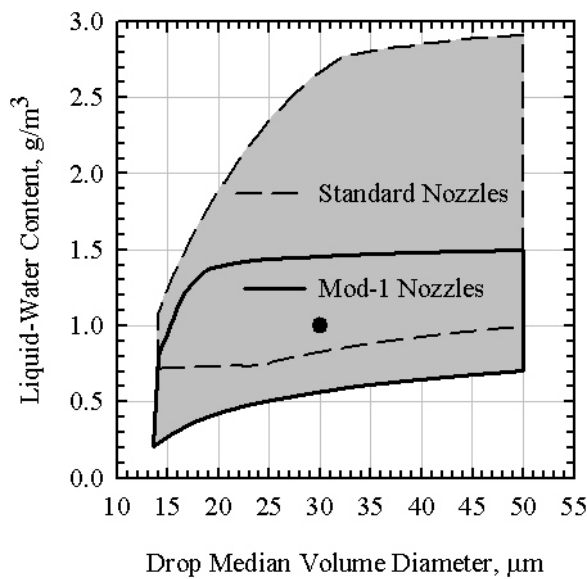
For the conditions of case 14 it is only necessary to select a new scale static temperature a little lower than the result determined by the Ruff scaling method. With c_s , V_s and δ_s unchanged, the modifications are:

- (1) Arbitrarily, set the scale static temperature a few degrees lower than the value originally found. Thus, $t_{st,S} = 5^\circ\text{F} (-15^\circ\text{C})$.
- (2) Find a new LWC_S for the new static temperature to maintain $n_{0,S} = n_{0,R}$. Note that for this example, $\beta_{0,S}$ for the modified scale conditions is the same as the original, which also matched $\beta_{0,R}$. The result is $LWC_S = 0.93 \text{ g/m}^3$.
- (3) Calculate a new scale icing time so that $A_{c,S} = A_{c,R}$. Then, $\tau_s = 5.2 \text{ min}$.

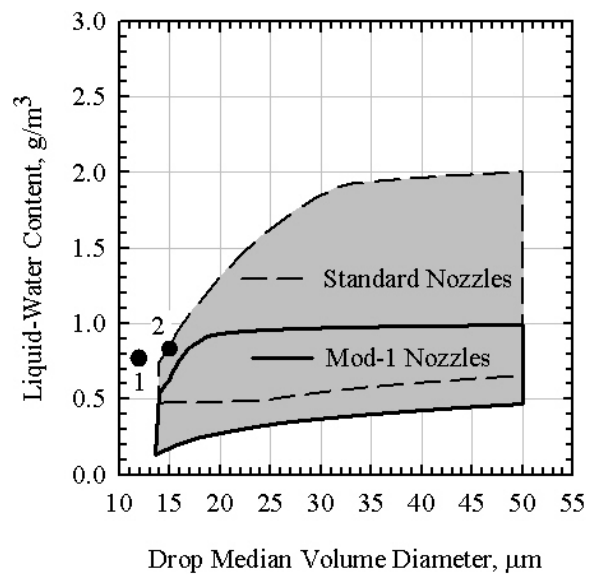
(4) Determine the new scale total temperature from equation (A.17). The static temperature change from 6.6 to 5°F has a negligible effect on the Mach number, so $M_{a,S}$ does not have to be re-calculated. $t_{tot,S}$ is then found to be 26.5°F (-3°C).

For case 15 both a lower scale static temperature and a higher scale drop size are needed compared with the scale values in Table B.I. Figure B.2. (a) shows the facility cloud envelope with the reference condition as a solid circle. The initial scale cloud conditions are given as point 1 in figure B.2. (b). The adjustments are made as follows with c_s and V_s unchanged:

- (1) Set the scale static temperature a few degrees lower than the value in Table B.I to reduce the total temperature below 27°F. As for case 14 above, $t_{st,S}$ is lowered to 5°F (-15°C).
- (2) Determine the new scale total temperature from equation (A.17). The Mach number is effectively unchanged from the value in Table B.I because the static temperature undergoes only a small change. Then we find $t_{tot,S} = 26.5^\circ\text{F}$. This is sufficiently below 27°F to be acceptable.
- (3) Choose a slightly larger δ_s such that it is within the facility cloud envelope. In this example, a value of 15 μm is used.



(a) Envelope for $V = 200 \text{ mph} (89 \text{ m/s})$ (Reference).



(b) Envelope for $V = 346 \text{ mph} (155 \text{ m/s})$ (1/3-Scale).

Figure B.2. IRT Cloud Envelope with Conditions for Scaling Case 15, Table B.II.

- (4) Calculate the new $\beta_{0,S}$ corresponding to $\delta_S = 15 \mu\text{m}$. The result is 0.691.
- (5) Find the new LWC_S for the new static temperature and δ_S such that $n_{0,S} = n_{0,R}$. The result is $LWC_S = 0.83 \text{ g/m}^3$.
- (6) Reevaluate the scale accumulation parameter so that $\beta_{0,S}A_{c,S} = \beta_{0,R}A_{c,R}$. $A_{c,S} = 2.29$.
- (6) Calculate a new scale icing time from the final $A_{c,S}$. The result is $\tau_S = 5.2 \text{ min}$. This completes the calculation of all the revised scale conditions.

The revised scale cloud conditions for case 15 are shown as point 2 on figure B.2. (b).

Adjustments to the scale conditions for case 17 in Table B.I will be discussed next. Figure B.3. (a) shows the facility cloud envelope with the reference condition as a solid circle. The scale cloud conditions from Table B.I are indicated as point 1 in figure B.3. (b). The scale total temperature for this case is above freezing, and the scale drop size is outside the calibrated envelope for the IRT. Thus, again it is necessary to reduce the scale static temperature and increase the scale drop size from the scale values in Table B.I.

The adjustments are made in the same way as for case 15, except that larger changes are necessary. Again, c_S and V_S are unchanged:

- (1) Set the scale static temperature sufficiently lower than the value in Table B.I. that the total temperature will be below 27°F . $t_{st,S}$ is set to 5°F (-15°C). Because the velocity and static temperature for this example is the same as for case 15, the Mach number and total temperature will also be the same. The resulting total temperature, $t_{tot,S} = 26.5^\circ\text{F}$. As before, this is sufficiently below 27°F to be acceptable.

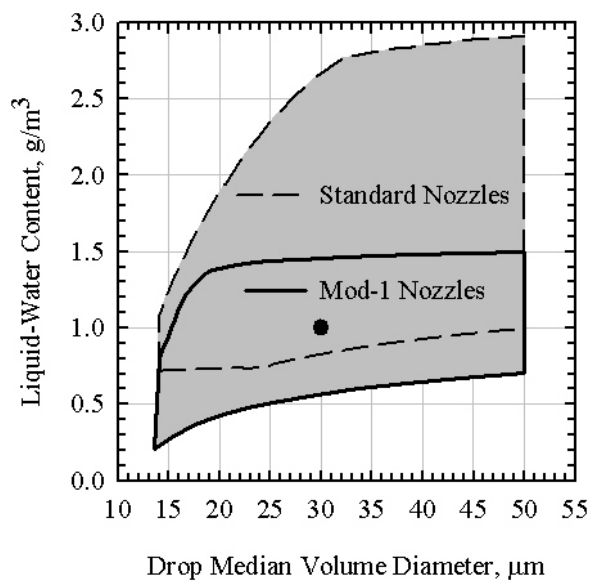
- (2) Choose a new δ_S such that it is within the facility cloud envelope. In this example, a value of $20 \mu\text{m}$ was expected to be large enough. It is desirable that this value not be any greater than necessary, but because we don't yet know the value of LWC_S that corresponds with the new temperature and drop size this initial guess for δ_S may need to be adjusted later.

- (3) The $\beta_{0,S}$ corresponding to $\delta_S = 20 \mu\text{m}$ is calculated to be 0.767.

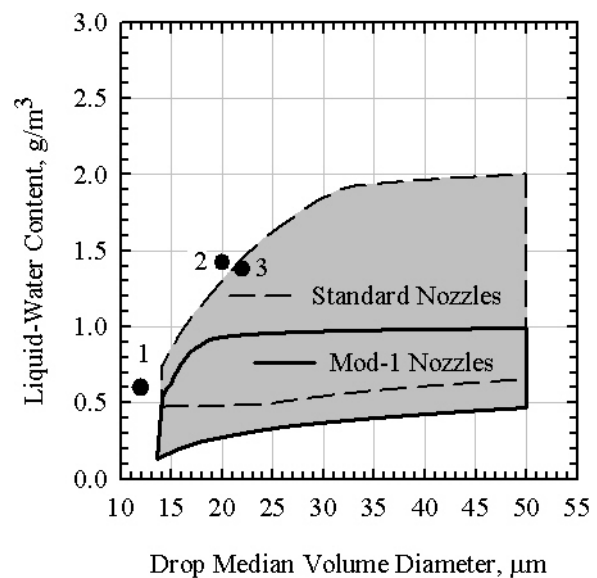
- (4) The LWC_S required to keep $n_{0,S} = n_{0,R}$ with the new static temperature and δ_S is 1.42 g/m^3 .

- (5) The scale accumulation parameter, $A_{c,S}$, is found to be 2.04 by matching $\beta_{0,S}A_{c,S}$ to $\beta_{0,R}A_{c,R}$.

- (6) Calculate the scale icing time from $A_{c,S}$. $\tau_S = 2.7 \text{ min}$.



(a) Envelope for $V = 200 \text{ mph}$ (89 m/s) (Reference).



(b) Envelope for $V = 346 \text{ mph}$ (155 m/s) (1/3-Scale).

Figure B.3. IRT Cloud Envelope with Conditions for Scaling Case 17, Table B.II.

These new scale cloud conditions for case 17 are shown as point 2 on figure B.3. (b). As can be seen from the figure, the $\delta_S - LWC_S$ combination was still just outside the calibrated map of the tunnel. Consequently, a slightly larger δ_S will be selected and the calculations repeated. The static temperature does not have to be changed. The procedures are the same as steps (2) – (6) above, and the resulting values are:

- (1) $\delta_S = 22 \mu\text{m}$
- (2) $\beta_{0,S} = 0.789$
- (3) $LWC_S = 1.38 \text{ g/m}^3$
- (4) $A_{e,S} = 1.99$
- (5) $\tau_S = 2.7 \text{ min}$

The final scale cloud conditions for case 17 are plotted as point 3 on figure B.3. (b). The $\delta_S - LWC_S$ combination now is within the calibrated envelope of the facility. This solution requires a fairly large modification to δ_S in a range of drop sizes for which the effect on ice shape has not been tested. Thus, while a solution is possible, we do not know how well the final result will simulate the desired accretion.

Appendix C References

1. von Glahn, Uwe H., "Use of Truncated Flapped Airfoils for Impingement and Icing Tests of Full-Scale Leading-Edge Sections," NACA RM E56E11, July 1956.
2. Saeed, Farooq, Selig, Michael S. and Bragg, Michael B., "Design of Subscale Airfoils with Full-Scale Leading Edges for Ice Accretion Testing," AIAA-96-0635, January 1996 and *J. Aircraft*, vol. 34, no. 1, January-February 1997, pp 94-100.
3. Saeed, Farooq, Selig, Michael S. and Bragg, Michael B., "Experimental Validation of the Hybrid Airfoil Design Procedure for Full-Scale Ice Accretion Simulation," AIAA-98-0199, January 1998.
4. Code of Federal Regulations, Title 14, Chapter 1, Federal Aviation Administration, Department of Transportation, Part 25, "Airworthiness Standards: Transport Category Airplanes," Appendix C, U.S. Government Printing Office, Washington DC, revised as of January 2001.
5. Bragg, M.B., Gregorek, G.M. and Shaw, R.J., "An Analytical Approach to Airfoil Icing," AIAA-81-0403, January 1981.
6. Bragg, Michael B., "A Similarity Analysis of the Droplet Trajectory Equation," *AIAA J*, vol. 20, no. 12, December 1982, pp 1681-1686.
7. Ruff, G.A., "Analysis and Verification of the Icing Scaling Equations," AEDC-TR-85-30, Vol 1 (Rev), March 1986.
8. Langmuir, Irving and Blodgett, Katharine B., "A Mathematical Investigation of Water Droplet Trajectories," Army Air Forces Technical Report No. 5418, February 1946.
9. Wright, W.B., "Users Manual for the Improved NASA Lewis Ice Accretion Code, LEWICE 1.6," NASA CR 198355, June 1995.
10. Olsen, W. and Walker, E., "Experimental Evidence for Modifying the Current Physical Model for Ice Accretion on Aircraft Surfaces," NASA TM 87184, 1986.
11. Anderson, David N. and Shin, Jaiwon, "Characterization of Ice Roughness from Simulated Icing Encounters," AIAA-97-0052 and NASA TM 87184, January 1997.
12. Hansman, R. John, Jr. and Turnock, Stephen, R., "Investigation of Surface Water Behavior During Glaze Ice Accretion," *J. Aircraft*, vol. 26 no. 2, February 1989, pp 140-147.
13. Olsen, William and Newton, James, "Experimental and Analytical Evaluation of Existing Icing Scaling Laws," unpublished draft of NASA Technical Memorandum, 1986.
14. Charpin, Francois and Fasso, Guy, "Essais de givrage dans la grande soufflerie de Modane sur maquettes a echelle grandeur et echelle reduite," *L'Aeronautique et l'Astronautique*, no 38, 1972, pp 23 – 31. English translation published as "Icing Testing in the Large Modane Wind Tunnel on Full Scale and Reduced Scale Models," NASA TM-75373, March 1979.
15. Armand, Claude, Charpin, Francois, Fasso, Guy and LeClere, Guy, "Techniques and Facilities used at the ONERA Modane Centre for Icing Tests," AGARD-AR-127, Appendix A6, November 1978.
16. Sibley, E.J. and Smith, R.E., "Model Testing in an Icing Wind Tunnel," Lockheed Aircraft Corporation, California Division, Report LR10981, October 1955.
17. Dodson, E.D., "Scale Model Analogy for Icing Tunnel Testing," Boeing Airplane Company, Transport Division Document no. D6-7976, 1962.
18. Chen, Shu-Cheng, unpublished GLC 305 icing studies in NASA Glenn IRT, March, April, September and October 1998.
19. Anderson, David N., "Acceptable Tolerances for Matching Icing Similarity Parameters in Scaling Applications," AIAA-2001-0832, January 2001.
20. Wright, William B., "Validation Report for LEWICE 2.0," NASA CR 208690, January 1999.
21. Messinger, B.L., "Equilibrium Temperature of an Unheated Icing Surface as a Function of Airspeed," *J. Aeron. Sci.* vol. 20 no. 1, January 1953, pp 29-42.
22. Tribus, Myron; Young, G.B.W.; and Boelter, L.M.K., "Analysis of Heat Transfer Over a Small Cylinder in Icing Conditions on Mount Washington," *Trans ASME* vol 70, 1948, pp 971-976.
23. McAdams, William H., *Heat Transmission*, McGraw-Hill, New York, 1954.
24. Kreith, Frank, *Principles of Heat Transfer*, International Textbook Co., Scranton, 1958.

25. Gelder, Thomas F. and Lewis, James P., "Comparison of Heat Transfer from Airfoil in Natural and Simulated Icing Conditions," NACA TN 2480, September 1951.
26. Poinssatte, Philip E., "Heat Transfer Measurements from a NACA 0012 Airfoil in Flight and in the NASA Lewis Icing Research Tunnel," NASA CR 4278, March 1990.
27. Van Fossen, G.J.; Simoneau, R.J.; Olsen, W.A.; and Shaw, R.J., "Heat Transfer Distributions Around Nominal Ice Accretion Shapes Formed on a Cylinder in the NASA Lewis Icing Research Tunnel," AIAA-84-0017 and NASA TM-83557, January 1984.
28. Shapiro, Ascher H., *The Dynamics and Thermodynamics of Compressible Fluid Flow*, Ronald Press Co., New York, 1954, pp 1070-1074, and 1122-1123.
29. Pruppacher, Hans R. and Klett, James D., *Microphysics of Clouds and Precipitation*, Reidel, Boston, 1980.
30. Oleskiw, Myron M., Kind, Richard J. and McCullough, Telamon, "Further Assessment of a Proposed Additional Scaling Parameter and of Non-Matching Freestream Temperature for Glaze Icing Tests," AIAA-2002-0520, January 2002.
31. Kind, R.J., "A Critical Assessment of the Similarity Requirements for Sub-Scale Simulation of Ice Accretion on Aircraft," section 4.1 in *Ice Accretion Simulation*, final report of AGARD/FDP Working Group 20, AGARD Report AR-344, in press, October 1997.
32. Kind, R.J., Dillon, T., Gaydos, J.A. and Oleskiw, M., "Evidence for the Importance of Scaling Viscous Effects in the Water Film in Glaze Icing Tests," AIAA-98-0196, January 1998.
33. Anderson, David N., "Methods for Scaling Icing Test Conditions," AIAA-95-0540 and NASA TM 106827, January 1995.
34. Anderson, David N., "Further Evaluation of Traditional Icing Scaling Methods," AIAA-96-0633 and NASA TM 104140, January 1996.
35. Anderson, David N. and Ruff, Gary A., "Evaluation of Methods to Select Scale Velocities in Icing Scaling Tests," AIAA-99-0244, January 1999.
36. Miller, Dean R., Addy, Harold E., Jr. and Ide, Robert F., "A Study of Large Droplet Ice Accretions in the NASA-Lewis IRT at Near-Freezing Conditions," AIAA-96-0934, NASA TM 107142 and Army Research Laboratory ARL-MR-294, January 1996.
37. Addy, Harlod E., Jr., Miller, Dean R. and Ide, Robert F., "A Study of Large Droplet Ice Accretion in the NASA Lewis IRT at Near-Freezing Conditions; Part 2," NASA TM 107424, May 1996.
38. Anderson, David N. and Tsao, Jen-Ching, "Evaluation and Validation of the Messinger Freezing Fraction," AIAA-2003-1218, January 2003.
39. Bilanin, A. J., "Proposed Modifications to the Ice Accretion/Icing Scaling Theory," AIAA-88-0203, January 1988.
40. Hansman, R. John, Jr. and Turnock, Stephen R., "Investigation of Microphysical Factors which Influence Surface Roughness During Glaze Ice Accretion," 4th International Workshop on Atmospheric Icing of Structures, Paris, September 1988.
41. Hansman, R.J., Breuer, K.S., Hazan, D., Reehorst, A. and Vargas, M., "Close-up Analysis of Aircraft Ice Accretion," AIAA-93-0029, January 1993.
42. Bilanin, Alan J. and Anderson, David N., "Ice Accretion with Varying Surface Tension," AIAA-95-0538 and NASA TM 106826, January 1995.
43. Bartlett, C. Scott, "An Analytical Study of Icing Similitude for Aircraft Engine Testing," DOT/FAA/CT-86/35 and AEDC-TR-86-26, October 1986.
44. Bartlett, C. Scott, "Icing Scaling Considerations for Aircraft Engine Testing," AIAA-88-0202, January 1988.
45. Oleskiw, Myron M., De Gregorio, Fabrizio and Esposito, Biagio, "The Effect of Altitude on Icing Tunnel Airfoil Icing Simulation," *Proceedings of the FAA International Conference on Aircraft Inflight Icing*, DOT/FAA/AR-96/81,II, August 1996, pp 511 – 520.
46. Anderson, David N., "Effect of Velocity in Icing Scaling Tests," AIAA-2000-0236, January 2000.
47. Feo, A., "Icing Scaling with Surface Film Thickness Similarity for High LWC Conditions," AE/PRO/4420/184/INTA/00, Instituto Nacional de Técnica Aeroespacial, October 2000.
48. Feo, A. and Urdiales, M., "Stagnation Point Probe in a Water Spray Immersed in an Airstream," φAE/TNO/0452/003/INTA/95, Instituto Nacional de Técnica Aeroespacial, February 1995.

49. Anderson, David N. and Feo, Alejandro, "Ice-Accretion Scaling Using Water-Film Thickness Parameters," AIAA-2002-0522, January 2002.
50. Feo, A., "Similarity of Water Film Weber Number and Film Thickness in Icing Scaling," AE/TNO/4420/264/INTA/01, Instituto Nacional de Técnica Aeroespacial, October 2001.
51. Kind, Richard J., "Assessment of Importance of Water-Film Parameters for Scaling of Glaze Icing," AIAA-2001-0835, January 2001.
52. Kind, Richard J. and Oleskiw, Myron M., "Experimental Assessment of a Water-Film-Thickness Weber Number for Scaling of Glaze Icing," AIAA-2001-0836, January 2001.
53. Kind, R.J., "Scaling of Icing Tests – A Review of Recent Progress," AIAA-2003-1216, January 2003.
54. Feo, Alejandro, INTA, personal communication, 1997.
55. Feo, A., "An Icing Scaling Law Considering Liquid Film Thickness Similarity," AE/TNO/4420/154/INTA/98, Instituto Nacional de Técnica Aeroespacial, July 1998.
56. Soeder, Ronald H. and Andracchio, Charles R., "NASA Lewis Icing Research Tunnel User Manual," NASA TM 102319, June 1990.
57. Soeder, Ronald H., Sheldon, David W., Andracchio, Charles R., Ide, Robert F., Spera, David A. and Lalli, Nick M., "NASA Lewis Icing Research Tunnel User Manual," NASA TM 107159, June 1996.
58. Irvine, Thomas B., Oldenburg, John R. and Sheldon, David W., "New Icing Cloud Simulation System at the NASA Glenn Research Center Icing Research Tunnel," AIAA-98-0143, January 1998 and NASA TM-1999-208891, June 1999.
59. Irvine, Thomas B., Kevdzija, Susan L., Sheldon, David W. and Spera, Daid A., "Overview of the Icing and Flow Quality Improvements Program for the NASA Glenn icing Research Tunnel," AIAA-2001-0229, January 2001.
60. Ide, Robert F., "Liquid Water Content and Droplet Size Calibration of the NASA Lewis Icing Research Tunnel," NASA TM 102447, January 1990.
61. Ide, Robert F., "Operating Envelopes and Calculation Procedure for Spray Settings for the NASA-Lewis Icing Research Tunnel," unpublished NASA Lewis document, November 1998.
62. Ide, Robert F. and Oldenburg, John R., "Icing Cloud Calibration of the NASA Glenn Icing Research Tunnel," AIAA-2001-0234, January 2001.
63. "Calibration and Acceptance of Icing Wind Tunnels," SAE ARP 5905, expected to be published 2003.
64. Anderson, David N., "Rime-, Mixed- and Glaze-Ice Evaluations of Three Scaling Laws," AIAA-94-0718 and NASA TM 106461, January 1994.
65. Anderson, David N., "Evaluation of Constant-Weber-Number Scaling for Icing Tests," AIAA-96-0636 and NASA TM 107141, January 1996.
66. Ruff, Gary A. and Anderson, David N., "Quantification of Ice Accretions for Icing Scaling Evaluations," AIAA-98-0195, January 1998.
67. Hauger, H. and Englar, K., "Analysis of Model Testing in an Icing Wind Tunnel – Theory and Limitations," Douglas Aircraft Report S.M. 14993, 1954.
68. Anderson, David N. and Ruff, Gary A., "Scaling Methods for Simulating Aircraft In-Flight Icing Encounters," NASA TM 107538, October 1997.
69. Bartlett, C. Scott, "An Empirical Look at Tolerances in Setting Icing Test Conditions with Particular Application to Icing Similitude," DOT/FAA.CT-87/31 and AEDC-TR-87-23, August 1988.
70. DeGregorio, F. and Esposito, B., "Prove Sperimentali sull'Accrescimento del Ghiaccio al Variare della Quota," CIRA Report MC-3E-CIRA-5-TR-0023, February 1996.
71. DeGregorio, F. and Imperato, L., "Experimental Assessment of Icing Scaling Laws," CIRA Document MC-3E-CIRA-7-TR-0033, October 1996.
72. *U.S. Standard Atmosphere, 1976*, U.S. Government Printing Office, Washington, DC, 1976.
73. Ingelman-Sundberg, M., Trunov, O.K., and Ivaniko, A., "Methods for Prediction of the Influence of Ice on Aircraft Flying Characteristics," Swedish-Soviet Working Group on Flight Safety, 6th Meeting, Report No. JR-1, 1977.
74. Anderson, David N. and Tsao, Jen-Ching, "Additional Results of Ice-Accretion Scaling at SLD Conditions," AIAA-2003-0390, January 2003.

75. Anderson, David N., Botura, Galdemir C. and Broeren, Andy P., A Study of Scaling for Intercycle Ice Accretion Tests,” AIAA-2001-0834, January 2001.
76. “NIST Thermophysical Properties of Air and Air Component Mixtures – NIST Airprops Version 1.0,” National Institute of Standards and Technology, US Department of Commerce, July 1998.
77. Mechtly, E.A., “The International System of Units – Physical Constants and Conversion Factors (Revised),” NASA SP-7012, 1969.
78. Abbott, Ira H. and von Doenhoff, Albert E., *Theory of Wing Sections*, Dover Publications, New York, 1959, p321.

REPORT DOCUMENTATION PAGE			<i>Form Approved</i> <i>OMB No. 0704-0188</i>	
Public reporting burden for this collection of information is estimated to average 1 hour per response, including the time for reviewing instructions, searching existing data sources, gathering and maintaining the data needed, and completing and reviewing the collection of information. Send comments regarding this burden estimate or any other aspect of this collection of information, including suggestions for reducing this burden, to Washington Headquarters Services, Directorate for Information Operations and Reports, 1215 Jefferson Davis Highway, Suite 1204, Arlington, VA 22202-4302, and to the Office of Management and Budget, Paperwork Reduction Project (0704-0188), Washington, DC 20503.				
1. AGENCY USE ONLY (Leave blank)		2. REPORT DATE March 2004	3. REPORT TYPE AND DATES COVERED Final Contractor Report	
4. TITLE AND SUBTITLE Manual of Scaling Methods			5. FUNDING NUMBERS WBS-22-728-41-17 NCC3-884	
6. AUTHOR(S) David N. Anderson				
7. PERFORMING ORGANIZATION NAME(S) AND ADDRESS(ES) Ohio Aerospace Institute 22800 Cedar Point Road Brook Park, Ohio 44142			8. PERFORMING ORGANIZATION REPORT NUMBER E-14272	
9. SPONSORING/MONITORING AGENCY NAME(S) AND ADDRESS(ES) National Aeronautics and Space Administration Washington, DC 20546-0001			10. SPONSORING/MONITORING AGENCY REPORT NUMBER NASA CR-2004-212875	
11. SUPPLEMENTARY NOTES Project Manager, Thomas H. Bond, Turbomachinery and Propulsion Systems Division, NASA Glenn Research Center, organization code 5840, 216-433-3900.				
12a. DISTRIBUTION/AVAILABILITY STATEMENT Unclassified - Unlimited Subject Category: 03 Available electronically at http://gltrs.grc.nasa.gov This publication is available from the NASA Center for AeroSpace Information, 301-621-0390.			12b. DISTRIBUTION CODE	
13. ABSTRACT (Maximum 200 words) This manual reviews the derivation of the similitude relationships believed to be important to ice accretion and examines ice-accretion data to evaluate their importance. Both size scaling and test-condition scaling methods employing the resulting similarity parameters are described, and experimental icing tests performed to evaluate scaling methods are reviewed with results. The material included applies primarily to unprotected, unswept geometries, but some discussion of how to approach other situations is included as well. The studies given here and scaling methods considered are applicable only to Appendix-C, icing conditions. Nearly all of the experimental results presented have been obtained in sea-level tunnels. Recommendations are given regarding which scaling methods to use for both size scaling and test-condition scaling, and icing test results are described to support those recommendations. Facility limitations and size-scaling restrictions are discussed. Finally, appendices summarize the air, water, and ice properties used in NASA scaling studies, give expressions for each of the similarity parameters used, and provide sample calculations for the size-scaling and test-condition scaling methods advocated.				
14. SUBJECT TERMS Aircraft icing; Icing testing; Scaling for icing tests; Ice-accretion physics			15. NUMBER OF PAGES 80	
			16. PRICE CODE	
17. SECURITY CLASSIFICATION OF REPORT Unclassified	18. SECURITY CLASSIFICATION OF THIS PAGE Unclassified	19. SECURITY CLASSIFICATION OF ABSTRACT Unclassified	20. LIMITATION OF ABSTRACT	